IMAGE: A MAP OF THE STARS OF THE ORION CONSTELLATION

JournalPreview

London Journal of Medical & Health Research

Volume 24 | Issue 8 | Compilation 1.0

Great Britain Journals Press

WWW.JOURNALSPRESS.COM

Journal Content
In this Issue

Great Britain Journals Press

A Short Study on Relationship between 'ABO' Blood Groups and Coronavirus Disease 2019

Dr. Pradip Kuma R Das, Dr. Eshita Das, Miss Chandrima Bhattacharyya & Miss Mekhola Sen

ABSTRACT

A Short study based on 204 patients with RT-PCR and Rapid Antigen Test proven SARS-CoV2 infection occurred in an urban municipality areas of total population more than 2 lakhs from March 2020 to August 2021, finding the relationship of covid -19 positive patients and their blood groups to search the link between susceptibility, severity and mortality with the blood groups. Current clinical observation suggest that gender and age of the patients are important risk factors in the susceptibility of Covid-19 infection. It is evident from the study that among the 'ABO' Blood group system, B positive groups are more affected and AB positive groups are less affected but the severity or complications leading to death is evident among more in Blood Group 'A' Positive and less in O positive cases. Among the negative groups. It has been shown that very less incidence is noted in O negative group. Why the negative groups are least affected, it is not clear to the researchers but it can be studied in details in near future.

Keywords: covid-19, coronavirus, ABO blood group system, susceptibility, severity.

Classification: NLM Code: WC506

Language: English

LJP Copyright ID: 392841

Great Britain Journals Press

London Journal of Medical & Health Research

Volume 24 | Issue 8 | Compilation 1.0

A Short Study on Relationship between 'ABO' Blood Groups and Coronavirus Disease 2019

Dr. Pradip Kuma R Das[α], Dr. Eshita Das[σ], Miss Chandrima Bhattacharyya[ρ] & Miss Mekhola Sen[ω]

ABSTRACT

A Short study based on 204 patients with RT-PCR and Rapid Antigen Test proven SARS-CoV2 infection occurred in an urban municipality areas of total population more than 2 lakhs from March 2020 to August 2021, finding the relationship of covid -19 positive patients and their blood groups to search the link between susceptibility, severity and mortality with the blood groups. Current clinical observation suggest that gender and age of the patients are important risk factors in the susceptibility of Covid-19 infection. It is evident from the study that among the 'ABO' Blood group system, B positive groups are more affected and AB positive groups are less affected but the severity or complications leading to death is evident among more in Blood Group 'A' Positive and less in O positive cases. Among the negative groups. It has been shown that very less incidence is noted in O negative group. Why the negative groups are least affected, it is not clear to the researchers but it can be studied in details in near future.

Keywords: covid-19, coronavirus, ABO blood group system, susceptibility, severity.

Author α: Mbbs, Dtm & H, Ph.D.
σ: Dr. Eshita Das, M. D, (Pediatrics).
ρ: M.SC, (Physiology).
ω: M.SC (Food & Nutrition).

I. INTRODUCTION

An outbreak of Severe Acute Respiratory Distress Syndrome diseases due to Novel Corona virus was reported on December 8, 2019 from the city of Wuhan, Hubei Province, China with a population of 11 million by the presentation of total 41 cases of pneumonia. Initially it was named as coronavirus 2019, the virus was later designated as Corona Virus Disease 2019 (COVID-19) by World Health Organization. Within a very short spell the epidemic spreads to different areas of China and later to 216 countries throughout the world as off now affecting more than thirty-two cores and death occurred more than two cores.

The patients appeared with varying clinical manifestations mainly fever with dry cough, sore throat, respiratory distress, weakness, giddiness and loss of smell in nose and loss of taste sensation, loose motions, red eyes and skin rashes. A study based on 250 patients with RT-PCR and Rapid Antigen Test proven SARS-CoV2 infection occurred in an urban municipality areas of total population more than 2 lakhs from March 2020 to August 2021, the clinical manifestations were Fever (100%), Cough (82.5%), weakness 77.5%), loss of sensation of taste in their tongue and loss of smell in their nose(35%) Body ache (35%), Throat pain and irritation (27.5 %), breathlessness (27.5%), Chest pain (20%), Dizziness and Giddiness (15%), loss of appetite (12.5%), Joint pains (7.5%), Loose motion, vomiting with pain abdomen (12.5%), red eyes (5%), allergic Skin rashes (2.5). A study of CT scan thorax reveals the most important radiological features as done by HRCT Thorax in the Covid-19 infected patients. Only 5 patients (2%) showed normal radiological pictures. But 245 patients (98%) showed various types of radiological features ranging from increased Bronco-vascular prominence (7.5%), Minimal Subsegmental Atelectasis (12.5%), Multifocal areas of Ground glass opacities (40%), Atypical Pneumonia 22.5%), Bilateral Pneumonia (7.5%), Pleural Effusion (5%) which indicate the suspicion of Covid-19 infections. The SARS Cov2 epidemic

has been announced as Public Health Emergency of International concern (PHEIC) by the World Health Organization on 30.01.2020 due to prolonged disease transmission and human-to-human transmission has been reported to different countries like Italy, Germany, Spain, America, Japan, Australia, India and others. People coming from abroad are forced to remain in quarantine period of 14 days for preventing the spread of transmission of entry of virus into the developing countries like India which is also a thick population density country, may have not their health infrastructure so developed to cope up with this divesting infection, is facing such type of global concern.

II. REVIEW OF LITERATURE

According to Chen N et al. SARS COV-2 reveals with respiratory distress symptom at its previous stage at local seafood market at Wuhan, China. Females were less susceptible than male for the reason of having female X chromosome and sex hormone that build innate and adaptive immunity. [1]

Cheng Y et al. states that, among 45 participant staffs 35 were affected by SARS-CoV and show the symptoms. Among them 'O' Blood group are found less that Non 'O' Blood group are found with SARS-CoV affected.[2]

According to Po XU et al. by examining with immunohematology analyzer among 3694 Han people who are disease free individual distribution od ABO blood group is found as O> A>B>AB, i.e., distribution of B blood group is found more that AB blood group. [3]

American College of Emergency Physicians (ACEP) says that, Covid-19 assessment tools like D-Dimer, CT- scan od chest, ferritin level, CRP (C-Reactive Protein) can clearly investigate Covid-19 circumstances within patients and can create positive disease management.[4]

III. METHODOLOGY

Clinical diagnosis of Covid-19 infected patients confirmed by RTPCR testing, other blood examination, D-Dimer test, St X-ray, HRCT Thorax etc. and local control population study.

Table 1: Survey of Covid-19 Positive Patients in Relation to Blood Groups

S L. No	Blood Group	Male	Female	Total No. of PTS
1	A POSITIVE	14	19	33
2	A NEGATIVE	0	0	0
3	B POSITIVE	40	42	82
4	B NEGATIVE	01	0	01
5	AB POSITIVE	12	15	27
6	AB NEGATIVE	0	01	01
7	O POSITIVE	35	23	58
8	O NEGATIVE	01	01	02
9	TOTAL	103	101	204

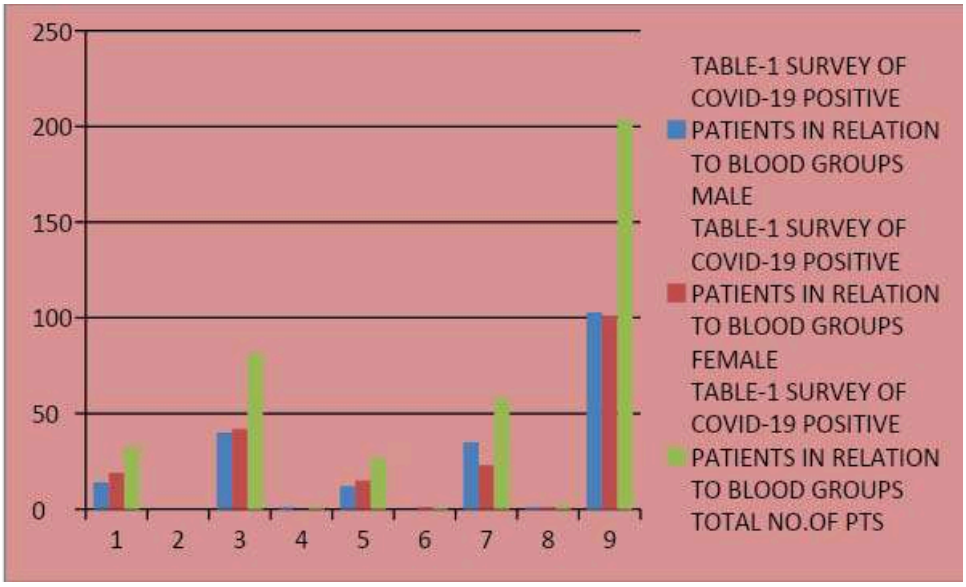

Chart-I

Table-1 & Chart-I shows that out of 204 numbers of positive Covid-19 patients examined so far it is evident that 33 patients (14-male,19-female) having A+ Blood Group, 82 Patients (40-male, 42-female) have B+ Blood Group, 27 (12 male,15 female) possess AB+ Blood Group, 58 (35 male, 23 female) possess O+ Blood group and 1male B-, 1 female AB- and 1 male with 1 female O- blood group.

Table 2: Age & Sexwise Blood Grouping

Blood Group	Agewise (Male)				Agewise (Female)				Total
	20-30 yrs	31-40 yrs	41 -50 yrs	51 yrs Above	20-30 Yrs	31-40 yrs	41 -50 yrs	51 yrs Above	204
A+	01	02	04	07	04	02	06	07	33
A-	0	0	0	0	0	0	0	0	0
B+	13	07	04	16	12	07	09	14	82
B-	0	0	0	01	0	0	0	0	01
AB+	04	02	01	05	06	01	03	05	27
AB-	0	0	0	0	0	01	0	0	01
O+	06	10	11	08	07	04	08	04	58
O-	0	01	0	0	0	0	0	01	02

Table-2 shows the age and sex-wise relationship of ABO Blood Group system with the covid-19 infected patients. It is evident from the Table that highest number of male patients belonging B+ group (40) and female patients belonging to B+ group (42) are characteristically divided into the age groups between 20-30 years (13) in male patients and in the same age group (14) in female patients, whereas in the age group between 5i years and above the number goes to 16 in males and 14 in females. In case of O+ group the figure is different in the age groups. In that case the age group between 31-40 yrs (10) and 41 -50 yrs (11) in male patients and in female patients the figure is 4 & 8 respectively. Different picture is also noted in male and female patients possessing A + group in their variant age groups.

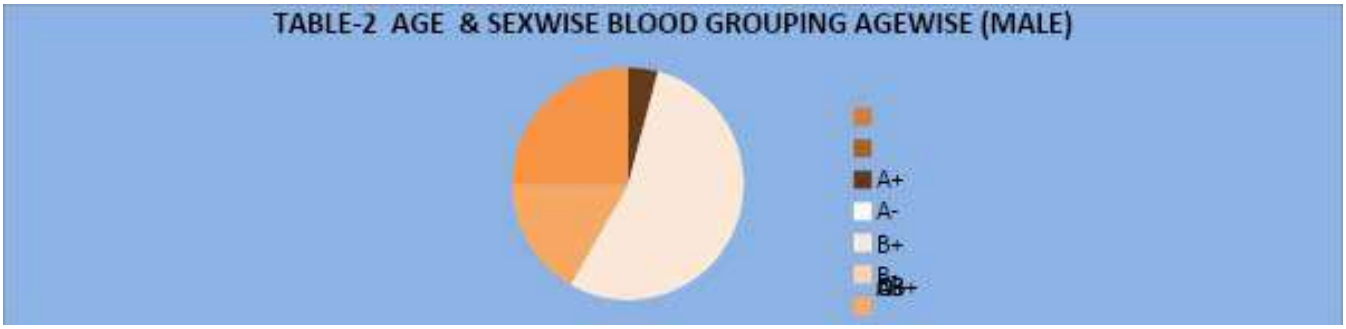

Chart-2

Table-2 & Chart-2 shows age-wise and sex-wise reflection of covid-19 positive patients.

Having different Blood groups but B positives are more affected than other groups.

Table-I: Sex Wise Categorization of Covid-19 Infected Patients

Male	Female
103	101

Table –I shows out of total patients diagnosed as COVID-19 under study it is evident that 103 patients (50.49%) are male and 101 patients (49.50%) are female.

Table-II: Age Wise Categorization of Covid-19 Infected Patients

20-30 Yrs (Male)	31-40 Yrs (Male)	41- 50 Yrs (Male)	51 Yrs and Above (Male)	Total (Male)
24	22	20	37	103
20-30yrs (Female)	31-40yrs (Female)	41-50 Yrs (Female)	51 Yrs & Above (Female)	Total (Female)
29	15	26	31	101

Table-II reveals that the patients under study are categorized as per their ages into three groups. Among them 53 patients (24 male & 29 female) belong to the age group between 20-30 years, 37 patients (22 male and 15 female) belong to 31 to 40 years, 46 patients (20 male & 26 female) belong to the age group of 41 to 50 yrs and 68 patients (37 male and 31 female) fall into the group of 51 yrs and above. From the Table-II, it has been shown that in the younger age group (20 to 30 Years) the affection is 25.98%, next to the age group (31-40) is 18.13%, in the age group between 41 to 50 years the percentage of affection is 22.5, whereas in the older age group (51 years and above) the affection is 33.33%. In our country the older age group is affected (33.33%) in compare to the western countries where the affection is more than 72% above the age group of 60 years. As age advances, immunity power of our body diminishes as well as co-morbidities increases. For that reason, their mortality rate increases (3%) in compare to our country where mortality rate is 1.8 %, although infectivity rate is high in our country.

Table-III: Presentation of Symptoms

Fever	Weakness	Body ache	Joint Pain	Throat Pain	Cough Dry or productive	Breathlessness	Loss of Taste sensation And loss of smell	Chest Pain	Tingling or Numbness	Giddiness or Dizziness	Loss of Appetite	Nasal stuffiness
204	155	70	15	55	165	55	43	40	5	30	25	10

Younger patients presented with loss of smell and taste sensation but aged patients came with breathlessness.

Table –III shows the various presentation of symptoms came to the doctors' chamber. In our study, it is noted that out of infected with Covid-19 204 patients, 100 per cent presented with fever of short or long duration, then presented with marked weakness (155) by 75.98 % along with dry cough or productive cough (165) by 80.89%. Most interesting finding is that younger patients (43) presented with loss of sensation of taste in their tongue and loss of smell in their nose by 21 per cent. Moreover, Body ache (70) by 34.31%, Throat pain and irritation in the throat during deglutition (55) by 26.96 %, breathlessness (55) mostly by the aged patients by 26.9%, Chest pain (40) by 19.6%, Dizziness and Giddiness (30) by 14.7%, loss of appetite (25) by 12.25%, Joint pains (15) by 7.35%. Astonishingly 10 (4.90%) presented with nasal stuffiness and five cases (2.45%) presented with allergic skin rashes in the abdomen, hands and legs without taking any drugs previously, excluding any drug rash and she had no food allergy recorded from her personal history.

Table-IV: Oropharyngeal and Nasopharyngeal Swab Testing Procedure

Rt Pcr Test	Rapid Antigen Test
194	10

Table-IV reveals that most of the testing procedures were done in Serampore Walsh Hospital from where Oropharyngeal and nasopharyngeal swabs were taken as per Standard Protocol and sent to NICED center, Kolkata for RT-PCR testing. out of 204 patients studied, 194 patients (95.09%) were tested RT-PCR and 10 patients (4.90%) were tested Rapid Antigenic mode as day goes number of infections increases to cope up with that situation Rapid Test were performed.

Table V: Abnormal Biochemical Testing of PTS

Liver Function Testing		D-Dimer Testing		C-Reactive Protein Testing	
Normal Finding in PTS	Abnormal Finding in PTS (Sgpt & Sgot U/Llevel)	Normal Finding in PTS	Abnormal Finding in PTS (Above 500 Ng/Ml)	Normal Finding in PTS	Abnormal Finding in PTS (More Than 6 Ng/Ml)
35	05	36	04	30	10

Table V shows that apart from Covid-19 testing other tests like Liver Function Tests- SGOT, SGPT, D-DIMER, C-Reactive Proteins were done to correlate any other organ affection by Covid-19

It has been shown that out of 40 patients, 35 patients (87/5%), showed no abnormal liver function but 5 Patients (12.5%) revealed abnormal liver function as evidenced by raised SGPT & SGOT levels.

Similarly, by estimating D-Dimer level it has been found that 4 (10%) patients showed raised D-Dimer level and 10 Patients (25%) revealed raised level of C-Reactive Proteins which indicates that Covid-19 infections in some cases can rise to Cytokine storms.

Table VI: Hematological Testing

Hemoglobin In Gm/Dl			Leucocyte Count Per Cubic Millilitre		
Below 10 Gm%	10+ To 12 Gm%	12+ To 14 Gm%	Below 4000	4000+ To6000	6000+ To 9000
25	125	54	16	136	52

Table-VI reveals that the all-infected patients under study have low level of hemoglobin. Out of them 25 patients (12.25%) have hemoglobin below 10 gm%, 125 Patients (61.27%) possess hemoglobin 10 to 12 gm % and 54 patients (26.47%) showed their hemoglobin range between 12 to 14 gm%. 16 patients (7.84%) showed leukopenia (leucocyte count below 4000) but the other patients showed leucocyte count within normal range. (4,000 to 9000).

Normal Picture	Increased Bronco Vascular Prominence	Minimal Subsegmental Atelectasis	Multifocal Areas of Ground Glass Opacities	Atypical Viral Pneumonia	Bilateral Pneumonia	Pleural Effusion
10	15	25	80	40	10	05

Table-VII reveals the most important radiological features as done by HRCT Thorax in the Covid-19 infected patients. Only 2 patients (5%) showed normal radiological pictures. But 38 patients (95%) showed various types of radiological features ranging from increased Bronco-vascular prominence (7.5%), Minimal Subsegmental Atelectasis (12.5%), Multifocal areas of Ground glass opacities (40%), Atypical Pneumonia 22.5%), Bilateral Pneumonia (7.5%), Pleural Effusion (5%) which indicate the suspicion of Covid-19 infections. In our study it has been found that 15 patients (37.5%) showed Atypical Pneumonia, Bilateral Pneumonia and Pleural Effusion which needs to be treated urgently otherwise patient can go to life saving measures. But in our study, 16 patients (40%) revealed the radiological features of Multifocal areas of Ground Glass opacities which also gave us a clue for suspicion of Covid-19 infections particularly in the background of Pandemic infection.

IV. RESULTS

Table –I shows out of total patients diagnosed as COVID-19 under study it is evident that 22 patients are male and 18 patients are female. Table-II reveals that the patients under study are categorized as per their ages into three groups. Among them 14 patients belong to the age group between 20-40 years, 15 patients belong to 41 to 60 years and 9 patients fall into the group of 61 to 80 years and only 2 patients belong to 81 to 100 years. From the Table-II, it has been shown that in the younger age group (20 to 40 Years) the affection is 35%, next to the age group (41-60) is 37.5%, whereas in the older age group (above 60) the affection is 27.5%. In our country the younger group is affected more (72.5%) in compare to the western countries where the affection is more than 72% above the age group of 60 years. As age advances, immunity power of our body diminishes as well as co-morbidities increases. For that reason, their mortality rate increases

(3%) in compare to our country where mortality rate is 1.8 %, although infectivity rate is high in our country. In our study it is noted that the lowest age of infectivity to Covid-19 is 23 years and highest age is 92 years old, both of them are quite well after treatment. Table –III shows the various presentation of symptoms came to the doctors' chamber. In our study, it is revealed that out of infected with Covid-19, 250 patients (100 %) presented with fever of short or long duration, then presented with marked weakness by 19 (77.6 %) along with dry cough or productive cough by33 (82.5%). Most interesting finding is that younger patients by number 14 (35%) presented with loss of sensation of taste in their tongue and loss of smell in their nose. Moreover 14 patients (35%) are presented by body ache, Throat pain and irritation in the throat during deglutition is manifested by 11 (27.5 %) patients, only breathlessness mostly by the 11 (27.5%) aged patients, Chest pain by 8 patients (20%), Dizziness and Giddiness by 6 patients (15%), loss of appetite by 5 patients (12.5%), Joint pains (03) by 7.5%. Astonishingly only 2 (5%) presented with nasal stuffiness and only one case presented with allergic skin rashes in the abdomen, hands and legs without taking any previously, excluding any drug rash and she had no food allergy recorded from her personal history. Table-IV reveals that most of the testing procedures were done in Serampore Walsh Hospital from where Oropharyngeal and nasopharyngeal swabs were taken as per Standard Protocol and sent to NICED center, Kolkata for RT-PCR testing. out of 40 patients studied, 32 patients (80%) were tested RT-PCR and 8 patients (20%) were tested Rapid Antigenic mode as day goes number of infections increases to cope up with that situation Rapid Test were performed. Table V shows that apart from Covid-19 testing other tests like Liver Function Tests- SGOT, SGPT, D-DIMER, C-Reactive Proteins were done to correlate any other organ affection by Covid-19 It has been shown that out of 40 patients, 35 patients (87/5%), showed no abnormal liver function but 5 Patients (12.5%) revealed abnormal liver function as evidenced by raised SGPT & SGOT levels. Similarly, by estimating D-Dimer level it has been found that 4 (10%) patients showed raised D-Dimer level and 10 Patients (25%) revealed raised level of C-Reactive Proteins which indicates that Covid-19 infections in some cases can rise to Cytokinetic storms. Table-VI reveals that the all-infected patients under study have low level of hemoglobin. Out of them 5 patients (12.5%) have hemoglobin below 10 gm%, 25 Patients (62.5%) possess hemoglobin 10 to 12 gm % and 10 patients (25%) showed their hemoglobin range between 12 to 14 gm%. Only 3 patients (7.5%) showed leukopenia (leucocyte count below 4000) but the other patients showed leucocyte count within normal range. (4,000 to 9000). Table VII reveals the most important radiological features as done by HRCT Thorax in the Covid-19 infected patients. Only 2 patients (5%) showed normal radiological pictures. But 38 patients (95%) showed various types of radiological features ranging from increased Bronco-vascular prominence (7.5%), Minimal Subsegmental Atelectasis (12.5%), Multifocal areas of Ground glass opacities (40%), Atypical Pneumonia 22.5%), Bilateral Pneumonia (7.5%), Pleural Effusion (5%) which indicate the suspicion of Covid-19 infections. In our study it has been found that 15 patients (37.5%) showed Atypical Pneumonia, Bilateral Pneumonia and Pleural Effusion which needs to be treated urgently otherwise patient can go to life saving measures. But in our study, 16 patients (40%) revealed the radiological features of Multifocal areas of Ground Glass opacities which also gave us a clue for suspicion of Covid-19 infections particularly in the background of Pandemic infections.

Objectives:

To find out the relationship of ABO blood groups and Covid-19 infected patients.

V. DISCUSSIONS

It is revealed that out of 204 number of positive Covid-19 patients (Table-1) examined so far it is evident that 33 patients (14-male,19-female) having A+ Blood Group, 82 Patients (40-male, 42-female) have B+ Blood Group, 27 (12 male,15 female) possess AB+ Blood Group, 58 (35 male, 23 female) possess O+ Blood group and 1 male B-, 1 female AB- and 1 male with 1 female O- blood group. Table-2 shows the age and sex-wise

relationship of ABO Blood Group system with the covid-19 infected patients. It is evident from the Table that highest number of male patients belonging B+ group (40) and female patients belonging to B+ group (42) are characteristically divided into the age groups between 20-30 years (13) in male patients and in the same age group (14) in female patients, whereas in the age group between 5i years and above the number goes to 16 in males and 14 in females. In case of O+ group the figure is different in the age groups. In that case the age group between 31-40 yrs (10) and 41 -50 yrs (11) in male patients and in female patients the figure is 4 & 8 respectively. Different picture is also noted in male and female patients possessing A + group in their variant age groups.

VI. CONCLUSION

Very younger and older patients are very much susceptibility to Covid-19 so far. Susceptibility of Covid-19 infection has got certain relationship with the ABO Blood Group system. Here we have tried to find the link between them in our clinical and laboratory research works. It has been shown that O+ Blood group patients are less affected that other groups and B+ groups are more affected and severity of infections goes to A+ groups.

REFERENCES

1. Chen N Zhou M Dong X et al, Epidemiological and clinical characteristics of 99 of 2019 novel coronavirus pneumonia in Wuhan, China: a descriptive study, Lancet,2020: (Published in Jan 29, https://doi.org/10.1016/SO140-6736 (20)30211-7.
2. Cheng Y, Cheng G et al. ABO Blood Group and susceptibility to severe acute respiratory syndrome, JAMA 2005 March 21: 293 (12); 1450-1.
3. Yu P Xiong Y et al. Distribution of ABO and RhD blood group among Healthy Han population in Wuhan, J Clin Hemato/(China), 2015 (28):837.
4. American College of Emergency Physician (ACEP), (2020): Covid-19 severity classification.

Body Weight Changes, Histological Features and Anti-Hyperglycemic Effects of Cocoyam-Soya Bean-Bambara Groundnut Flour Blend-Fed Streptozotocin (STZ)-Induced Diabetic Rats

Professor Uro-Chukwu, Henry Chukwuemeka, Prof. Ezekwe, Afamefula Sunday, Dr. Okorie Uchechukwu, Dr. Eleazu, Chinedu & Miss Uro-Chukwu, Frances Chidinma

Alex Ekwueme Federal University

Background: Diabetes mellitus (DM) has a global prevalence of 536.6 million people, which is an estimated rise of 12.2% by 2045. Diabetes management is expensive, hence alternate management options are being explored. The World Health Organization recognizes some plants and plant-based meals as excellent diabetes treatment agents. These include cocoyam (CYN), soya bean (SB), and Bambara groundnut (BGN). The purpose of this study was to evaluate these extracts' hypoglycemic, weight changes and histological effects.

Methodology: CYN, SB, and BGN were sourced and processed to generate high-quality flour, which were pelletized and oven-dried at 60°C, before storage. The eighty-two male albino rats weighing between 134 and 247 g, were administered with low-dose fructose to induce insulin resistance. Type 2 diabetes mellitus (T2DM) was induced with intraperitoneal injection of streptozotocin, following which 28 days intervention formulations were administered. Throughout the investigation, the weights of the rats were recorded while on the 28th day, their organs and blood samples were collected from killed rats for histological examination and blood glucose analysis respectively.

Keywords: rat weight, histology, diabetes, flour blend.

Classification: NLM Code: WK 810

Language: English

Great Britain Journals Press

London Journal of Medical & Health Research

Volume 24 | Issue 8 | Compilation 1.0

Body Weight Changes, Histological Features and Anti-Hyperglycemic Effects of Cocoyam-Soya Bean-Bambara Groundnut Flour Blend-Fed Streptozotocin (STZ)-Induced Diabetic Rats

Professor Uro-Chukwu, Henry Chukwuemeka[α], Prof. Ezekwe, Afamefula Sunday[σ], Dr. Okorie Uchechukwu[ρ], Dr. Eleazu, Chinedu[CO] & Miss Uro-Chukwu, Frances Chidinma[¥]

ABSTRACT

Background: Diabetes mellitus (DM) has a global prevalence of 536.6 million people, which is an estimated rise of 12.2% by 2045. Diabetes management is expensive, hence alternate management options are being explored. The World Health Organization recognizes some plants and plant-based meals as excellent diabetes treatment agents. These include cocoyam (CYN), soya bean (SB), and Bambara groundnut (BGN). The purpose of this study was to evaluate these extracts' hypoglycemic, weight changes and histological effects.

Methodology: CYN, SB, and BGN were sourced and processed to generate high-quality flour, which were pelletized and oven-dried at 60°C, before storage. The eighty-two male albino rats weighing between 134 and 247 g, were administered with low-dose fructose to induce insulin resistance. Type 2 diabetes mellitus (T2DM) was induced with intraperitoneal injection of streptozotocin, following which 28 days intervention formulations were administered. Throughout the investigation, the weights of the rats were recorded while on the 28th day, their organs and blood samples were collected from killed rats for histological examination and blood glucose analysis respectively.

Results & Discussion: The investigation revealed an average random blood glucose (RBG) levels that varied significantly over time for each group, displaying a consistent pattern of changes across the entire group from week 1 to week 4 (F=79.106, p<0.01) (F=76.755, p<0.001), with significant differences between groups (F= 13.963, p<0.001). Group A diabetic rats exceeded the normal control group in terms of anti-diabetic efficacy, rat body weight gain of 8.85% over four weeks period, an increase in liver weight in the intervention formulation groups and an unchanged pancreatic weight. Histological examinations revealed varied levels of tissue regeneration and intra-hepatic inflammation in pancreatic and hepatic cells between groups treated with different intervention formulations. Conclusion: Group A rats, treated with formulation 1 (16.6% CY+16.6 %SB+16.6%BGN) had histological characteristics identical to the normal control group, exceeding the standard control groups. This showed that these formulations successfully stopped STZ-induced organ damage and resulted in successful organ healing. Furthermore, the Cocoyam-Soya bean-Bambara groundnut flour blend demonstrated hypoglycemic, tissue regeneration, and hepato-pancreatic protective effects in STZ-induced diabetic rats, showing its potential as a therapeutic supplement in the treatment of diabetes mellitus.

Keywords: rat weight, histology, diabetes, flour blend.

Author α: Department of Medical Biochemistry College of Medicine Alex Ekwueme Federal University Ndufu- Alike Ikwo Ebonyi State.

σ: Department of Medical Biochemistry College of Medical Sciences Rivers State University PortHarcourt, Nigeria.

ρ: Department of Biochemistry Faculty of Science Alex Ekwueme Federal University Ndufu- Alike Ikwo Ebonyi State Nigeria.
ↀ: Department of Biochemistry Faculty of Science Alex Ekwueme Federal University Ndufu- Alike Ikwo Ebonyi State Nigeria.
¥: Institute for Nutraceutical, Nutrition and Public Health Research & Development, Nigeria.

I. INTRODUCTION

Diabetes mellitus, an endocrine and metabolic disease, affects an estimated 536.6 million people globally (10.5%), and it is expected to rise by 12.2% among those aged 20 to 79, potentially affecting 783.2 million people by 2045[1]. Hyperglycemia is caused by abnormalities in pancreatic cells or insufficient insulin secretion, which can lead to a variety of health issues including ketoacidosis, heart failure, renal failure, and blindness[2]. Diabetes mellitus is becoming increasingly common in low-income countries such as Nigeria, with higher rates of occurrence, prevalence, and daily adjusted life years (DALYs) than in high-income countries[3].

Diabetes management requires large financial resources, a workforce, healthcare infrastructure, and the treatment of associated problems[4]. This leads to lower productivity, a shorter life expectancy, and a lower quality of life for individuals. The enormous financial burden and problems of addressing diabetes complications provide a significant barrier in countries with poor healthcare systems and inadequate resources[5]. As a result, there is an urgent need to find more cost-effective techniques for reducing the prevalence, severity, and effects of diabetes using available resources, particularly in developing countries.

It has been discovered that complementary management strategies like adopting suggested eating patterns and increasing physical activity, can considerably lower the risk factors linked to diabetes. As a result, there are fewer new instances, the condition is less severe, and the consequences associated with it are reduced[6]. Diabetic Medical Nutrition Therapy, the nutritional management of diabetes, is centred on developing a customized nutrition treatment plan based on evidence that takes into account many variables, such as how well an individual's lifestyle and insulin are matched[7]. Research has demonstrated that dietary changes can lessen the difficulties associated with diabetes mellitus[8].

It is well known that eating plant-based foods and plants can effectively treat diabetes. The use of medicinal plants to treat diabetes and other illnesses has been recognized by the World Health Organisation[9]. Antioxidant and anti-inflammatory bioactive components are present in some of these therapeutic plants. Examples include the Fabaceae bean Bambara groundnut (vigna underground), which is high in lipids (10%), protein (15–17%), and carbs (57–67%)[10,11]. Furthermore, major amounts of vital vitamins and minerals, including vitamin A, niacin, riboflavin, and carotene, as well as important phytochemicals and bioactive compounds, such as phenolics[12], dietary fibres[13], fatty acids, including PUFA and MUFA[14], peptides, and amino acids are also present in bambara groundnuts.

Tocopherols, tocotrienol, and oxysterols, in particular, have many advantageous characteristics, including immune system stimulation, antioxidant and antimicrobial effects, decreased platelet aggregation, hormone metabolism regulation, and enzyme detoxification[15]. It has been discovered that phenolic chemicals inhibit enzymes that help convert starch to glucose, such as α-amylase and α-glucosidase[16]. Furthermore, in diabetic rats, Bambara groundnut can enhance peripheral glucose absorption, which results in hypoglycemic effects[17].

Although high in carbohydrates, roots and tubers with a low glycaemic index include cocoyam. Research has demonstrated that cocoyam possesses immunomodulatory and anti-hyperglycemic qualities in both in vitro and in vivo settings. Though in different proportions, these foods include bioactive substances such as polyphenols, flavonoids, amino acids, and peptides. Titerpenoids, alkaloids, flavonoids, phenolics, and peptides are among the bioactive ingredients that have been shown to activate

hepatic enzymes and pancreatic β-cells in rats, resulting in the normalization of blood glucose levels[18].

Many studies have indicated that the phytochemicals found in cocoyam have antioxidant and hypoglycemic qualities[19]. Eleazu and colleagues[20] suggested that these chemicals may have anti-diabetic properties because they can suppress acute pancreatitis and delay or regulate the conversion of starch to glucose. Aloe vera leaf extract[21], Mangifera indica seed kernel[22], and allium sativum L bulb extract[23] are other plants that have been linked to anti-diabetic effects. The purpose of this study was to evaluate in diabetic rats the anti-hyperglycemic and biochemical benefits of eating cocoyam flour, a plant-based diet.

Glycine max. (L) Merrill, sometimes known as soya beans, are a leguminous crop that is high in protein and oil. It is eaten in a variety of ways, including tofu, textured vegetable protein (TVP) or textured soy protein (TSP), tempeh, roasted, boiled, in soymilk, mayonnaise, miso, cheese, and soy yoghurt. In terms of nutrition, each 100g of it has 30–50g of protein, 20–35g of carbs, and 15–25g of fats. PUFA makes up the majority of the lipid composition (63%), followed by MUFA (21.5%) and SFA (15%). In addition to vitamins E, K, A, and C, minerals including calcium, iron, zinc, salt, potassium, magnesium, copper, and phosphorus, soya beans also include folates, thiamine, riboflavin, pyridoxine, and niacin. Bioactive peptides, oxalates, isoflavones, and phytic acids are some of the phytochemicals found in soybeans. Antioxidant qualities are exhibited by the soybean's inositol triphosphate (IP3) and inositol tetraphosphate (IP4).

It has been discovered that the peptides exhibit immunomodulatory and antioxidative properties and in both human and animal studies, soybean and its bioactive components dramatically reduce blood levels of triglycerides and cholesterol[24]. Because isoflavones interact with β-estrogen receptors in the liver, they increase the number of hepatic receptors for LDL-C, which helps break down cholesterol and oxidize fatty acids, which is why lipid levels have decreased[25]. This study aimed to evaluate in greater detail the anti-hyperglycemic and biochemical benefits of feeding diabetic rats a plant-based diet called Bambara groundnut flour.

II. MATERIALS AND METHODS

2.1 Collection and Preparation of the Plant Food Material

The Vigna subterranean had been recognised by a plant taxonomist after it was purchased from a reputable local market. The sample was processed by giving it a thorough wash, peeling it, and soaking it in water for ten minutes. It was then washed, brought to a boil, and dried in an oven set to 60°C until it reached a uniform weight. After that, the dried weight was converted into pellets, coarsely crushed into flour, and baked at 60°C until a consistent weight was attained. The pelletized foods were kept in a tightly closed container until they were needed to feed the rats. Plant taxonomist NCe 005 recognized the roots of a *Colocasia Esculenta* variety known as edeofe in South East Nigeria, which was purchased from a well-known local market. Similar processing procedures were applied to the sample, including washing, peeling, soaking, rinsing, boiling, and oven drying at 60°C, until a consistent weight was noted.

The dry weight had to be ground into fine flour to create pellets, which had to be dried in an oven at 600C until they reached a constant weight. Then, for eventual use in feeding the rats, these pelleted feed items were stored in a sealed container. A botanist confirmed the origins of the glycine max. (l) Merrill roots, which were then thoroughly cleaned, peeled, and soaked in water for ten minutes. The roots were obtained from a reputable local market. The roots were then cleaned, brought to a boil, and dried at 600 degrees Celsius in an oven until they reached a consistent weight. To ensure a consistent weight, the dry weight was again ground into fine flour, pelletized, and dried in an oven at 60° degrees Celsius. Before feeding the rats, the resultant pelletized feed was kept in a sterile, airtight container.

III. EXPERIMENTAL ANIMALS

A reliable breeder provided sixty-four male albino rats, weighing between 134 and 249 grammes. They were kept in groups of eight per cage and their weights were recorded every week. Using a permanent marker, each rat in a group was assigned a number between 1 and 8 on its tail. After that, for a week leading up to the start of the experiment, they were given commercial rat meal and unrestricted access to water while being kept in a 12-hour light/12-hour dark cycle at a room temperature of 27°C to 30°C. The work complied with the NRC's[26] ethical criteria for using, caring for, and treating laboratory animals.

3.1 Induction of Insulin Resistance using Low Fructose Diet

Male albino rats that had been acclimated were given a diet that included 10% fructose at a low dose to establish insulin resistance. Fructose (30 grams) was dissolved in 300 millilitres of water to generate this diet. After a week-long acclimatization period, the rats were given this fructose solution as their drinking water at a rate of 25 millilitres ad libitum for two weeks. Rat feeds were freely available to all of the rats in an equal amount.

3.2 Induction of Type 2 Diabetes Mellitus using STZ

Male albino rats that had been acclimated were given a diet that included 10% fructose at a low dose to establish insulin resistance. Fructose (30 grams) was dissolved in 300 millilitres of water to generate this diet. After a week-long acclimatization period, the rats were given this fructose solution as their drinking water at a rate of 25 millilitres ad libitum for two weeks. Rat feeds were freely available to all of the rats in an equal amount.

All groups were treated for a total of 28 days as part of the trial. Metformin 200 mg/kg/day orally administered via an oral dispenser and commercial rat meal were administered to the standard and normal control groups, respectively. The remaining groups were given various intervention formulations, as described by Nnadi and colleagues[27], which consisted of 50% intervention feed and 50% commercial rat feed (Table 1). In the experimental protocol, the precise group assignments were specified.

Table 1: Groups and Assigned Intervention Formulations

Groups	Status	Formulations	Formulation Composition
A	Intervention Group	1	16.6%CY: 16.6%SB: 16.6%BGN: 50%RF
B	Standard Control	RF + Metformin	100 Commercial Rat Feed (RF)
C	Normal Control	RF	100 Commercial Rat Feed (RF)
D	Negative Control	RF	100 Commercial Rat Feed (RF)
E	Intervention Group	2	12.5%CY: 12.5%SB: 25%BGN: 50%RF
F	Intervention Group	4	12.5%CY: 25%SB: 12.5%BGN: 50%RF
G	Intervention Group	7	0%CY: 50%SB: 0%BGN: 50%RF
H	Intervention Group	5	0%CY: 0%SB: 50%BGN: 50%RF
I	Intervention Group	6	50%CY: 0%SB: 0%BGN: 50%RF
J	Intervention Group	3	25%CY: 12.5%SB: 12.5%BGN: 50%RF

RF = Commercial Rat Feed
CY = Cocoyam
SB = Soya Bean
BGN = Bambara groundnut

3.3 Estimation of Blood Glucose

At the end of 28 d, the rats were fasted overnight and the following morning, their final body weights measured using a weighing scale, and the blood glucose concentrations were estimated using a glucometer (Acu-check activeR).

3.4 Organ Harvest & Weight Changes Examination

After the rats were fed for 28 days, they were put to sleep using ethyl acetate, which was put inside cotton wool in a beaker with a 1000 mL capacity. After that, the experimental rat was put in the beaker and given a quick moment to become completely unconscious. In addition to the body weight and feed consumption, the pancreas and liver were collected and weighed during this period. An electronic weighing balance (Modelscout Pro Ohaus Corporation, USA) was used to measure the weights. The data were analyzed and compared with the blood glucose levels that were monitored over time.

3.5 Histological Studies of Pancreas and Liver

After the animals were sacrificed, the livers and pancreas of those under diethyl ether anaesthesia were taken. After being dissected, the organs were stored in 10% buffered formalin, dried off using many alcohol treatments, and then embedded in paraffin wax. Hematoxylin and eosin (HE) dye were used to stain thin slices of 4-5 µm that were cut with an American optical microtome, Model 82. The sections were then mounted on glass slides. A microscope was then used to examine the stained samples.

3.6 Statistical Analysis

The results were presented as the standard error of the mean (SEM), which was obtained from measurements taken three times, with eight rats in each group. Version 20.0 of the Statistical Package for the Social Sciences (SPSS Inc., Chicago, IL) was used for the analysis. One-way analysis of variance (ANOVA) was used to compare the mean values, and Tukey's posthoc test was used to identify statistically significant differences between the means at $P<0.05$.

IV. RESULTS

Effect on Blood Glucose

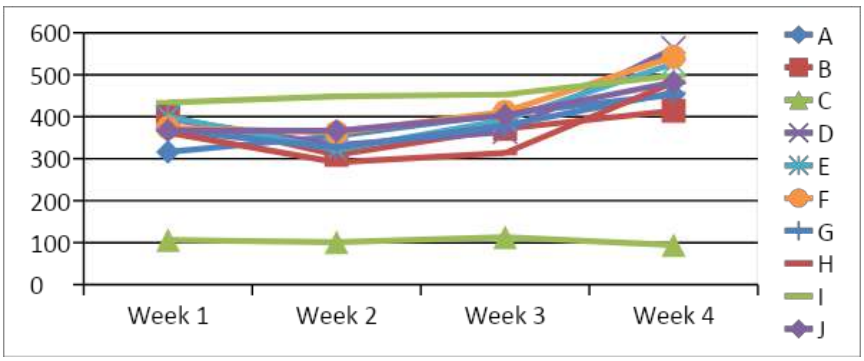

Figure 1: Trend of Mean Random Blood Glucose Concentration for Groups A-J Over Time

The trend line graph in Figure 1 illustrates the average blood glucose levels over time for each Group. Except for a minor drop in week two, the results showed an overall increase in mean glucose levels throughout time. The average glucose levels in Group C were the lowest and stayed comparatively constant throughout time. Comparing each group's mean glucose levels over time to the others, the ANOVA analysis showed that each group's mean levels fluctuate significantly ($F=13.963$, $p<0.001$). Additionally, the data showed a comparable pattern for every Group from week 1 to week 4, indicating that they were substantially parallel ($F=79.106$, $p<0.01$), with a noteworthy upward tendency from week 1 to week 4.

Effect on Rat Body Weight Over Time

Table 2: Showing the Results of the Analysis of Rat Body Weight Values within each group over time

Groups	Week 1 Mean (SEM)	Week 2 Mean (SEM)	Week 3 Mean (SEM)	Week 4 Mean (SEM)	Day of Sacrifice Mean (SEM)
A	225.43(14.91)	222.00(18.36)[a]	226.00(15.73)[a]	232.57(16.46)[a]	204.86 (16.76)[a]
B	238.00(16.69)	217.75(23.12)[a]	244.50(26.07)[a]	253.00 (30.47)[a]	228.00 (28.59)[a]
C	276.88(10.17)	288.00(11.17)[b]	301.75(9.78)[b]	301.38(8.86)[b]	280.75 (9.46)[b]
D	192.50(10.22)	211.50(11.03)[a]	210.00(9.81)[a]	233.00(10.62)[a]	224.00(8.17)[a]
E	222.17(15.96)	218.83(15.43)[a]	214.17(14.64 [a]	234.50(15.47)[a]	207.33(12.72)[a]
F	249.14(14.59)	220.43(10.17)[a]	228.86(10.24)[a]	250.57(12.90)[a]	230.86(13.69)[a]
G	246.00(33.45)	217.86(11.81)[a]	213.71(11.03)[a]	230.14(13.65)[a]	205.29(11.91)[a]
H	237.67(32.57)	207.33(16.07)[a]	213.67(17.91)[a]	245.67(14.23)[a]	220.00(12.53)[a]
I	198.17(18.99)	190.17(21.56)[a]	193.50(26.86)[a]	197.50(29.42)[a]	208.00(32.60)[a]
J	226.00(6.91)	219.40(7.60)[a]	222.60(8.14)[a]	225.60(8.21)[a]	206.00(6.14)[a]
F(p-value)	1.48	4.02	5.22	3.65	3.07
p-value	0.184	0.001	<0.001	0.002	0.006

Repeated Measures Test
Mean values along the column with different alphabetical superscripts indicate significance (p<0.05)

Equal Level (Mean difference among Groups)		Parallelism (Pattern of all groups across time points) i.e. within/between group interactions		Flatness (Trend)	
F-value	p-value	F-value	p-value	F-value	p-value
4.141	0.001	4.060	0.001	5.663	0.004

Table 2 showed changes in rat body weight of the different groups over time. Group C had the best weight gain followed by the standard control group and the rats in Group A.

Comparing Rat Body Weight with Blood Glucose Level of Various Groups over Time

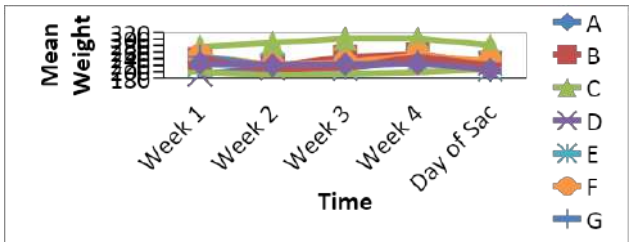

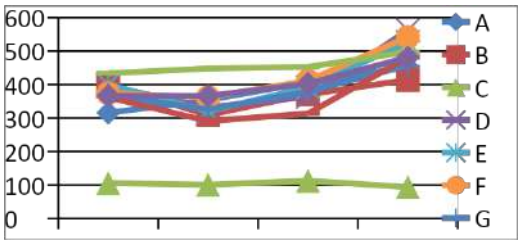

Figures 2(a & b) show comparison graphs of the mean random blood glucose (right) and mean body weight (left) over some time (1-4 weeks) for rats with and without diabetes. The groups with the highest weight and weight gain over time were those with normoglycemia (Group C, Right). Likewise, Group I experienced the least amount of weight gain due to extremely high blood glucose.

Relating Blood Glucose Concentration, relative Weight of liver, pancreas and weight variation

Table 3: Result of the Analysis of Blood Glucose Concentration, relative Weight of liver, pancreas and weight variation

Group	Blood Glucose Concentration Mean (SEM)	Relative Weight of Liver Mean (SEM)	Relative Weight of Pancreas Mean (SEM)	Weight Variation Mean (SEM)
A	293.14(42.38)^{b}	3.74(0.12)^{ab}	0.240(0.08)	-51.29(16.34)^{b}
B	282.25(48.77)^{b}	3.02(0.27)^{ab}	0.165(0.00)	-37.25(15.95)^{ab}
C	76.38(2.81)^{a}	2.69(0.15)^{a}	0.170(0.01)	6.25(3.49)^{a}
D	338.67(6.86)^{b}	4.42(0.41)^{b}	0.185(0.03)	-34.25(17.32)^{ab}
E	302.00(30.98)^{b}	3.40(0.14)^{ab}	0.150(0.01)	-50.67(19.12)^{b}
F	361.14(19.38)^{b}	3.81(0.16)^{ab}	0.223(0.02)	-59.43(7.92)^{b}
G	318.00(43.35)^{b}	3.77(0.25)^{ab}	0.247(0.03)	-48.43(14.09)^{b}
H	327.50(45.15)^{b}	3.78(0.23)^{ab}	0.237(0.03)	-57.67(8.37)^{b}
I	285.25(74.12)^{b}	3.64(0.40)^{ab}	0.183 (0.02)	-50.83(30.84)^{b}
J	241.00(35.47)^{b}	3.61(0.14)^{ab}	0.207 (0.02)	-68.00(6.4)^{b}
F (p-value)	4.664	3.333	1.262	1.884
p-value	<0.001	0.003	0.296	0.076

Mean values along the column with different alphabetical superscripts indicate significance ($p<0.05$)

Table 3 presents the findings of the mean analysis for the mean glucose concentration, the relative weights of the pancreas, liver, and rats' weight fluctuations. The glucose concentration in Group C was found to be considerably ($p<0.01$) lower, according to the results. There was no discernible variation in the glucose concentration across the other groups. The relative weight of the liver followed the same trend in terms of glucose concentration, with group C having the lowest mean weight and group D having the highest mean weight. There was no discernible variation in the pancreatic relative weight. Except for the control groups, there was no discernible difference ($p>0.05$) in the mean weight variation between the groups.

Liver Histology

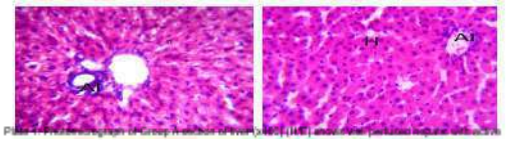

hepatocyte (H) and mild portal aggregate of inflammation (PAI)

Plate 1: Group A

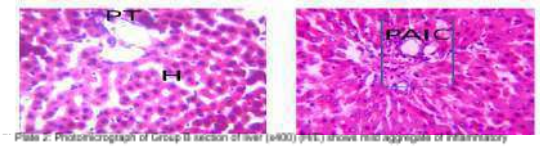

cell (PAIC) otherwise normal with active hepatocyte (H)

Plate 2: Group B

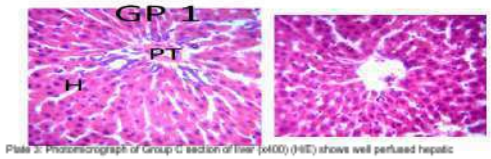

tissue with portal triad (PT) and active hepatocyte (H) and central vein (CV)

Plate 3: Group C

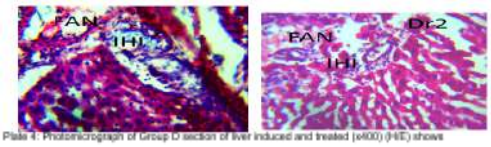

severe degeneration with focal area necrosis (N) and severe intra hepatic inflammation (IHI)

Plate 4: Group D

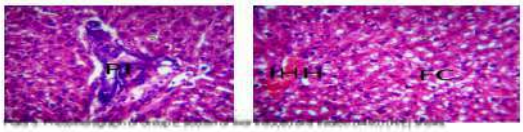

Plate 5: Group E

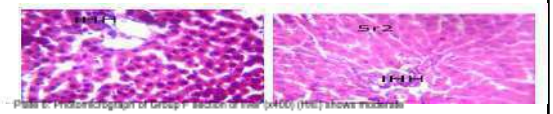

regeneration with mild intra hepatic inflammation

Plate 6: Group F

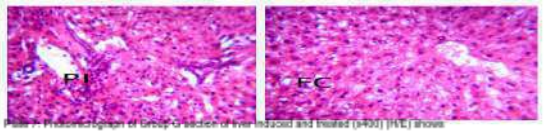

moderate regeneration with mild portal inflammation (PI) and mild fatty changes (FC).

Plate 7: Group G

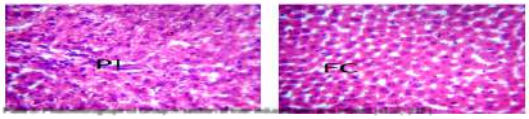

Plate 8: Group H

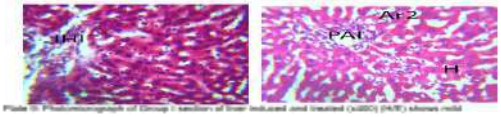

Plate 9: Group I

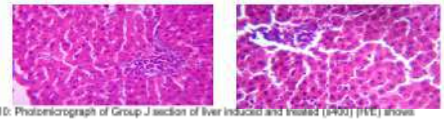

moderate regeneration with mild intra hepatic inflammation (IHI)

Plate 10: Group J

Pancreas Histology

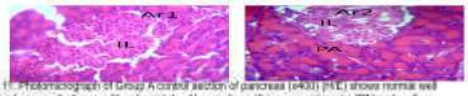

Plate 11: Group A:

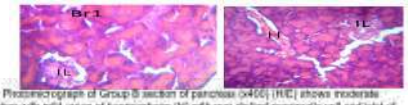

Plate 12: Group B

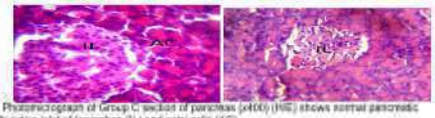

Plate 13: Group C

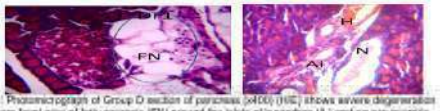

Plate 14: Group D

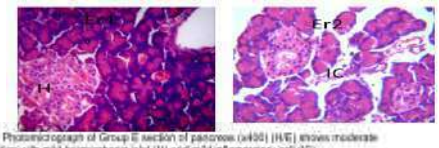

Plate 15: Group E

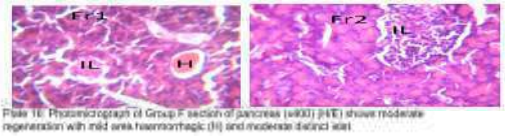

Plate 16: Group F

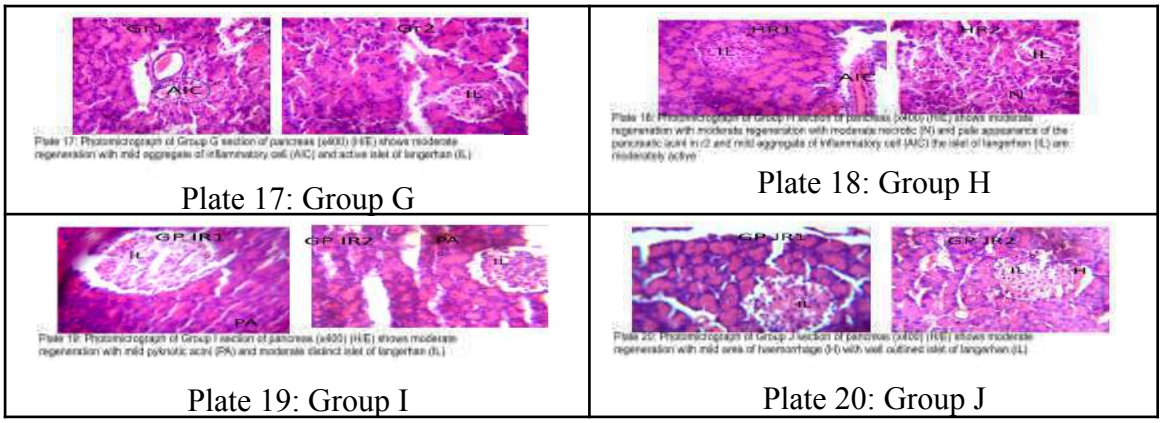

Plate 17: Group G

Plate 18: Group H

Plate 19: Group I

Plate 20: Group J

Plates 1–20: The liver and pancreas histological characteristics for the different control and intervention groups. The different treatment groups were compared using the histological characteristics of the normal control. In both organs, Group A on Formulation 1 showed stronger amelioration and regeneration than the standard controls, with identical histological characteristics to the normal control.

V. DISCUSSION

5.1 Effect on Blood Glucose Level

The results of this study indicated that each group's mean random blood glucose (RBG) over time differed significantly ($F= 13.963$, $p<0.001$) from the other and that the group as a whole changed in a roughly similar way from week 1 to week 4. As a result, the group was deemed to be significantly parallel ($F=79.106$, $p<0.01$), significant ($F=76.755$, $p<0.001$), and showing a positive trend. In this study, there were essentially two comparison groups: the intervention groups and the control groups.

Group C had the lowest mean concentration of RBG, which was explained by the group's lack of diabetes. Over the weeks, the diabetic control's RBG value was higher than that of the other controls, the standard control, B. Groups E, F, G, and H among the intervention groups showed reduced RBG values with a consistent trend over time (Figure 1). When the RBG values of the diabetic rats in the intervention and control groups were compared, the former showed lower values than the standard and diabetic controls, indicating that the RBG control was better with the intervention flour formulations than when the diabetic rats were fed commercial rat feeds either on their own or in addition to metformin, an anti-diabetic medication.

The trend over time indicated that Group C had better RBG control than Group H, which was better than Groups B, G, E, A, J, and finally F, D, and I. This suggests that the use of formulation 5 for the intervention had better RBG control than the standard anti-diabetic drug metformin and that all intervention formulations—except for formulation 6 (Group I)—were better at controlling RBG than the use of commercial rat feeds alone for STZ-induced diabetic rats (Figure 1).

The findings suggested that, although the reduction in hyperglycemia was not linear over time and showed levels of fluctuations as occur even in human subjects on anti-diabetic medications, the intervention formulations, like the standard anti-diabetic drugs, might have been responsible for it in the STZ-induced diabetic rats. This situation has made the use of anti-diabetic drug combinations for glycemic control necessary[28]. The inclusion of phenolic compounds and other bioactive components in the formulations may likely account for the hypoglycemic effects of the products.

Plants generate phenolic compounds as secondary metabolites, and these compounds have anti-diabetic properties. This is because they activate the 5' adenosine monophosphate-activated protein kinase (AMPK) pathway, which stimulates

skeletal muscle cells to take up glucose. They improve glucose metabolism in tumour necrosis factor-α (TNFα)-treated insulin-resistant mice hepatocytes by blocking gluconeogenesis and promoting glycogenesis[29]. Oboh and colleagues have reported that it also increases the inhibitory activity of α-amylase and α-glucosidase in rats with streptozotocin-induced diabetes when given anti-diabetic medications[30].

The presence of phenolics has been linked in many different studies to a decrease in blood glucose levels while fasting[31]. Among other bioactive components, a gas chromatographic study of cocoyam, soybean, and Bambara groundnut, and their blends showed the presence of phenolic compounds[32]. Additional BACs included in the formulations probably played a role in the hypoglycemic outcomes seen in this investigation. Monoterpenoid derivatives that inhibit α-amylase and α-glucosidase activity have been shown to have antidiabetic benefits[33].

Similarly, compounds containing artemisinin and its derivatives can reduce the symptoms of type 2 diabetes by reversing the imbalance in the ratio of insulin, glucagon, and somatostatin content in islets[34], increasing insulin secretion[35], and inhibiting α-glucosidase activity[36]. Haemoglobin A1c (HbA1c) levels are elevated after long-term artemisinin consumption[37]. Additionally, artemisinin deacetylated lysine residues on several transcription factors, increasing insulin secretion, and upregulated the expression of SIRT1 in islet ß-cells, which affected glucose/lipid metabolism[37]. As reported by Kitada and Koya[38], pancreatic ß-cells are similarly protected by the stimulation of silent information regulator-1 (SIRT1) expression. By indirectly stimulating the γ-Aminobutyric acid (GABA) signaling pathway in mice models, artemisinins can cause neogenesis in ß-cell-like STZ-induced ß-cell death[39]. According to studies, artemisinins can change α cells that produce glucagon into ß cells that produce insulin[40]. Thiadiazole, a heterocycle containing nitrogen and sulphur, has isomers and derivatives with biological activities associated with the =N–C–S–moiety or strong aromaticity of the ring, and it also acts as a carbonic anhydrase inhibitor, which reduces the production of glucose in the liver in patients with type 2 diabetes[41].

Some substances, such as thiourea and naphthalene, have positive pharmacological and therapeutic effects that help treat type 2 diabetes (T2DM); in particular, sulfonylureas stimulate insulin secretion from pancreatic β-cells, and thiourea derivatives inhibit the formation of advanced glycation end products, α-glucosidase, and protein tyrosine phosphatase 1B (PTP1B)[42]. By lowering fasting blood glucose and serum lipid levels, increasing insulin sensitivity, and reducing hepatic steatosis in obese diabetic (db/db) mice, naphthalene's inhibitory effect on FABP4 significantly improves glucose and lipid metabolism and it has equally demonstrated strong PPARγ agonistic activity, which decreased blood glucose levels[43]. These bioactive substances may be responsible for the hypoglycemic effects of the combination of Bambara groundnut, cocoyam, and/or soybeans[36, 44, 45].

5.2 Effects of the Mean Blood Glucose Level on the Rat Body Weights

A comparative analysis of Figures 2a and 2b showed that weight growth was greater in the groups with normal or regulated blood glucose concentrations than in the hyperglycemic state. The normal control group experienced a weight gain of 24.50 g at week 4, which corresponded to a mean Random Blood Glucose level of 106.25 mg/dl and represented 8.85%. With RBG concentrations ranging from 315.83 mg/dl in week 1 to over 563 mg/dl in week 4, all STZ-induced diabetic groups experienced hyperglycemia, which was associated with reduced weight growth.

Group I experienced the least amount of weight gain and, ironically, the highest RBG during weeks 1-3 (Figure 2). Prior studies comparing control and diabetic rats showed that the diabetic group had weight loss and high blood glucose, while the active, healthy controls had weight increases[46]. According to this study, diabetics with uncontrolled blood glucose experienced a more noticeable weight loss in week 4 compared to week 1 (Table 2; Figure 2).

The administration of STZ, the hyperglycemic state, and the use of the anti-diabetic medication metformin can all contribute to weight loss in diabetic rats. Because STZ alkylates DNA in rats, causing hyperglycemia and necrotic lesions, animals given the drug experience lower body weight[46]. There is a connection between diabetic animals' lower body weight and hyperglycemia.

The type and frequency of the diet, the sex of the diabetic rats, the dosage of the STZ used to induce T2DM, the length of the intervention trial, and the genetic composition are some of the variables taken into account when calculating changes in body weight in diabetic rats. Researchers have experimented with different doses of STZ to cause hyperglycemia in rats of various strains. 45 mg/kg[46]; 50 mg/kg[47]; 70 mg/kg[48]; and 90 mg/kg[49] were some of the levels that were employed.

An intra-peritoneal dose of 45 mg/kg of STZ was used in this trial. This amount was thought to be safe for the strain because only 13% of deaths were reported, which might have been caused by metformin toxicity, STZ toxicity, diabetes complications, or a combination of these. The standard control in this trial exhibited better weight growth because they were able to control their blood sugar better than other diabetic groups. The blood glucose control in Group B may have been attributed to the anti-diabetic medication metformin. According to Kotb and colleagues[50], there is limited research that associates the metformin medication with weight loss despite blood glucose regulation.

This has been attributed to several factors, including decreased appetite[51], attenuation of neuropeptide-Y (NPY)[52], stimulation of glucagon-like peptide-1 (GLP-1), which inhibits food intake[53], and activation of lipolysis through the inhibition of adipogenesis, carbohydrate absorption, and bile salt uptake[53], all of which inhibit energy production. However, our findings in this work suggest that metformin had a positive effect on weight gain.

The various outcomes from the several diabetic rat groups can be explained by the fact that different formulations included various bioactive substances in different quantities. On intervention formulations, groups F and H had comparatively better blood glucose levels and better weight gain than other groups. Formulations 5 and 4, respectively, were assigned to groups H and F. Based on the available research, the bioactive components included in both formulations were stilbene and phenolics[36,44,45.] Furthermore to the previously mentioned anti-diabetic effects of phenols, stilbene, which is found in cocoyam and soybean flour, also reduces the expression of peroxisome proliferator-activated receptor gamma (PPARγ), lessens IR, and upregulates GLUT4, enhances glucose and fatty acid catabolism [54], lowers serum cholesterol and the LDL/HDL ratio, attenuates obesity-induced inflammation in adipocytes[55], as demonstrated by a decrease in inflammatory cytokines TNF-α, IL-6, and monocyte chemo-attractant protein-1 (MCP-1)[56]. Rats with managed diabetes mellitus may gain weight due to these actions, which also cause hypoglycemia consequences.

5.3 Effects of the Mean Blood Glucose Level on the Relative Organ Weights

Investigation indicates that in the absence of a successful intervention, the frequency and intensity of STZ-induced lesions in the pancreas, liver, kidney, and gastrointestinal tract steadily rise over time[57]. The weight of the pancreas did not significantly differ between the groups in this study, suggesting that the weight of the pancreas remained relatively unchanged, but the weight of the liver increased significantly between the diabetic control, which had the highest value, and the normal control, which recorded the lowest value (Table 3).

There was no statistically significant difference in the relative weight of the liver between the diabetic groups in the standard control group and the intervention formulation groups. This suggests that the anti-diabetic medication's mitigating effects and the food extract formulations' effects may have prevented the progression of the organ damage caused by STZ. It was noteworthy to note that the variation in the blood glucose concentration and the mean relative weight of the liver followed a similar pattern, with

the negative control exhibiting the highest values for both blood glucose and relative weight of the liver, and the normal control displaying the lowest values for both.

Diabetes Mellitus has been linked to weight changes in several organs, including the pancreas, liver, and kidney. Some studies have observed an increase in liver weight, while others have shown a decrease in liver weight. The greater rate of catabolism was linked to reports of weight decrease in the liver[58]. In other investigations, it was noted that the liver weight of the diabetic control rats rose proportionately to their body weights when compared to the non-diabetic rats, particularly when the former was on plant extract. This increase was explained by an increased build-up of triglycerides in the liver[19].

An increase in liver weight was also noted by other studies[59]. Other similar studies carried out in experimental settings showed increases in the body weight and liver ratio of diabetic rats in comparison to controls[60]. The study revealed that the pancreas had not undergone significant alteration. Campbell-Thompson and colleagues found that the diabetic group had a larger mean liver weight than the non-diabetic group during autopsies, although the diabetic group had a lower pancreas weight[61].

As compared to non-diabetic rats, Zafar and colleagues found that the mean values of the pancreas weight in some of the diabetic rats were unchanged[46]. Certain studies have connected the disruption and eventual removal of the pancreatic islets and the selective destruction of cells that produce insulin to the decrease in pancreatic weight[36]. In addition to the effects of STZ-induced hyperglycemia and hypo-insulinemia, other plausible explanations include the possibility that the direct alkylating activity of STZ can cause cellular necrosis and the selective elimination of beta cells[46]. As a result, according to a number of investigations, the weight of the pancreas decreased or remained unchanged in diabetic groups, although the weight of the liver and kidney increased.

5.4 Effects on Organ Histology

The findings of the study, the rats in the negative control group's liver specimens had significant intrahepatic inflammation, a localized area of necrosis, and severe degeneration—all indications of the damaging effects of STZ and hyperglycemia on the liver. The results aligned with earlier research that documented hepatocyte fatty deposits, deformed sinusoids, inflammatory alterations, and necrosis characteristics surrounding the triad on the tenth day in STZ-induced diabetic rats[62].

The diabetic rats in the intervention groups showed varied degrees of regeneration and mild intra-hepatic inflammation in response to formulations 1–7, suggesting that the formulation effectively stopped the STZ-induced organ damage and sparked effective regeneration of the destroyed liver cells (Plates 1 -10). This investigation also revealed that the pancreas of the diabetic control exhibited significant intrahepatic inflammation, focal area of necrosis, and severe degradation of pancreatic cells, indicating unchecked damage by the STZ and hyperglycemia (Plate 14).

The histological appearance of the conventional anti-diabetic medication used in the standard control was comparable to that of the patients in group A on formulation 1. Variable degrees of regeneration and minor inflammatory cell aggregation were observed in all other groups on intervention formulations (Plates 11–20).

Limitations (if applicable)

Nil

VI. CONCLUSION

On STZ-induced diabetic rats, a blend of cocoyam, soybean, and Bambara groundnut flour produced hypoglycemic effects; however, the extent of blood sugar reduction differed depending on the blend formulation. In addition to exerting superior glycemic control over the anti-diabetic medication metformin, Group A, which received formulation 1, also improved liver and pancreatic tissue regeneration. The results also showed that the rat and liver weights increased as a result of these

formulations in the groups with improved RBG control, while the pancreatic weight remained constant.

Therefore, it could be suggested that in addition to lowering blood glucose, consuming a combination of these plant-based foods could help prevent organ damage, repair damaged organs, and prevent overall weight gain in people with diabetes mellitus. As such, it should be considered a useful addition to the nutritional management of diabetes.

ACKNOWLEDGEMENTS

The authors wish to sincerely appreciate and acknowledge the technical support from Dr Eleazu Chinedu and Dr Uchechukwu Okorie of the Department of Biochemistry, Alex Ekwueme Federal University, Ndufu Ikwo, Ebonyi State Nigeria.

REFERENCES

1. Sun, H., Saeedi, P., Karuranga, S., Pinkepank, M., Ogurtsova, K., Duncan, B.B., Stein, C., Basit, A., Chan, J.C.N., Mbanya, J.C., Pavkov, M.E., Ramachandaran, A., Wild, S.H., James, S., Herman, W.H., Zhang, P., Bommer, C., Kuo, S., Boyko, E.J., Maqliano, D. J., (2022). IDF Diabetes Atlas: Global, Regional and Country-level diabetes prevalence estimates for 2021 and projections for 2045. *Diabetes Research and Clinical Practice*, 183, 109119. https://doi.org/10.1016/j.diabres.2021.109119
2. Van Belle, T.L., Coppieters, K.T. and Von Herrath, M.G. (2011).Type 1 diabetes: etiology, immunologyand therapeutic strategies. *Physiological Reviews*, 91:1.
3. Lin, X,. Xu, Y., Pan, X., *et al.,* (2020) Global, regional, and national burden and trend of diabetes in 195 countries and territories: an analysis from 1990 to 2025. Sci Rep, 10, 14790
4. Kirigia JM, Sambo HB, Sambo LG and Barry SP. (2009).Economic burden of diabetes mellitus in the WHO African region. BMC International Health and Human Rights, 9:6.
5. Sobngwi E, Mauvais-Jarvis F, Vexiau P, Mbanya JC and Gautier JF. (2001).Diabetes in Africans. Epidemiology and clinical specificities. Diabetes Metab., 27(6):628-634.
6. Piero MN. (2006) Hypoglycemic effects of some Kenyan plants traditionally used in management of diabetes mellitus in eastern province, Msc thesis, Kenyatta University.
7. Wylie-Rosett, J and Delahanty, L.M (2017) Nutrition in the Prevention and Treatment of Disease (Fourth Edition) Pp 691-707. https://doi.org/10.1016/B978-0-12-802928-2.00031-X
8. Forouhi, G.N., Misra, A., Mohan, V., Taylor, R., Yancy, W (2018) Dietary and nutritional approaches for prevention and management of type 2 Diabetes, Science and Politics of Nutrition, BMJ 361 Doi:https://doi.org/10.1136/bmj.k2234
9. Piero MN, Njagi JM, Kibiti CM, Ngeranwa JJN, Njagi ENM and Miriti PM. (2012).The Role of Vitamins and Mineral Elements in Management of Type 2 Diabetes Mellitus: A Review South As. J. Biol.Sci., 2(Supp.1):107–115.
10. Arise, A. K., Amonsou, E. O. & Ijabadeniyi, O. A. (2015) Influence of extraction methods on functional properties of protein concentrates prepared from South African Bambara groundnut landraces. *International. Journal of Food Science and. Technology*. 50, 1095–1101. https,//doi.org/10.1111/ijfs.12746.
11. Oyeyinka AT, Pillay K, Siwela M.(2019), Full title- in vitro digestibility, amino acid profile and antioxidant activity of cooked Bambara groundnut grain. Food Biosci.31:100428. doi: 10.1016/j.fbio.2019.100428.
12. Salawu, (2016). Comparative study of the antioxidant activities of methanolic extract and simulated gastrointestinal enzyme digest of Bambara nut (Vigna subterranean) FUTA J. Res. Sci., 1: 107-120.
13. Yao, D.N., Kouassi, K.N., Erba, D., Scazzina, F., Pellegrini, N., Casiraghi, M.C. (2015) Nutritive Evaluation of the Bambara Groundnut Ci12 Landrace [*Vigna subterranea* (L.) Verdc. (*Fabaceae*)] Produced in Côte d'Ivoire. *International Journal of Molecular Sciences*. 16(9): 21428-21441.doi. org/10.3390/ijms160921428.

14. Baptista, A., Pinho, O., Pinto, E., Casal, S., Mota, C., & Ferreira, I.M.P.I.V.O (2016) Characterization of protein and fat composition of seeds from common beans (phaseolus vulgaris L.), cowpea (Vigna unguiculata L.Walp) and Bambara groundnuts (Vigna subterranean L. Verde) from Mozambique. *Journal of Food Measument and Characterization,* 1-9.
15. Barbieri, R., Coppo, E., Marchese, A., Daglia, M., Sobarz-Sánchez, E., Nabavi, S. F, & Nabavi, S. M. (2017) Phytochemicals for human disease: An update on plant-derived compounds antibacterial activity. *Microbiology Research*. 196, 44-68. doi: 10.1016/j.micres.2016.12.003. Epub 2016 Dec 19. PMID: 28164790.
16. Iwai, K., Kim, M., Onodera, A & Matsue, H. (2006). α-Glucosidase Inhibitory and Antihyperglycemic Effects of Polyphenols in the Fruit of *Viburnum dilatatum* Thunb. *Journal of Agricultural and Food Chemistry, 54* (13), 4588-4592 DOI: 10.1021/jf0606353.
17. Ruzaidi, A., Abbe, M., Amin, L., Nawalyah, A.G., Muhajir, H., Pauliena, M.B.S.M.J., Muskinah, M.S (2008) Hypoglycemic properties of Malaysia cocoa (Theobromacacao) polyphenols-rich extract. Int Food Res. J., 15:305-312.
18. Prabhakar, P.K., and Doble, M (2008) A Target Based Therapeutic Approach Towards Diabetes Mellitus Using Medicinal Plants. Current Diabetes Reviews,4(4); 291-308. Bentham Science Publishers Ltd.S
19. Eleazu CO, Iroaganachi M & Eleazu KC (2013) Ameliorative potentials of cocoyam (*Colocasia esculenta* L.) and unripe plantain (*Musa paradisiaca* L.) on the relative tissue weights of streptozotocin-induced diabetic rats. *J Diabetes Res*.1–8 https://doi.org/10.1155/2013/160964.
20. Eleazu CO, Okafor PN & Ijeh II (2014). Biochemical basis of the use of cocoyam (Colocassia esculenta L.) in the dietary management of diabetes and its complications in streptozocin-induced diabetes in rats. *Asia Pac J Trop Dis*., 4, S705-S711.
21. Sharma V., Ramawat K.G,, Mérillon J.M (2013), Isoflavonoids. *Natural Products*. Springer; Berlin/Heidelberg, Germany: 1849-1863.
22. Gupta R & Gupta RS (2011). Antidiabetic efficacy of Mangifera indica seed kernels in rats: a comparative study with glibenclamide. *Diabetologia Croatica*, 40(4), 107-116. https://link.gale.com/apps/doc/A278950690/AONE?u=anon~331d941d&sid=googleScholar&xid=08ea4a9b.
23. Shakya, V., Saxena R and Shakya A (2010) Effect of ethanolic extract of Allium sativum bulbs on Streptozotocin induced diabetic rats, Journal of Chemical and Pharmaceutical Research 2(6): 171-175.
24. Esteves, E. A., Bressan, J., Costa, N. M. B., Martino, H. S. D., Donkin, S. S., & Story, J. A. (2011). Modified soybean affects cholesterol metabolism in rats similarly to a commercial cultivar. Journal of Medicinal Food, Vol.
25. Dewell, A., Hollenbeck, C. B., and Bruce, B. (2002). The Effects of Soy-Derived Phytoestrogens on Serum Lipids and Lipoproteins in Moderately Hypercholesterolemic Postmenopausal Women. J Clin Endocrinol Metab., 87(1):118-121
26. NRC (National Research Council) (1985) Guide for the care and use of laboratory Animals. Bethesda (MD): *National Institute of Health*, 8523.
27. Nnadi, N.N., Ezekwesili, C.N., Ezeigwe, O.C (2022) Effects of Formulated Unripe Plantain and Millet Dietary Feeds in Alloxan-Induced Diabetic Albino Rats. International Journal of Innovative Research and Advanced Studies (IJIRAS), 9 (6).
28. Azeez, T.A (2023) The pattern of antidiabetic drugs and glycemic control among type 2 diabetes patients in an endocrinology clinic in Lagos, Nigeria. https,//doi.org/10.110//2023.06.25.23291774.
29. Huang, D.W., & Shen, S.C. (2012). Caffeic acid and cinnamic acid ameliorate glucose metabolism via modulating glycogenesis and gluconeogenesis in insulin-resistant mouse hepatocytes. *Journal of Functional Foods,* 4(1),358–66. doi: 10.1016/j.jff.2012.01.005.
30. Oboh, G., Ogunbadejo, M.D., Ogunsuyi, O.B., Oyeleye, S.I (2020) Can gallic acid potentiate the antihyperglycemic effect of acarbose and

metformin? Evidence from streptoztocin-induced diabetic rat model. Archives of Physiology and Biochemistry. https://doi.org/10.108/13813455.2020.1716014.
31. Oršolić N, Sirovina D, Odeh D, Gajski G, Balta V, Šver L, et al.(2021), Efficacy of caffeic acid on diabetes and its complications in the mouse.; 26(11):3262. doi: 10.3390/molecules 26113262.
32. Eleazu CO, Eleazu KC & Iroaganachi MA (2016a). Effect of cocoyam (*Colocasia esculenta*), unripe plantain (*Musa paradisiaca*) or their combination on glycated hemoglobin, lipogenic enzymes, and lipid metabolism of streptozotocin-induced diabetic rats, Pharmaceutical Biology, 54(1), 91-97, DOI: 10.3109/13880209.2015.1016181.
33. Garba HA, Mohammed A, Ibrahim MA & Shuaibu MN (2020). Effect of lemongrass (*Cymbopogon citratus* Stapf) tea in a type 2 diabetes rat model. *Clin. Phytosci.* 6, 19. doi: 10.1186/s40816-020-00167-y.
34. Guo X-x, Wang Y, Wang K, Ji B-p and Zhou F (2018). Stability of a type 2 diabetes rat model induced by high-fat diet feeding with low-dose streptozotocin injection. *Journal of Zhejiang University-Science* B 19, 559-569
35. Xiang, M., Chen, Z., He, L., Xiong, G., and Lu, J. (2019). Transcription profiling of artemisinin-treated diabetic nephropathy rats using high-throughput sequencing. *Life Science*. 219, 353–363. doi:10.1016/j.lfs. 2019.01.032.
36. Kim J.A, Jung W.S., Chun, S.C., Yu, C.Y., Ma, K.H., Gwag, J.G., Chung, I.M (2006) A correlation between the level of phenolic compound and antioxidant capacity in cooked-with-rice and vegetable soya bean (Glycine max L) varieties. European Food Research & Technology, 224: 259-270.
37. Han, P., Wang, Y., Zhan, H., Weng, W., Yu, X., & Ge, N. (2019). Artemether ameliorates type 2 diabetic kidney disease by increasing mitochondrial pyruvate carrier content in db/db mice. *American Journal of Translational Research,*11(3),1389-1402.
38. Kitada, M., & Koya, D. (2013). SIRT1 in type 2 diabetes: mechanisms and therapeutic potential. *Diabetes Metabolism Journal*, 37 (5), 315–325.
39. Ben-Othman, N., Vieira, A., Courtney, M., Record, F., Gjernes, E., Avolio, F., Hadzic B, Druelle, N,, Napolitano, T., Navarro-Sanz, S., Silvano, S., Al-Hasani, K., Pfeifer, A., Lacas-Gervais, S., Leuckx, G., Marroquí, L., Thévenet, J,, Madsen, O. D., Eizirik, D. L., Heimberg, H., Kerr-Conte, J., Pattou, F., Mansouri, A., & Collombat, P., (2017). Long-term GABA administration induces alpha cell-mediated beta-like cell neogenesis. *Cell* 168 (1-2), 73–85.e11. doi,10.1016/j.cell.2016.11.002
40. Li X., Watanabe K., Kimura I. (2017) Gut Microbiota Dysbiosis Drives and Implies Novel Therapeutic Strategies for Diabetes Mellitus and Related Metabolic Diseases. *Frontiers in Immunology,* 8:1882. doi: 10.3389/fimmu.2017.01882.
41. Ibrahim, S.I., Ameh, D.A., Atawodi, S.E., & Umar, I.A. (2016). Carbonic Anhydrase: A New Therapeutic Target for Managing Diabetes. *Journal of Metabolic Syndrome*, 5, 196. doi:10.4172/2167-0943.
42. Ullah, I., Hassan, M., Khan, K.M., Sajid, M., Umar, M., Hassan, S., Ullah, A., El-Serehy, H.A., Charifi, W., Yasmin, H.(2022). Thiourea derivatives inhibit key diabetes-associated enzymes and advanced glycation end-product formation as a treatment for diabetes mellitus. *International Union of Biochemistry and Molecular Biology Life*,75(2):161-180. doi: 10.1002/iub.2699.
43. Furukawa A, Arita T, Fukuzaki T, Mori M, Honda T, Satoh S, Matsui Y, Wakabayashi K, Hayashi S &. Nakamura KJ (2012). "Synthesis and biological evaluation of novel (–) cercosporamide derivatives as potent selective PPARγ modulators." Bioorg Med Chem Lett. 54, 522-533.
44. Adedayo, B.C., Anyasi, T.A., Taylor, M.J.C, Rautenbauch, F., Rose-Hill, M and Jideani, V.A (2021) Phytochemical composition and antioxidant properties of methanolic extracts of whole and dehulled Bambara groundnut (Vigna subterranean) seeds. Scientific Reports 11. Article 14116. https://doi.org/10.1038/s41598-021-93525-10.

45. Eleazu CO (2016b). Characterization of the natural products in cocoyam (*Colocasia esculenta*) using GC–MS, Pharmaceutical *Biology* 5412, 2880-2885, DOI: 10.1080/13880209.2016.1190383.
46. Zafar, M., and Naqvi, S.M.H (2010) Effects of STZ-induced Diabetes on the relative weights of kidney, liver and pancreas in Albino Rats: A Comparative Study. International Journal of Morphology 28(1):135-142.
47. Oscika, T. M.; Yu, Y.; Panagiotopoulos, S.; Clavant, S. P.; Kirizis, Z.; Pike, R. N.; Pratt, L. M.; Russo, L. M.; Kemp, B. E.; Camper, W. D. & Jerums, G.(2000), Prevention of albuminuria by aminoguanidine or ramipril in streptozotocin-induced diabetic rats is associated with the normalization of glomerular protein kinase C. Diabetes, 49(1):87-93.
48. [48] Kang, N., Alexander, G., Park, J. K., Maasch, C., Buchwalow, I., Luft, L. C., & Haller, H. (1999). Differential expression of protein kinase C isoforms in streptozotocin-induced diabetic rats. *Kidney International*, 56(5),1737-50.
49. Mozaffari, M.S; Warren, B.K., Russel, C.M., and Schaffer, S.W (1997) Renal function in the noninsulin-dependent diabetic rat: Effects of unilateral nephrectomy. Journal of Pharmacological and Toxicological Methods, 37 (4): 197-203.
50. Kotb, A. S., Abdel-Hakim, S., Ragy, M., Elbassuoni, E., & Abdel-Hakeem, E. (2022). Metformin ameliorates diabetic cardiomyopathy in adult male albino rats in type 2 diabetes. *Minia Journal of Medical Research*, 33(4), 128-138.
51. Petersen MC, Samuel VT, Petersen KF and Shulman GI.(2020) Non-alcoholic fatty liver disease and insulin resistance. The Liver: Biology and Pathobiology 6th ed chap 37;455-471.
52. Kalsbeek, M.J., Wolff, S.E., Korpel, N.L., Fleur, S.E., Romijn, J.A., Fliers, E., Kalsbeek, A., Swaab, D.F., Huitinga, I., & Hol, E.M. (2020). The impact of antidiabetic treatment on human hypothalamic infundibular neurons and microglia. JCI insight,5.
53. Mobasher, M.A (2021) Metformin: An AMPK-dependent antidiabetic drug with novel medical applications. International Journal of Cancer and Biomedical Research, 5(2): 1-12.
54. Tan, Y. and Chang, S.K.C. (2017). Digestive enzyme inhibition activity of the phenolic substances in selected fruits, vegetables and tea as compared to black legumes. *Journal of Functional Foods* 38: 644–655. doi.org/10.1016/j.jff.2017.04.005.
55. Yang, Z., Wang, M., Zhang, Y., Cai, F., Jiang, B., Zha, W., Yu, W. (2020). Metformin ameliorates diabetic cardiomyopathy by activating the PK2/PKR pathway. *Frontiers in Physiology*, 11:425.
56. Yan, F., Xiaohong, T., Shuling, B., Jun, F., Weijan, H., Hao, T., Dehua, L (2012) Autologous transplantation of adipose-derived mesenchymal stem cells ameliorates streptozotocin-induced diabetic nephropathy in rats by inhibiting oxidative stress, pro-inflammatory cytokines and the p38 MAPK signalling pathway. International Journal of Molecular Medicine, 30 (1): 85-92
57. Piyachaturawat, P.; Poprasit, J.; Glinsukon, T. & Warichanon, C.(1988), Gastric mucosal lesions in Streptozotocin-diabetic rats. Cell. Biol. Intern. Rep., 12(1):53-63.
58. Meyer, C., Stumvoill, M., Nadkarni, V., Dostou, J., Mitrakou, A., Gerich, J (1998) Abnormal Renal and Hepatic Glucose Metabolism in Type 2 Diabetes Mellitus, J. Clin. Invest., 102 (3): 619-624.
59. Lee, S. I., Kim, J. S., Oh, S. H., & Park, K. Y. (2008). Anti-hyperglycemic effect of Fomitopsis pinicola extracts in streptozotocin-induced diabetic rats. *Journal of Medicinal Food*, 11(3), 518–524.
60. Zhuo, J., Zeng, Q., Cai, D., Zeng, X., Chen, Y., Gan, H., Huang, X., Yao, N., Huang, D., Zhang, C (2018) Evaluation of type 2 diabetic mellitus animal models via, interactions between insulin and mitogen-activated protein kinase signalling pathways induced by a high fat and sugar diet and streptozotocin. Molecular Medicine Reports, 17(4): 5132-5142
61. Campbell-Thompson, M., Wasserfal,l C., Montgomer,y E. L., Atkinson, M. A., Kaddis, J. S. Pancreas Organ Weight in Individuals With

Disease-Associated Autoantibodies at Risk for Type 1 Diabetes. *Journal of the American Medical Association,* 2012; 308(22), 2337–2339. doi,10.1001/jama.2012.15008.

62. Teoh SL, Latiff AA, Das S. (2009) A histological study of the structural changes in the liver of streptozotocin-induced diabetic rats treated with or without Momordica charantia (bitter gourd). Clin Ter.,160 (4):283-286.

This page is intentionally left blank

Needle Sofinnovation: Over Coming Unprecedented Challenges Intransdermal Drug Delivery with Micro Needles

Sumit Kumar Gupta, Simran Sah Kalwar, Aakrshan Kumar, Aditi Bhardwaj, Shivani Sharma, Sushil Kumar Mali & Ram Prakash Yadav

RIMT University

ABSTRACT

Drug delivery through the skin offers distinct advantages, including bypassing the liver's initial metabolism, maintaining consistent drug levels in the blood, and ensuring safety and adherence to treatment, which surpasses traditional oral or injectable methods. Microneedle technology has emerged as a revolutionary approach in this regard, offering enhanced delivery efficiency and patient acceptance. The main obstacle to transdermal administration, however, is the fact that only a small number of strong medications with optimal physicochemical characteristics can intercellularly and passively diffuse across skin barriers to reach therapeutic concentration using this method. Innovative strategies have been pursued to improve the drug's skin penetration.

Keywords: skin, TDDS; microneedle; microscale fabrication techniques; coating techniques, mechanical properties; therapeutics.

Classification: NLM Code: QV 785

Language: English

LJP Copyright ID: 392843

Great Britain Journals Press

London Journal of Medical & Health Research

Volume 24 | Issue 8 | Compilation 1.0

Needle Sofinnovation: Over Coming Unprecedented Challenges Intransdermal Drug Delivery with Micro Needles

Sumit Kumar Gupta[α], Simran Sah Kalwar[σ], Aakrshan Kumar[ρ], Aditi Bhardwaj[ↀ], Shivani Sharma[¥], Sushil Kumar Mali[§] & Ram Prakash Yadav[χ]

ABSTRACT

Drug delivery through the skin offers distinct advantages, including bypassing the liver's initial metabolism, maintaining consistent drug levels in the blood, and ensuring safety and adherence to treatment, which surpasses traditional oral or injectable methods. Microneedle technology has emerged as a revolutionary approach in this regard, offering enhanced delivery efficiency and patient acceptance. The main obstacle to transdermal administration, however, is the fact that only a small number of strong medications with optimal physicochemical characteristics can intercellularly and passively diffuse across skin barriers to reach therapeutic concentration using this method. Innovative strategies have been pursued to improve the drug's skin penetration.

Microneedles, a microscale physical enhancement technique, have expanded the spectrum of medications that may be delivered transdermally and intradermally. These microneedles are usually between 0.1 and 1 mm in length, offering a minimally invasive yet highly effective method for drug administration. This review discusses the challenges associated with microneedle based TDDS, including formulation issues, skin permeability, and manufacturing complexities.We highlight recent advancements in microneedle design, materials, and fabrication techniques, shedding light on their potential to overcome these hurdles. One may create solid, coated, hollow, or dissolvable microneedles using a range of materials, including silicon, stainless steel, and polymers. Despite extensive research, several obstacles hinder the long-term, cost-effective production, and effectiveness of microneedles for transdermal drug delivery. This analysis identifies gaps in production technology and reviews characterization techniques. Microneedles show promise in various applications, including medicine delivery, vaccination administration, illness diagnosis, and cosmetics, indicating their versatility and wide-ranging potential.

Keywords: skin, TDDS; microneedle; microscale fabrication techniques; coating techniques, mechanical properties; therapeutics.

Author α: College of Pharmacy, B-pharmacy, RIMT University, Mandi Gobindgarh, Punjab (147301), India.
σ: Health Care Science, BMLT, CT University, Ludhiana, Punjab (142024), India.
ρ ↀ ¥: College of Pharmacy, Associate Professor, RIMT University, Mandi Gobindgarh, Punjab (147301), India.
§ χ: College of Pharmacy, B-pharmacy, RIMT University, Mandi Gobindgarh, Punjab (147301), India

I. INTRODUCTION

For thousands of years, people have been using various chemical substances on their skin for a variety of reasons. These substances were utilized for medicinal purposes, to protect the skin, and even for cosmetic purposes [1]. In ancient times, the Greeks developed a balm by combining water, olive oil, and lead (II) oxide. The olive oil served as a barrier, while the lead (II) oxide had a tightening effect [2]. It wasn't until 1893 that Bourget proved the efficacy of salicylic acid in treating acute rheumatoid arthritis, which

London Journal of Medical & Health Research

challenged the notion that the skin was impenetrable [3,4].

In the early 1900s, researchers made a significant discovery regarding lipophilic agents, which were found to enhance the permeability of the skin. Through Wolf's tape-stripping technique, Blank conducted a study and determined that the stratum corneum (SC) serves as the primary obstacle for the penetration and permeation of active pharmaceutical ingredients (APIs) [5,6].

The utilization of skin as a means of delivering drugs to systemic circulation was not adopted for commercial or scientific purposes until 1954. It was during this time that the effectiveness of 2% nitroglycerin ointment in managing angina pectoris was demonstrated. Consequently, this ointment became the initial commercially available formulation designed for transdermal delivery of active pharmaceutical ingredients into the systemic circulation [4,7].

1.1 Skin Structure

The skin, which accounts for approximately 15% of the body's mass and covers an area of 1.5 to 2.0 square meters, is widely recognized as the largest and most intricate organ in the human body. The first skin layer, i.e. the epidermis layer, is approximately 150–200 mm thick and is composed of viable cells. The structure consists of five layers based on the level of cell keratinization i.e. stratum corneum (SC, horny layer), stratum lucidum (clear layer), stratum granulosum (granular layer), stratum spinosum (spinous or prickle layer), and stratum germinativum (basal layer) [8].Its vital role lies in safeguarding the body against detrimental environmental elements such as dehydration, disease-causing micro-organisms, and various forms of stress [9-12]. Moreover, the skin possesses distinctive attributes that render it suitable for the safe and efficient administration of medications. Specifically, topical, and transdermal delivery methods primarily target the skin for drug absorption. Nevertheless, the stratum corneum layer, the outermost lipophilic layer of the skin measuring 20 to 50 micrometers in thickness, often poses a challenge to the passive diffusion of drugs into the skin [13,14] (Figure 1). The epidermis is composed of dead keratinocytes, the lipid matrix, and corneodesmosome, creating the well-known 'bricks and mortar' structure. The 'bricks' are keratinized corneocytes, while the 'mortar' is the continuous lipid matrix. Only moderately lipophilic compounds with a log P of 1.0–3.0 can penetrate the skin's lipid-enriched structure to reach the underlying skin layers. The covalent bonds between corneocytes and the lipid matrix form a strong bond, serving as the primary protective barrier function of the skin, which is also known as the main barrier limiting drug delivery rate [15].

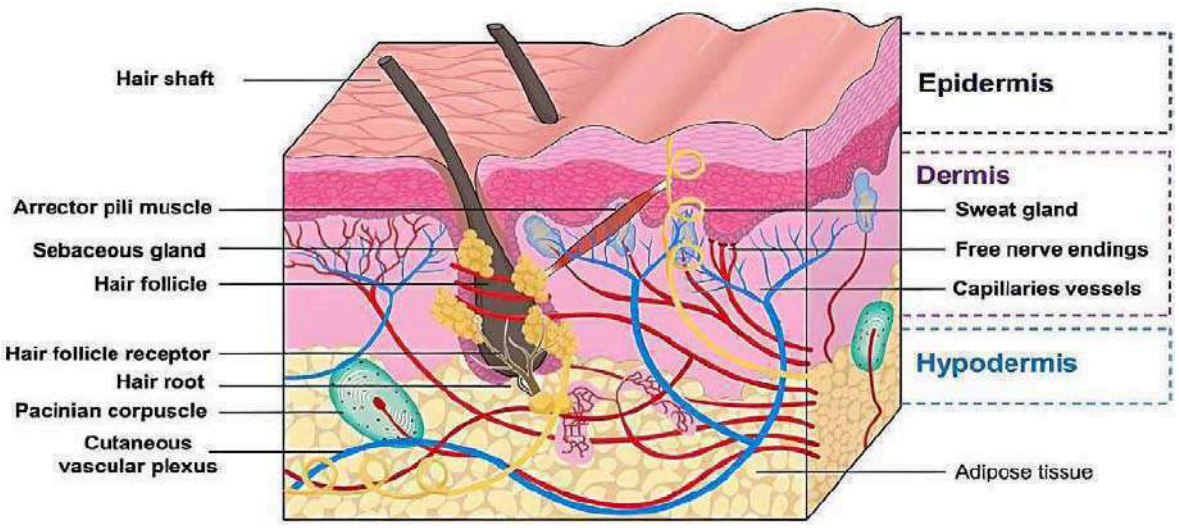

Figure 1: The Diagram Illustrates the Layers of Human Skin. Image Reproduced with Authorization from [16]

1.2 Transdermal Drug Delivery System (TDDS)

Transdermal drug delivery is gaining popularity as a preferred method of drug administration. This approach enables drugs to enter the bloodstream through the skin while retaining their effectiveness. As a result, it offers advantages such as increased bioavailability, sustained release, reduced side effects, and improved physiological and pharmacological responses [17,18]. For example, in testosterone replacement therapy, transdermal delivery overcomes the limitations of oral and intramuscular methods by bypassing first-pass metabolism in the liver, thereby reducing the required dosage. Moreover, it eliminates the need for frequent injections and maintains a higher concentration of testosterone in the blood [19,20]. However, the transdermal delivery of drugs is greatly influenced by the chemical characteristics of the drugs, impacting their absorption through the skin. As a result, only a limited number of drugs can be effectively delivered in therapeutic doses through this route [21].The transdermal drug delivery system necessitates the drugs to follow a complex path to penetrate through multiple layers of the skin, which consist of both aqueous and lipid domains, and ultimately enter the bloodstream [22,23]. For a drug molecule to successfully traverse the stratum corneum (SC) layer, it must possess specific characteristics. These include a molecular weight below 600 Da, a Log P value ranging from 1 to 3, a well-balanced SC/vehicle partition coefficient, and a low melting point that correlates with good solubility, as predicted by the ideal solubility theory [24]. Olanzapine is an example of a drug that possesses the necessary physicochemical properties for effective transdermal drug delivery. It is lipophilic (log P 2.8), has a low molecular weight of 312.4, and a low melting point (195 °C).The low bioavailability of olanzapine when taken orally and its vulnerability to loss during transportation result in only 40% of the intended dosage reaching the bloodstream. These attributes highlight olanzapine as a promising option for administration through transdermal drug patches [25,26]. It is evident that numerous drugs do not meet the rigorous criteria for transdermal delivery[27].

The primary obstacle in transdermal delivery lies in the fact that only a limited range of medications can be effectively administered through this route. Currently, transdermal drugs that have proven successful possess molecular masses that do not exceed a few hundred Daltons. Additionally, these drugs exhibit octanol-water partition coefficients that strongly favor lipids and require daily doses of milligrams or less [28-31]. Delivering hydrophilic drugs through the transdermal route has proven to be challenging. The transdermal delivery of peptides and macromolecules, including novel genetic treatments involving DNA or small-interfering RNA [32], has presented specific difficulties.

From a global standpoint, we propose that the progress in transdermal delivery systems can be classified into three generations of developmentFigure 2. The first generation involved the creation of many of today's patches through the careful selection of drugs that can penetrate the skin at therapeutic rates without requiring significant enhancement. The second generation brought about further advancements in delivering small-molecule drugs by enhancing skin permeability and the driving forces for transdermal transport. Moving forward, the third generation will facilitate the transdermal delivery of small-molecule drugs, macromolecules (such as proteins and DNA), as well as virus-based and other vaccines by specifically permeabilizing the skin's stratum corneum.

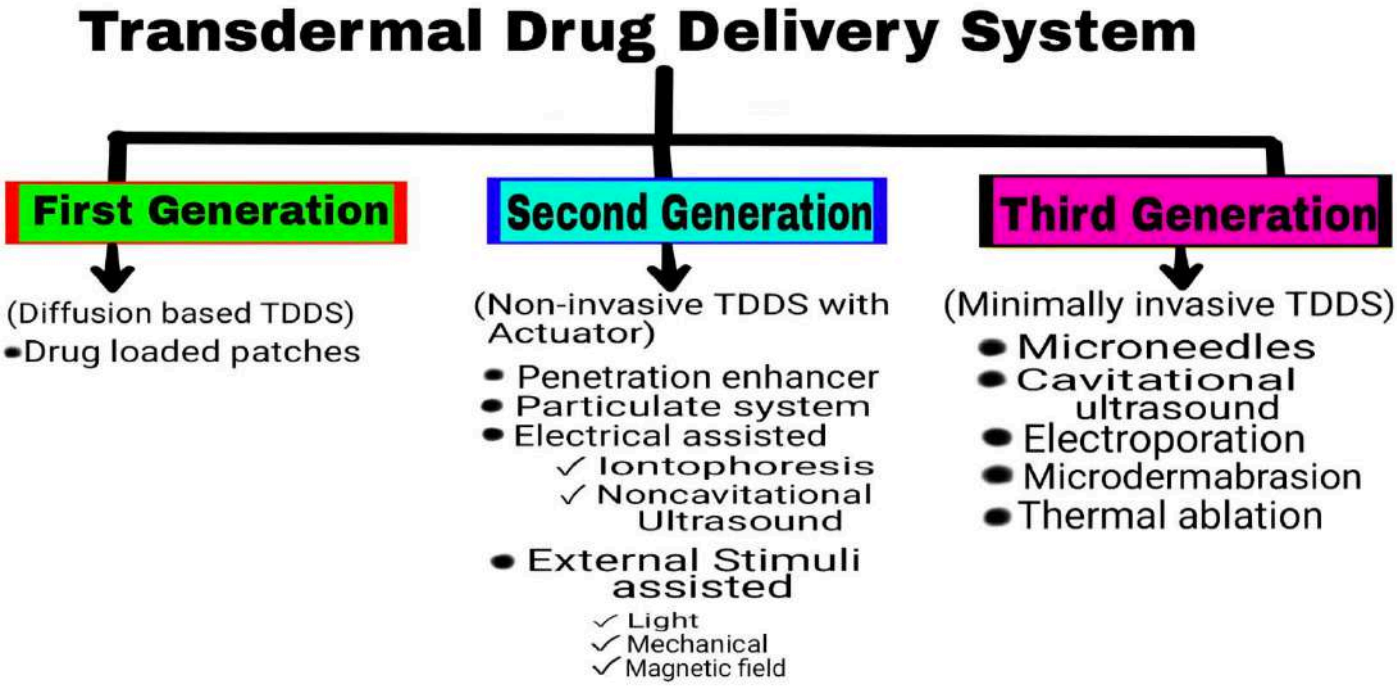

Figure 2: Generations of Transdermal Drug Delivery

1.3 Type of Transdermal Drug Delivery System

The transdermal drug delivery system (TDDS) is an innovative approach to delivering medication. It involves delivering a specific amount of medication through the outermost layer of the skin. This method ensures that the medication is released at a controlled rate over an extended period, allowing it to enter the bloodstream gradually. The TDDS can be classified as a unique type of drug delivery system that adheres to a zero-order drug release pattern [33].There are various methods of transdermal drug delivery available, which encompass:

1.4 Membrane Permeation Controlled TDD System

Within this particular transdermal drug delivery system, the drug reservoir is situated between the backing layer and the polymeric membrane. Illustrated in Figure 1(a), the drug reservoir region contains the drug that is distributed within the polymeric matrix solution to create a paste-like suspension. This suspension is subsequently released at a regulated pace through the rate controlling membrane, which can be either non-porous or micro porous [34]. Substances such as estradiol are administered through membrane penetration [35].

1.5 Matrix Diffusion Controlled Transdermal Drug Delivery System

In Figure 1(b), illustrates the presence of an occlusive base plate, drug reservoir, and polymeric membrane. The drug reservoir contains the drug, which is enclosed by the matrix. The matrix can consist of hydrophilic or lipophilic molecules. The drug and matrix together create a medicated disc-like structure, releasing the required amount of drug at a controlled rate into the systemic circulation. The drug is in a solution form within the matrix and is supported by an adhesive layer [36]. This method can be used to deliver drugs like nitroglycerine [37].

1.6 Reservoir Gradient Controlled Transdermal Drug Delivery System

This category is effective in addressing concerns associated with a non-zero release profile of the drug [38]. The drug and polymer matrix are merged in a reservoir, which can transform into a reservoir gradient along the diffusional pathway

across the layer. This process results in the controlled release of the drug, as illustrated in Figure 1(c). Glyceryl trinitrate is utilized as the drug in creating a deponit system for controlled delivery [34,39].

1.7 Microreservoir Dissolution Controlled Trans-Dermal Drug Delivery System.

The drug delivery system illustrated in Figure 1(d) combines matrix and reservoir dispersion types. It involves two main steps: creating the drug reservoir by suspending the drug in water-soluble or aqueous solutions, and then mixing/dispersing the suspension with a lipophilic polymer using strong mechanical force. This process leads to the formation of numerous microscopic reservoirs, ultimately resulting in the controlled release of the drug at a specific rate [34].

1.8 Microneedles- Innovating Drug Delivery Techniques.

A range of approaches can be employed to improve the delivery of drugs through the skin, such as the use of penetration enhancers, innovative formulation designs, and physical techniques [40]. Among these methods, microneedles have recently emerged as the most efficient and dependable approach for transdermal drug delivery. This recommendation is supported by various research studies conducted in academic institutions and industrial companies [41,42–44]. Microneedles, which are needles with sizes ranging from 25 to 2000 micrometers, have been found to puncture the layers of the skin in a precise and reversible manner, thereby disrupting the skin barrier function and creating numerous microchannels within the skin [45].

Microneedle technology has a rich history spanning over 40 years of development. The initial concept of microscale needles was introduced in a patent filed by Gerstel and Place, which was granted by the United States Patent and Trademark Office in 1976. The progress in the microfabrication industry has greatly facilitated the precise and controlled fabrication of microneedles. Subsequently, different types of microneedles, including solid, hollow, coated, dissolving, and swelling microneedles, have been developed in chronological order. Among these, the most recent design of microneedles for skin delivery is the hydrogel-forming swelling microneedle, which was developed in 2012 by Donnelly and his colleagues. In recent times, dissolving microneedles has garnered significant attention from researchers, leading to the invention of superior materials, novel designs, and optimized scalable production techniques. The extensive research conducted in this field has contributed to the growing popularity of microneedles. Furthermore, this evolving field has expanded to encompass cosmetic and diagnostic applications, as well as drug delivery to various tissues such as the eye, buccal mucosa, and gastrointestinal tract.

The initial microneedle design was patented in 1976, and a patent for a hollow microneedle device for intradermal drug delivery followed in 1996. A skin-piercing device was created in 1997, while silicon solid microneedles were first utilized for transdermal delivery of calcein in 1998. In 2000, researchers developed hollow microneedles for injecting a drug solution into the skin. The first coated microneedles were produced in 2004 to improve the transdermal delivery of desmopressin. Subsequently, in 2006, drug-loaded dissolving microneedles were manufactured to deliver bovine serum albumin and calceintransdermally. Finally, hydrogel-forming swelling microneedles were introduced in 2012 as the most recent type of microneedle.

Extensive research has delved into various aspects of microneedles, such as manufacturing processes [46,47], designs[48], drug delivery applications, safety measures[49], clinical studies [46], modeling, simulation [50], and more. Studies have shown that microneedles can penetrate the skin without reaching the dermis, where nerve fibers and blood vessels are located, to prevent pain or bleeding. Nguyen and colleagues recently explored the strategies for transdermal hormone delivery using microneedles, discussing trends, advancements, and challenges in transitioning from the lab to clinical settings[51]. Ali and coworkers also examined the skin's anatomy and

biomechanical properties concerning microneedle insertion and drug permeation, along with drug permeation modeling and clinical implementation of microneedles [52].

Transdermal delivery has seen significant improvement through the use of microneedles, expanding the possibilities for delivering small molecules [53,54], macromolecules [55–58], cosmeceuticals [59–61], and particulate systems [62–64]. Microneedles are versatile in transporting molecules of varying sizes and molecular weights. Different microneedle systems have been developed, each with their distinct characteristics including geometry, size, design, layout, density, composition, and materials. Microneedles can be made from a range of materials such as glass, sugar, metal, silicon, ceramics, and polymers. These materials must meet specific requirements for microneedle production, such as mechanical strength, biocompatibility, and safety. Among these materials, biodegradable, biocompatible polymers have emerged as promising options and have garnered significant attention and interest [65].Various polymers can be utilized to create a variety of microneedles, such as dissolving, swelling, solid, coated, and hollow microneedles. Commonly used polymers for this purpose are SU-8 photoresist, cyclic-olefin copolymer, polycarbonate, poly (methyl Metha-acrylate), poly-lactic-co-glycolic acid (PLGA), polyglycolic acid, polystyrene, polylactic acid, poly (vinyl pyrrolidone), polyvinyl alcohol, and sodium carboxy methyl cellulose. PLGA, chitosan, and hyaluronic acid are among the frequently employed polymers in microneedle production [40,66,67]. Recent research has also investigated a wide array of materials for microneedle fabrication, including natural, synthetic, and semisynthetic polymers, and particle composites [68–70]. Microneedles composed of natural materials have garnered significant attention due to their exceptional compatibility and minimal skin irritation [71,72]. Dabholkar provided a comprehensive overview of the utilization of natural materials, such as polysaccharides, polypeptides, and proteins, in the production of biodegradable microneedles [71]. These natural materials include cellulose and its derivatives, starch, and complex carbohydratepolymers like chitosan, alginates, pullulan, chondroitin sulfate, chitin, xanthan gum, and hyaluronic acid. Protein polymers such as gelatin, zein, fish scale, collagen, and silk fibroin are also examples of materials used. Damiri et al. further delved into the discussion of various carbohydrates for microneedle fabrication [73].

Various types of microneedles have been utilized in transdermal drug delivery. These include solid, hollow, coated, dissolving, and swelling microneedles (Figure 4). Figure 5 displays microscopic images of dissolving microneedles. Both academic institutions and industrial companies have made significant advancements in the fabrication of microneedles on different scales. The scientific literature contains several reviews that discuss the various fabrication techniques for microneedles, such as microelectromechanical systems, micro molding techniques, additive manufacturing (including fused deposition modeling, stereolithography, digital light processing, and photon polymerization), atomized spraying technique, X-ray technique, laser technique (including laser cutting and laser ablation), droplet-born air blowing, drawing lithography, pulling pipettes, and micro-injection molding. These methods have been extensively explored and documented in the scientific community [46,68,69,74].Among the various methods available, micro-molding stands out as the most commonly utilized technique for manufacturing microneedles in both academic and industrial environments [58,67,75]. Different microneedle-coating methods such as immersion coating, dip-coating, layer-by-layer coating, drop-coating, spray coating, electrohydrodynamic atomization, gas-jet drying, and piezoelectric inkjet printing are also employed. Ali et al. recently provided an overview of common techniques for producing dissolving microneedles, which include micro molding, drawing lithography (such as thermal drawing, electro-drawing, and magnetorheological drawing lithography), and additive manufacturing (3D printing) [68]. It is worth noting that 3D printing

has gained significant attention as a promising method for microneedle production [76–78].

The fabricated microneedles underwent comprehensive characterization in multiple studies. Researchers analyzed various aspects including microneedle formulations such as drug solubility, drug-excipient compatibility, and rheological and interfacial properties. They also examined the geometry and morphology of the microneedles before and after insertion, as well as their mechanical properties including axial force, transverse force, base strength, and skin penetration force. Additionally, investigations were conducted on microneedle dissolution, drug release, drug-loading capacity, drug distribution, skin penetration efficiency, and safety aspects such as biological safety, skin irritation, and skin recovery. Furthermore, the physicochemical stability of the microneedles was assessed in terms of hygroscopicity, swelling behavior, stability, water content, and solid state.

Microneedles insertion creates multiple microchannels in the skin [79,80]. The successful microporation of the skin by microneedles is confirmed through various characterization studies. These studies involve evaluating the morphology, measuring skin resistance and transepidermal water loss, conducting histological analysis, dye binding studies, assessing microchannel depth using confocal laser scanning microscopy and optical coherence tomography, examining pore uniformity, and studying pore closure kinetics. Following microneedle insertion, the pores gradually close due to the skin's viscoelasticity and natural healing process. Several research groups have investigated the kinetics of pore closure, as it can impact skin irritation and the risk of infection. Researchers have reported that pore closure significantly influences microneedle-mediated drug delivery [81-83].The time it took for pores to close varied from a few hours to 72 hours, depending on factors such as skin types (animal and human skin), experiment design (in vitro, in vivo, and clinical studies), occlusion, microneedle dimensions, and formulation pH [81,83,84]. Haridass and the team found that pores created by microneedle insertion (Nanopatch®) closed by 25% within 30 minutes and completely within 6 hours. As a result, microneedle-induced pores are temporary and reversible, resulting in rapid skin recovery within 1-2 days out of 39 [85].

Various advantages and disadvantages of microneedles have been explored in scientific literature. Microneedles address issues associated with hypodermic needles such as needlestick injuries, needle phobia, sharp waste, and the transmission of blood-borne pathogens. The painless and noninvasive nature of microneedle treatment enhances patient acceptance and compliance. Additionally, microneedles enhance drug bioavailability by bypassing first-pass hepatic metabolism and avoiding enzymatic degradation. Microneedles have the potential to offer a dose-sparing effect and a strong immunological response to vaccines. The temporary and reversible skin disruption caused by microneedle insertion helps reduce the risk of skin irritation and infection.There are several drawbacks associated with microneedles. One of the main concerns is that they can only hold a small amount of drugs. Additionally, polymeric microneedles may lack the necessary strength and mechanical properties to effectively penetrate the skin. Moreover, the viscoelasticity of the skin can limit the depth to which microneedles can penetrate. The variability in skin thickness, hydration level, and viscoelastic properties further complicates the task of achieving consistent penetration depth.

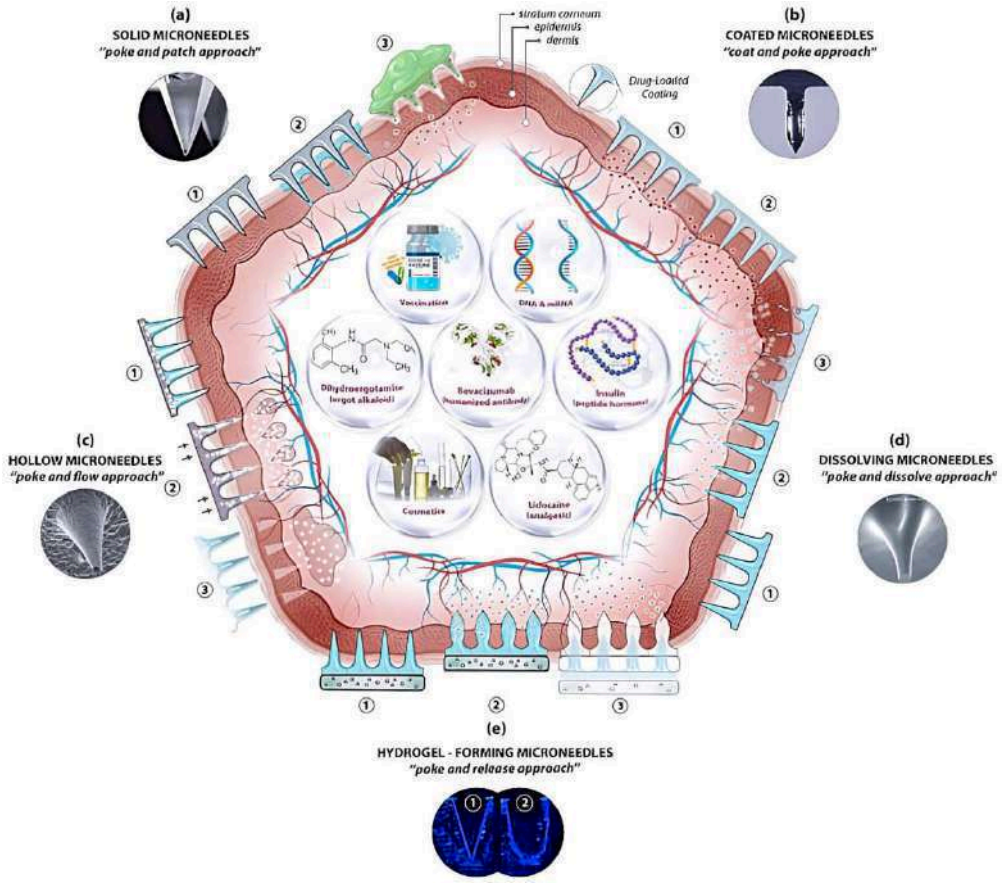

Figure 4: Diagram illustrating microneedle-facilitated transdermal drug delivery: (a) Solid microneedles enhance drug permeation by forming temporary hydrophilic microchannels in the skin. (b) Drugs are applied onto the microneedle surface and rapidly dissolve upon skin insertion. (c) Hollow microneedles pierce the skin, enabling drug solution injection. (d) Dissolving microneedles disintegrate upon skin entry, releasing the drug payload into the skin layers. (e) Swelling microneedles absorb skin fluid and expand to promote drug diffusion through the porous structure. Images reproduced with authorization from [86].

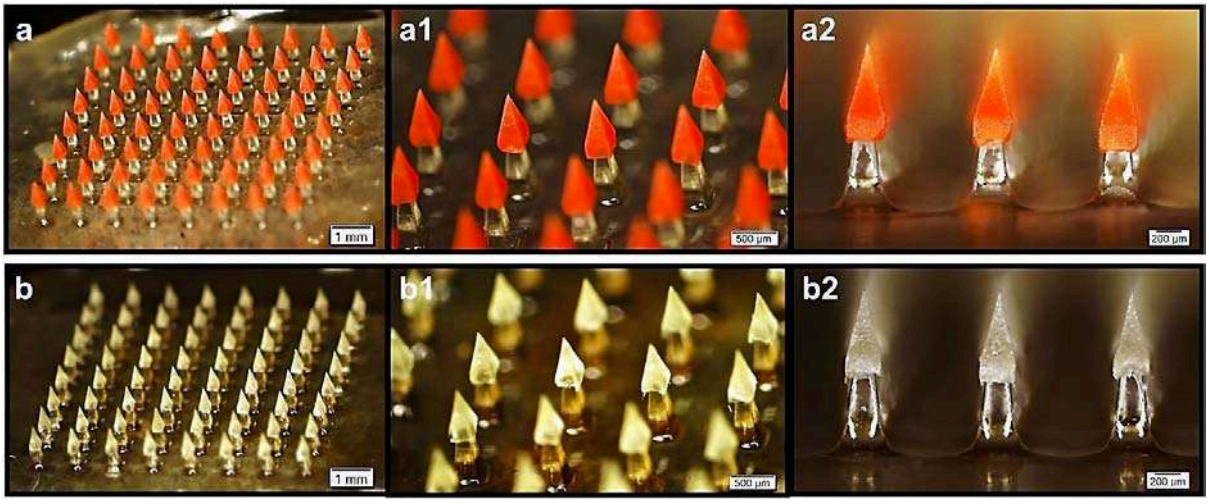

Figure 5: Images of chitosan-poly(L-lactide-co-D, L-lactide) microneedle array loaded with rhodamine B dextran (a, a1, a2) and ovalbumin (b, b1, b2) are depicted in the microscopic form. These images have been reprinted with permission from [87].

II. TYPE OF MICRONEEDLES FOR DRUG DELIVERY

2.1 Solid Microneedles

Solid microneedles typically involve a two-step process for drug administration. Initially, the solid microneedles are inserted into the skin and then removed, creating temporary hydrophilic microchannels. Following this, a drug-loaded topical formulation such as a gel, cream, lotion, ointment, or transdermal patch, is applied over the microchannels to facilitate drug delivery (Table 1) [80,88-90]. The microchannels formed by the insertion of solid microneedles enable passive diffusion of the applied drugs into the layers of the skin (Figure 2a). Upon the administration of the drug formulation to the affected area, the drug can be continuously delivered through microchannels created by microneedles until either the drug supply is exhausted, or the channels are sealed. The effectiveness of drug transportation into and across the skin is influenced by various factors such as the size, shape, sharpness, and density of the microneedles used for skin pretreatment [91,92]. Furthermore, the efficiency of microneedle-assisted delivery is greatly influenced by the physicochemical properties and molecular weight of the drugs [60].

Solid microneedles can be made from various materials such as glass, metal, silicon, and polymers. The common designs for solid microneedles include solid arrays, flexible patches, and roller types. The disruption of the skin caused by solid microneedles has proven beneficial for many biomolecules. Numerous studies have focused on using microneedles to administer substances like fluorescein isothiocyanate-labeled ovalbumin and insulin, ovalbumin-conjugated nanoparticles, human immunoglobulin G, calcein, bovine serum albumin, fluorescein isothiocyanate-coupled dextran, melanostatin, rigin, palmitoyl-pentapeptide, and genes [60,93,94]. In general, microneedle treatment significantly improves the delivery of most large molecules into the skin. Furthermore, the effectiveness of drug delivery is inversely related to the molecular weight of the drug [60,95].

Several research groups have explored the efficacy of solid microneedle therapy in delivering insulin intradermally, both in vitro and in vivo, resulting in a significant reduction in blood glucose levels [96,97]. Martanto et al. reported an 80% decrease in blood glucose levels in diabetic rats after the insertion of solid microneedles. Moreover, these microneedles improved insulin delivery to a level comparable to 0.05–0.5 units of insulin administered via subcutaneous injection [98]. Noteworthy, Qiu and team devised an insulin-loaded lyophilized hydrogel patch to achieve sustained and continuous drug delivery through microneedle-formed channels in the skin for up to eight hours. This novel formulation demonstrated a considerably longer duration of action compared to conventional subcutaneous injections. Additionally, insulin retained 90% of its bioactivity after being stored for six months at 4 ◦C [99].

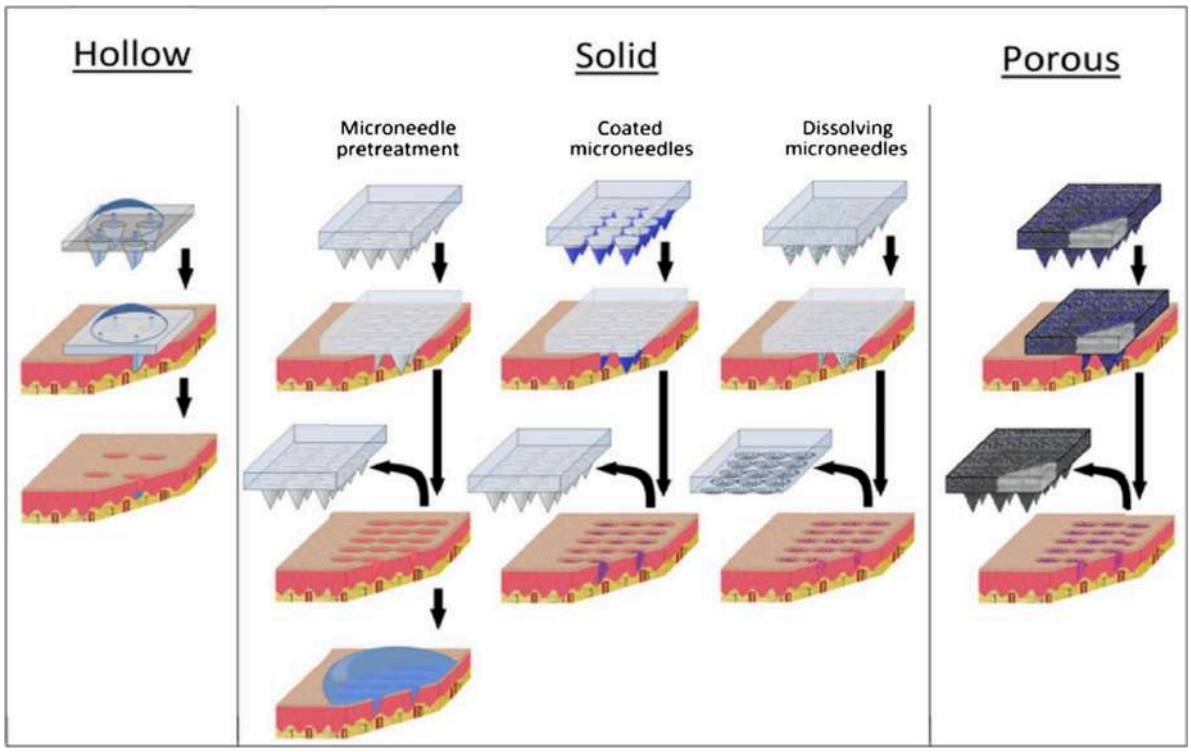

Figure 6: This Source Shows that Microneedles can be used for Drug Delivery with Various Structures Like Hollow, Solid, or Porous. Image Adapted from [114]

2.2 Hollow Microneedles

Hollow microneedles, which are downscaled hypodermic needles in micron size with a similar configuration (Table 1), enable the controlled injection or infusion of a drug solution into the skin layers (i.e., epidermis or dermis) in a non-invasive manner [100] (Figure 2c). Passive diffusion is the simplest method of drug transport through hollow microneedles. However, due to the slow permeation of drugs into the dense skin tissue, researchers have applied pressure to enhance drug delivery [101]. One notable advantage of hollow microneedles is their ability to accurately deliver a large quantity of drugs into the skin [102,103]. A properly engineered microneedle must possess ample mechanical durability to avoid fracturing while penetrating the skin and minimize the risk of bore obstruction, a prevalent issue with hollow microneedles. Scientists have created hollow microneedles with off-center bores on the side of the tip to prevent blockages and enable the medication to access the adjacent skin tissue. Scientific studies illustrate the effective application of hollow microneedles in improving the transdermal administration of various macromolecules, such as proteins, peptides, oligonucleotides, and vaccines.

Researchers have explored the use of hollow microneedles for painless and noninvasive insulin delivery, known as the "poke and flow" technique[104,96,105]. Studies have shown that intradermal delivery of insulin via hollow microneedles offers faster absorption and better treatment outcomes compared to traditional subcutaneous injections [106]. Additionally, retracting the microneedles partially has allowed for the injection of larger drug volumes. A study on children with type 1 diabetes demonstrated that insulin delivery through hollow microneedles led to quicker healing and reduced pain levels when compared to conventional injection

methods[107]. McAllister and colleagues found that applying a pressure of 10 psi allowed a glass microneedle to deliver 32 μL of insulin solution into the skin of a hairless rat over a period of 30 minutes [108]. Xenikakis and team, on the other hand, created two types of hollow microneedles through 3D printing and liquid crystal display techniques. The researchers analyzed the needle dimensions using scanning electron microscopy, the volumetric properties of microneedles and microchannels using microfocus computed tomography, and the mechanical properties and skin penetration efficiency using finite element analysis simulation. The resulting hollow microneedles successfully facilitated the delivery of insulin across human skin in laboratory settings [109].In addition, hollow microneedles have the potential to improve the transdermal delivery of various macromolecules. These include β-galactosidase, formaldehyde-inactivated botulinum toxoid [110], synthetic mRNA [111], cascade blue, dextran-cascade blue, FITC-dextran [112], human growth hormone, equine tetanus antitoxin [113], and ovalbumin-loaded PLGA nanoparticles [62]. To facilitate the injection of liquid formulations into the skin, 3M has developed a hollow microstructured transdermal system (hMTS). This system consists of hollow microneedles that are connected to a glass cartridge. By utilizing a spring-controlled mechanism, the hMTS device allows for self-injection of up to 1.5 mL of drug solution. Notably, the 3M™ hMTS device has demonstrated successful delivery of equine tetanus antitoxin and human growth hormone into the skin in vivo. Researchers have observed comparable pharmacokinetic profiles of these drugs in domestic swine when administered via hMTS or subcutaneous injection [113].

2.3 Coated Microneedles

An enhanced approach for enhancing transdermal drug delivery using solid microneedles involves applying drug formulations onto the needle surface (Table 1). Various coating methods (such as dip coating, casting, and deposition [115,116]) have been created and assessed for this purpose. Once the microneedles are inserted into the skin, the coating layer breaks down quickly, releasing the drug into the targeted skin layers [117] (Figure 2b). In comparison to the solid microneedles' two-step application process, this single-step technique (coated microneedles) is significantly more effective, precise, and convenient. It is important to note that most in vivo studies on transdermal macromolecule delivery have utilized coated microneedles. However, it is worth mentioning that coated microneedles can only accommodate a small amount of drugs due to their limited surface area.Furthermore, an overabundant coating could lead to a decrease in the mechanical strength and sharpness of microneedles. Therefore, microneedles that are coated are advantageous for highly potent molecules that necessitate a lower therapeutic dosage, like desmopressin, human growth hormone, interferon alpha, and various macromolecules[118,119]. Scientists should strive to enhance the coating procedure and formulation to attain a precise, dependable, and consistent amount of drugs coated onto the needles.

Coated microneedles have proven to be effective in facilitating the penetration of various macromolecules into the skin. These macromolecules include desmopressin, bovine serum albumin, interferon-alpha, parathyroid hormone, peptide A, insulin, recombinant human erythropoietin alfa, bovine pancreatic ribonuclease A, antisense oligonucleotides, erythropoietin, ovalbumin, and human growth hormone [119–125]. It is worth noting that coated microneedles have demonstrated the ability to deliver hydrophobic peptides into human skin in vitro and mouse skin in vivo [162]. In a study conducted by Li and colleagues, metal microneedles were coated with various molecules such as proteins, immiscible molecules, and nanoparticles, enabling the delivery of multiple therapies using a single microneedle array [163]. The bioavailability of human growth hormone and peptide A, when coated on solid microneedles, was found to be comparable to that of subcutaneous injections, thus highlighting the efficiency of coated microneedles in transdermal drug delivery [118,122].

Two prominent coated microneedle systems include the Macroflux® microneedle array

(titanium microneedles) and the 3M solid microstructured transdermal system (sMTS). The Macroflux® system has the capability to coat a variety of biomolecules (such as biologics, peptides, proteins, and vaccines) onto the surface of solid microneedles. Notably, parathyroid hormone 1-34 (PTH 1-34), a medication used for treating postmenopausal osteoporosis, has garnered significant attention in both preclinical and clinical trials [121]. It is worth mentioning that PTH remained stable in the final product even after being stored for two years at 25 ◦C, thereby eliminating the need for any cold-chain or special storage requirements.The PTH-coated microneedles caused a sudden surge in drug plasma levels, reaching Tmax three times faster than the control FORTEO® subcutaneous injection [128]. Similarly, Macroflux® desmopressin-coated microneedles facilitated swift drug delivery in vivo, providing an effective dose for antidiuretic effects without causing pain or skin irritation [129]. Moreover, the 3M sMTS (coated microneedles) demonstrated the ability to transport a drug payload of up to 0.3 mg. Peptide A exhibited significantly enhanced stability when coated on the sMTS [122].

2.4 DissolvingMicroneedles

Dissolving microneedles, a unique design of microneedles, -has attracted considerable interest from both academic and industrial fields(Table 1). Ali and his team recently conducted a comprehensive review on dissolving microneedles, focusing on their designs and materials for delivering macromolecules through the skin [68]. These microneedles contain therapeutic substances within their polymer structure[44]. Once inserted into the skin, the drug-filled microneedles break down and dissolve in the skin fluid, releasing the drug(Figure 2d). This innovative system provides either immediate or prolonged drug release, depending on how quickly the polymer materials dissolve and how long the microneedles are applied [130–134]. The primary challenge with dissolving microneedles is their strength, which decreases as the amount of drug they can hold increases. Furthermore, the physical and chemical properties of materials and design factors greatly impact the strength and drug release rate of these microneedles[135]. The robustness of microneedles is directly influenced by the aspect ratio of microneedle length to base dimensions [136]. Recent studies on dissolving microneedles have focused on the design and geometries of these microneedles [41,42,44, 137,138]. Various innovative microneedle designs have been proposed and assessed for their effectiveness in skin penetration and drug delivery [139]. Biodegradable and water-soluble polymers such as carboxymethylcellulose [140], maltose [141], chitosan [75, 142, 143], polyvinyl alcohol (PVA) [144], hyaluronic acid, and polyvinylpyrrolidone are suitable for developing dissolving microneedles. Additionally, it is preferable to use mild manufacturing conditions to enhance stability and preserve the bioactivity of biopharmaceutical drugs [68,145].

Researchers have demonstrated that dissolved microneedles may efficiently transfer insulin into the skin, lowering blood glucose levels in diabetic rats, dogs, and mice [146,147]. Particularly, there was a lot of curiosity in an insulin transdermal delivery system mediated by glucose-responsive microneedles [148, 149]. Specifically, there was no significant difference in the pharmacokinetic profile of insulin between subcutaneous injection and microneedle therapy [150]. Moreover, insulin's stability, bioactivity, and bioavailability were all enhanced by encapsulating the medication in dissolving microneedles [150]. For example, after a month at 25 or 37 ◦C, the insulin that has been encapsulated into starch and gelatin microneedles may still have over 90% of its bioavailability [151].Insulin-loaded microneedles with a relative bioavailability of 96.6 percent were created by Jung and coworkers using a gentle droplet-born air-blowing approach [152]. To decrease the blood glucose levels efficiently and quickly in diabetic mice, Yu and colleagues created a "smart insulin patch" using a crosslinked hyaluronic acid matrix containing glucose-responsive vesicles [153]. In a similar vein, Yang and colleagues created a glucose-responsive closed-loop device for glucagon and insulin transdermal administration. Changes in blood glucose levels have the potential to automatically modify the release of insulin and

glucagon. Using mice and minipigs that had been given type 1 diabetes, the researchers showed that their microneedle technology was successful over a prolonged period [154]. To create polymeric microneedles with the required drug release kinetics, Demir et al. used gelatin methacrylate, polyethylene glycol diacrylate, and MoS2 nanosheets. In both ex vivo and in vivo experiments, the MoS2 needles were able to pierce the skin of mice and pigs and release insulin. In addition, the amount of blood glucose decrease brought about by microneedles was comparable to subcutaneous injection in pigs and mice [155].

Numerous biopharmaceutical agents, including calcein, bovine serum albumin, immunoglobulin G [1], cyclosporin A [157], fluorescein isothiocyanate-labeled dextran [158], interferon-α-2b [159], polymyxin B [160], lysozyme [161,162], FITC-BSA [163], glucagon [164], human parathyroid hormone [165], vascular endothelial growth factor [166], monoclonal IgG [156], rhGH, desmopressin [167], and leuprolide acetate [168] are among the biopharmaceutical agents that are transdermally delivered by dissolving microneedles. A new tissue-interlocking microneedle based on hyaluronic acid was created by FakhraeiLahiji et al. to increase transdermal distribution of different biomolecules by enhancing needle- to-skin adhesion (Figure 7) [169].

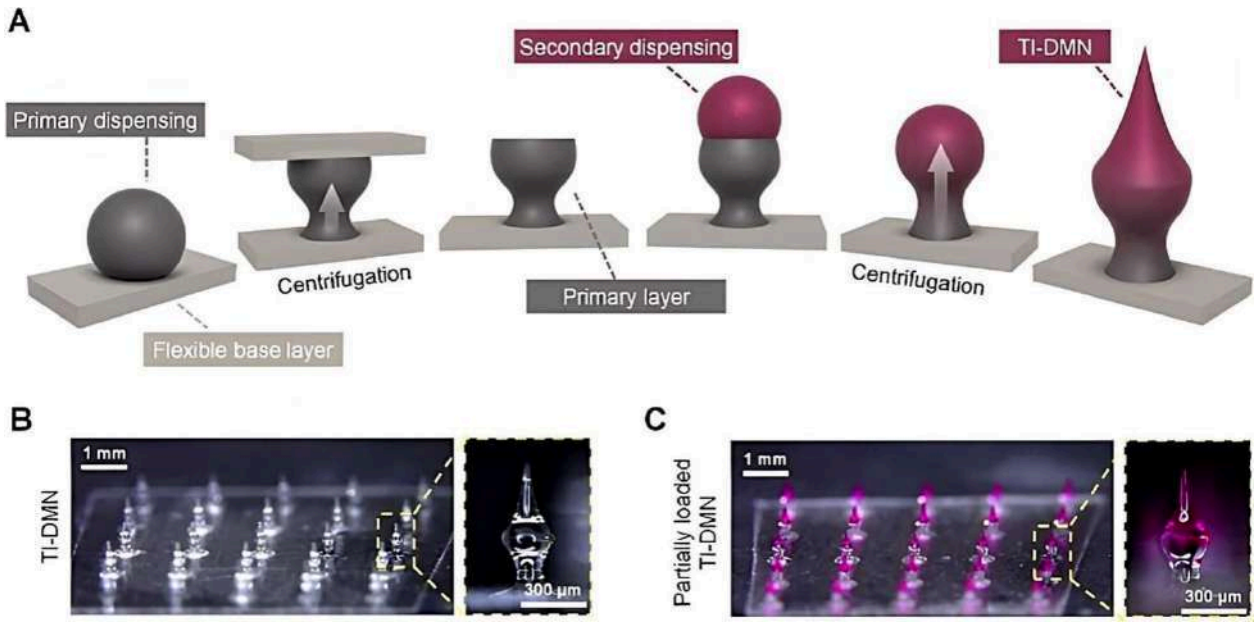

Figure 7: Illustration showing the tissue-interlocking, dissolving microneedles based on hyaluronic acid. (A) the stages involved in fabrication; (B) microscopic pictures; and (C) A microneedle partly loaded with Rhodamine B. Pictures reprinted from [169] with permission

Table 1: An Overview of the Many Methods used to Administer Drugs using Microneedles, together with Information on the Kind of Needles that Correspond with each Method

Drug delivery approach	Type of microneedle	Description	Reference
Poke and patch	Solid microneedle	medication is released via micropores created by microneedles.	[170]
Poke and flow	Hollow microneedle	The drug exits the bore.	[171]

Coat and poke	Drug-coated microneedle	Coating separation from the microneedle	[172]
Poke and release	Dissolving microneedle	Drug permeates the pores and dissolves there.	[173]

III. MICRONEEDLE PRODUCTION

3.1 Materials

The production of MNs in research labs and pharmaceutical businesses has been made possible by the introduction of microfabrication manufacturing technologies in recent decades [174]. As a result, the best materials for MN manufacture must be chosen using the following standards [175]:

- Delicate production without causing harm to delicate and unstable compounds.
- Regulated or quick release of drugs; and
- Enough mechanical strength to pierce the skin.

Silicon was used to create the first solid MNs [176] since the creation of MNs was made possible by silicone's flexibility and industrial high-precision microelectronics instruments. However, because of their brittle nature, its primary drawback is the silicon MN breaking. These days, MNs are made of many different materials (Table 1), including titanium, nickel-iron, glass [177,178], ceramics [179], stainless steel [180,181,182], and titanium. Metal MNs are mechanically strong enough to pierce the skin, but one drawback is that they may produce biological waste [183,184]. It's interesting to note that nitinol is utilized in vascular surgery because of its benefits in terms of biocompatibility, flexibility, and shape memory [185]. Polymeric MNs offer improved solubility and are more practical when it comes to tip breakage [186]. MN production utilizes water-soluble polymers [84,187–189] and engineering plastics like CMC, polyglycolicacid (PGA), polylactic-co-glycolic acid (PLGA), polyvinyl alcohol(PVA), polyvinylpyrrolidone (PVP), polylactic acid (PLA), chondroitin sulfate, and polycarbonate. On the other hand, dissolving MNs consist of sugars such as maltose [190,191], dextran [81], or galactose [193,194–196]. Table 2 provides an overview of the materials that are appropriate for MN manufacture.

Table 2: Suitable Materials for Microneedle (MN) Manufacturing

Material Type	Manufacturing Method	MN Type	Reference
Silicon	Etching, lithography	Solid, hollow, coated	[176,197,198,199]
Mesoporous silicon	Post-synthesis grafting method		[200]
Nitinol	Multiple-pulse laser microhole drilling	Hollow	[185]
α-aluminum(III)oxide(α-Al2O3),zirconia	Lithography and ceramic sintering, micro molding, two-photon polymerization(2PP)	Ceramic(solid), hollow	[179,201]
Nickel/iron	Laser-ablation, micro molding, electroless plating, wet etching	Solid, hollow, coated	[202,203]
Stainless steel	Laser cutting, laser ablation, etching, electroplating, electropolishing, lithography, and micro stereolithography	Solid, hollow, coated	[204,205,206,181, 182,207–212]
Glass	Pulling pipettes	Hollow	[178,212,213]
PLGA	2PP, micro molding	Hollow, solid, dissolving	[184,214]

Thermoplastic starch	Electro-discharge machining process	Dissolving	[215]
PLA	Fused deposition modelling (FDM), micro molding	Solid, dissolving	[105,216–218]
Titanium	Microelectromechanical systems (MEMS)	Solid,hollow, coated	[219,200]

The manufacturing process for MN should be durable, reliable, repeatable, and exact according on the material that is used [221]. MEMS, lithography techniques, laser cutting, laser ablation, metal electroplating, isotropic and anisotropic etching [199], injection molding [222], DAB method [223], surface/bulk micromachining, polysilicon micro molding [224], and additive manufacturing (AM) technologies (FDM [225], stereolithography (SLA) [226, 227,228], digital light processing (DLP), and 2PP [229] are some of the manufacturing methods for solid or hollow MNs and are covered in the following sections. Furthermore, a detailed description of coating MNs with an API-containing formulation is provided below.

3.2 Production Techniques for Microneedles

3.2.1 Laser Cutting

The processes of 3D laser cutting [204,205, 206,182,207,208], laser ablation [209–211], and electroplating or electroless plating of metal onto positive or negative MN molds [193] can all be used to create metal MNs.

Using an infrared laser, stainless steel or titanium sheets shaped like MNs are cut to create arrays of solid MNs (Figure 8). Some computer-aided design (CAD) software is used to produce the required form, geometry, and dimensions of MNs. After the laser beam conforms to the needle's predefined shape, MNs are cleaned in hot water and bent vertically at a 90-degree angle from the base plane.The next steps involve electro-polishing, washing, and compressed air drying the MNs in order to remove, thin down, and sharpen the tips. A single row of MNs with various geometries and two-dimensional rows of metallic MNs may be produced using this manufacturing process [204, 205, 206,182,207,208].

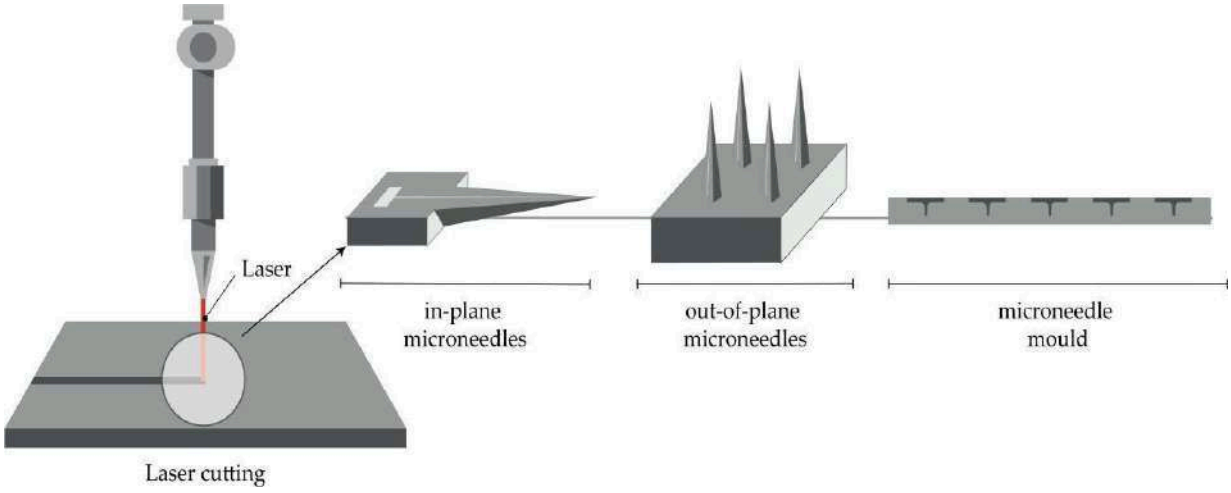

Figure 8: The Principle of Producing both in-Plane and out-of-Plane MNs and MN Molds by Laser Cutting [230]

Moreover, it is stated [231] that molds for a dissolving MN patch and hollow MNs [218] have been produced. In the first instance, PLA sheets that had previously been made using a

micromolding process were made to have holes made from their sides using a KrF laser (λ = 248 nm) [218]. The creation of MN patches on polymethylmethacrylate (PMMA) sheets using a CO2 laser was documented by Albarahmieh et al. Then, dissolving MNs containing terbinafine hydrochloride and methylhydroxy-4-benzoate were generated by pouring a chosen combination into PMMA molds [231].

3.2.2 Microelectro mechanical Systems (MEMS)

Micro-electro-mechanical systems (MEMS) techniques have been used to directly manufacture solid and hollow micro-needles (MNs) as well as molds for dissolving MNs from a suitable material substrate [232]. Three exact phases make up the production process: material deposition, patterning, and etching (Figure 1) [233,234]. Because of the etchant's differing material selectivity, these processes lead to the development of intricate three-dimensional (3D) structures [234]. In the initial stage, a thin layer is created on a substrate using chemical vapor deposition (CVD) or physical vapor deposition (PVD) that has a thickness ranging from a few nanometers to 100 μm [233,235,236]. Atoms are immediately transported from the source to the substrate during the gas phase of the PVD process, producing the film. Conversely, the CVD technique forms films as a result of a chemical reaction on the substrate surface [236].

During the second stage of the procedure, known as patterning, the required material is then transferred as a two-dimensional master pattern from the original photomask to the photosensitive-coated substrate. A silicon wafer is often used as the substrate, and one of the lithography processes—photolithography [237], ion beam lithography [238], or X-ray lithography [239]is utilized to create the transfer process using a radiation source.

Photolithography is the most widely used kind of lithography. This procedure is based on the observation that some materials, including metals, become opaque when subjected to UV light (λ = 193-236 nm), whereas glass remains clear. An opaque template called an optic mask is made during this operation to construct the required pattern in a wafer (Figure 9). The mask, made of a flat glass or quartz plate, only permits light to flow in a certain pattern [240]. The silicon substrate is first heated to around 900 °C with steam or humidified oxygen to form an oxide layer. It is then rotated and covered with an organic polymer known as photoresist material, which is UV-sensitive [236,139,241]. The solvent is eliminated, and the required photo-resistant pattern is formed when UV light and heat between 75 and 100 °C are applied [240]. Positive and negative resists can both be utilized in this stage. Compared to the negative resist, where the chemical bonds are reinforced, the positive resist exhibits photo-resistant polymer chains that break apart upon exposure to UV light, rendering the polymer more soluble in the developer's chemical solution (Figure 9) [241].

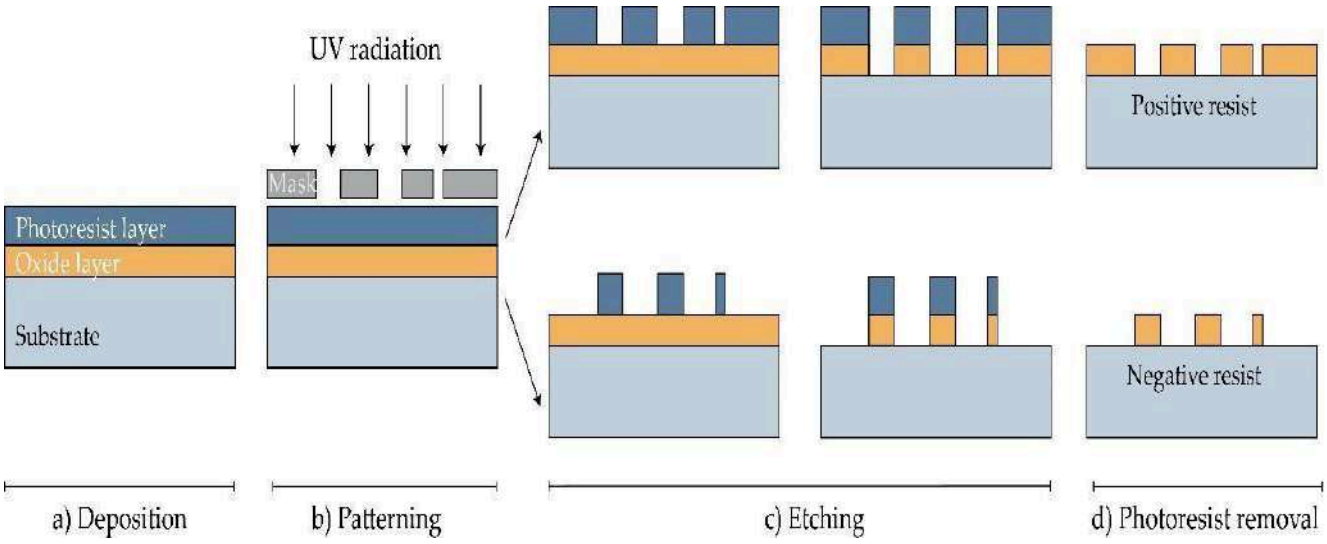

Figure 9: MNs are manufactured using photolithography [236]. (a) Deposition: To create an oxide layer on the Si wafer, it is either humidified or exposed to steam as a substrate. After that, a substrate is spin-coated with aphoto-resistive substance. (b) Patterning: The photoresistive material is subjected to UV light guided by a mask. (c) Etching: SiO2 layer is etched after the soluble resist material is eliminated. (d) Photoresist removal: The photoresist layer is eliminated in this stage [230]

Moreover, photolithography makes it possible to manufacture MN molds. In this instance, a stiff silicone cast with a positive image is created, and the selected material is then applied after the creation of a negative mold from poly (dimethylsiloxane) (PDMS) [236]. In order to create a pattern on the material's surface, the exposed portions of the substrate are etched away using a powerful acid or caustic chemical. There are two different kinds of etching: wet and dry etching [233]. By immersing the substrate in the chemical liquid during the wet etching process, extra material is eliminated, resulting in metallic or silicon MN arrays. Anisotropic etching is the process of etching at a different rate from isotropic etching, which is done at the same rate [233,242]. However, the use of a vapor phase or plasma etcher is necessary to accomplish the dry etching procedure. It is possible to distinguish between two primary forms of dry etching: ion-beam milling (IBM) and reactive ion etching (RIE). A reaction between the gas and the substrate is made possible in the RIE process by the gas's excitation into a reactive state. By adjusting the gas pressure, the amount of ions that affect the degree of isotropy may be changed. Ions can be accelerated by the electric field, which also increases the etching's direction. To physically remove the material to be etched, inert ions are accelerated from a source in the IBM method [241]. While RIE can produce structures, it has a poor etching rate and finds it difficult to maintain a high width-to-height ratio. The procedure known as the Bosch process, or deep reactive ion etching (DRIE), works well for producing off-plane MNs. Hollow MNs with a lumen of several hundred micrometers (width-to-height ratio of 30:1) are created using this technique [243]. The greatest results are obtained by combining isotropic dry and anisotropic wet etching to generatewell-defined and sharp MN tips, even though wet etching can lower production costs compared to dry etching [244,243,245].

3.2.3 Micromolding Method (SolventCasting)

The process of producing dissolving MNs typically involves pouring the liquid formulation into an MN mold that has already been constructed [202]. A silicon wafer is often used as the starting material for mold [184]. The wafer is then oxidized at 1000 ◦C. CVD is utilized to cover a wafer and lithography techniques are employed to form a needle geometry, which is then subjected to RIE (see Section 3.1.2). After filling the molds with a liquid polymeric solution, air pockets are

wafer and lithography techniques are employed to form a needle geometry, which is then subjected to RIE (see Section 3.1.2). After filling the molds with a liquid polymeric solution, air pockets are extracted using a vacuum or centrifuge [246,247]. The molds are then dried in the oven, and MNs are taken out after they have cooled (Figure 10) [224]. The benefits of this approach are found in the comparatively straightforward and economical manufacturing of MNs at room temperature [248]. Furthermore, it has been documented that MNs made from biodegradable polymers, comprising both natural and synthetic substances, possess the necessary shape and strength to effectively penetrate the skin [184, 248]. It is worth noting that micromolding has also been employed in the fabrication of ceramic MNs [208].

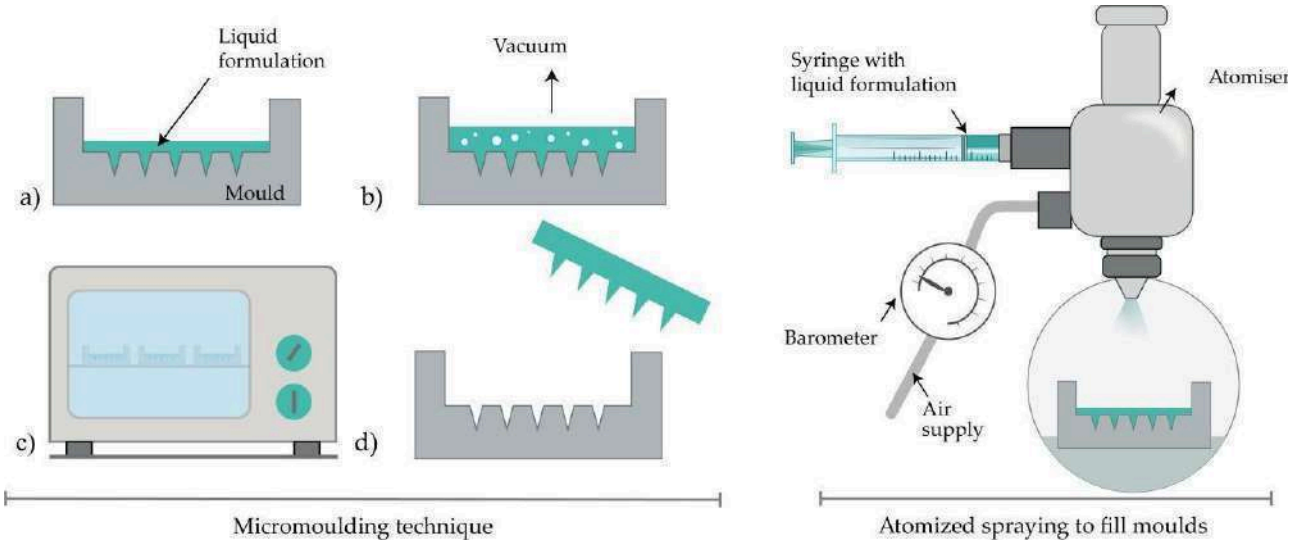

Figure 10: The process of producing MNs using micromolding involved many steps: (a) filling the mold with the liquid formulation; (b) vacuum degasification; (c) drying; and (d) extracting the MNs. Right: Filling molds with atomized spraying. Image from [230]

3.2.4 Laser Ablation

This approach to material processing, which includes metal processing, is top-down. Solid metal arrays are created when light pulses cause a desired shape to bulge on a metal plate [209]. However, the creation of plasma ions and electrons is unsuitable for the creation of structured materials because of the high-intensity laser pulses. Consequently, as seen in Figure 11, Omatsu presented a brand-new, efficient, and time- and money-saving fabrication technique for producing metal MNs based on circularly polarized optical vortices with nonzero total angular momentum. Tantalum MNs with a vertical height of more than 10 μm and noticeably tiny tip radii were fabricated, as the authors described [210].Evens et al. presented a brand-new technique in 2020 for creating solid polymer MNs with laser-ablated steel molds. Additionally, this mold was used in the injection molding procedure to create the polymer MNs. This low-cost manufacturing approach allows for the variation of MN height and the acquisition of acute tip radii [211].

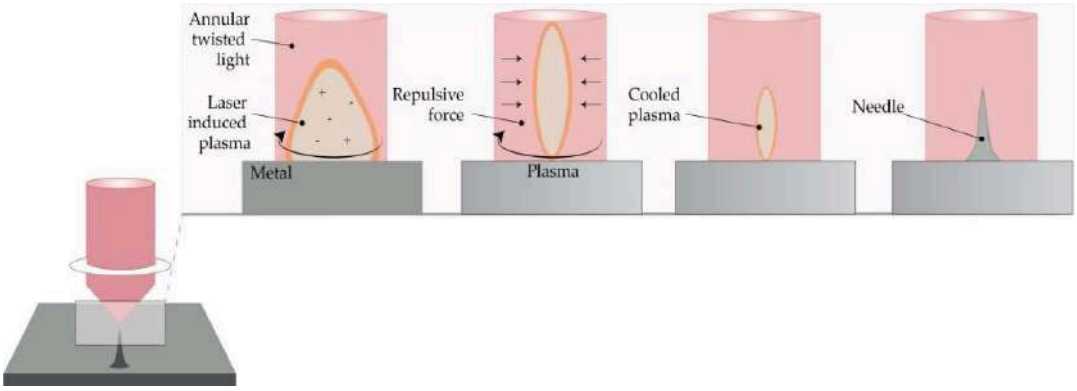

Figure 11: The Omatsu et al. (Modified from [210]) Principle of Metal MN Synthesis Utilizing Twisted Light with a Spin. Image from [230]

3.2.5 Atomized Spraying Method

This technique solves the issues related to the restricted ability to produce dissolving MNs in large quantities with the appropriate shape and physical properties. Additionally, it is possible to reduce the issues arising from the impacts of liquid viscosity and surface tension during the filling of the MN molds. Sugars (fructose, trehalose, and raffinose) or polymers (PVA, PVP, CMC, HPMC, and sodium alginate) can be used to make dissolving MN. In summary, an atomized spray is created via a nozzle that is attached to a liquid formulation and an air source (Figure 11). The mixture is poured into PDMS molds and allowed to air dry for two hours. This approach can also be used to make MN that dissolves in laminate-layered and horizontally layered structures [101].

3.2.6 Droplet - Born Air Blowing Method (DAB)

Conventional MN manufacturing procedures have resulted in drug inactivity owing to UV radiation and heat exposure. Among the drawing lithography techniques is the DAB approach, which was put out by Kim et al. [251]. This process, which uses air blowing to form polymer droplets into MNs, allows for manufacture in temperate climates without the need for heat or UV light [184].

To put it briefly, the procedure starts with the prepared solution being dispensed onto the upper and lower plates. Next, the higher plate is lowered to facilitate droplet contact.This causes the viscous solution to extend as the upper plate moves higher. Next, as shown in Figure 7 [251, 223,252,253], air blowing eliminates any remaining water and pulls the droplets off a substrate to solidify them in the appropriate form.

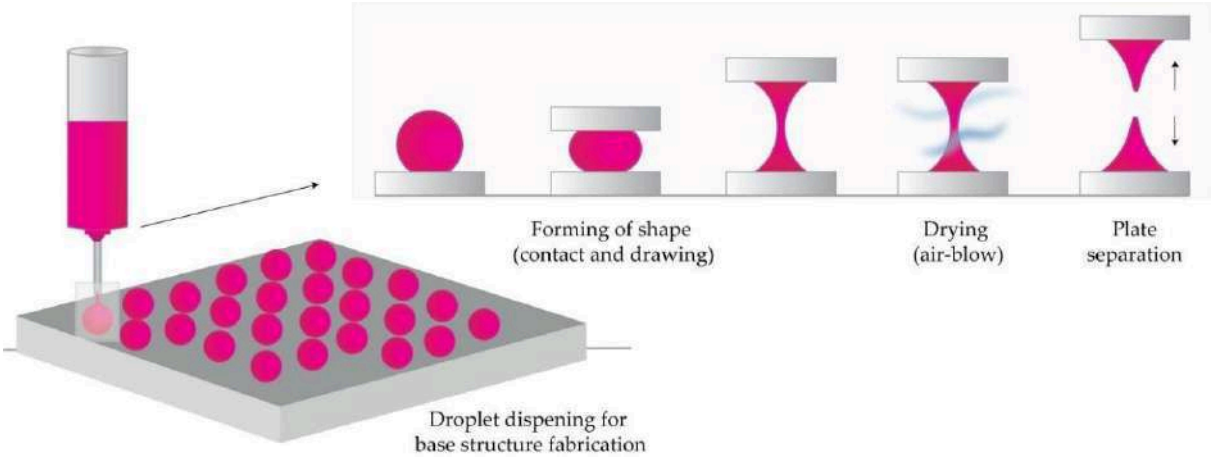

Figure 12: The Fundamental Idea Behind Droplet-Born Air Blowing (Dab) Techniques (As Amended by [253]). Image from [230]

Thus, direct control over drop size and API concentration is made possible by applying one drop of polymer per milliliter. Insulin-loaded dissolving MNs were created using this 10-minute procedure, and they were successful in lowering blood glucose levels in diabetic rats [223].

A new technique with a shadow mask made it possible to produce MN uniformly and solved droplet formation issues related to poor throughput. By using this technique, the authors reported optimized hole width and thickness of the shadow mask together with regulated medication dose [251].

3.3 Process of Additive Manufacturing (AM)

A recent area of study is additive manufacturing, sometimes referred to as 3D printing, which is used to make molds and MN arrays. Using computer-aided design software (CAD) to build a three-dimensional item is the initial stage in all AM technologies. To tessellate and slice the 3D shape into digital layers, the CAD model is first converted to an STL file. After that, the printer is configured with printing parameters, and the STL file is sent to it using specialized machine software. By layering appropriate material (such as liquids, ceramics, thermoplastic, plastic, photopolymer, powders, or even living cells), the printer creates the model [254–259].

MN arrays were effectively fabricated using additive manufacturing technologies, FDM [216,217], and photopolymerization-based methods such as SLA [226,227,228,260–263], DLP [135–138], and 2PP [214,229,264,265]. Compared to conventional manufacturing methods, these state-of-the-art technologies provide several benefits, such as affordability, ease of use, the capacity to construct intricate geometrical products with the flexibility to alter original designs at any point, and the ability to produce devices tailored to individual patients [259,266].

3.3.1 Two-Photon-Polymerization (2PP)

The 2PP approach makes it possible to fabricate 3D structures at minimal cost, layer by layer, from solid, liquid, or powder precursors in both microscale and nanoscale architectures. For the purpose of polymerizing resin into MN structure, a femtosecond or picosecond laser is directed within a liquid resin droplet [209,254]. Photopolymerization is accomplished by a mechanism that relies on the temporal and spatial overlap of photons [214]. The method has several benefits, including enhanced geometric control, scalable resolution, and a high degree of flexibility. It may also be carried out in traditional facilities [209,254].

The first report on employing 2PP to create MNs from Ormocer® (organically modified ceramic) materials was made by Doraiswamy et al. [201]. According to Trautmann et al., 2PP was used to create hollow MNs with internal laser-generated microchannels [264].Moreover, another research

team used 2PP to print ultra-sharp polymer MNs [265]. Using 2PP 3D, Cordeiro et al. reported a method for creating superior MN array master templates [229]. According to Gittard et al., 2PP may produce MNs with a variety of geometries, including rocket-shaped, mosquito fascicle-shaped, in-plane, and out-of-plane MNs [214].

3.3.2 Fused Deposition Modelling (FDM)

Using CAD software to design the MN and optimizing its shape in accordance with printer specifications is the first step in being ready to print it using a standard FDM printer [256,259]. The appropriate thermoplastic material is then fed into the printer via rollers in the form of a filament and heated by heating elements into a molten state to a temperature slightly over its softening point (glass transition temperature T_g). Gears guide the melted or softened material as it is pushed toward the head end of the printer, where it is extruded via a nozzle and placed layer by layer on a build plate. The material cools and solidifies in less than a second (Figure 8) [254–257]. 3D structures may be created by the printer's head moving in the x, y, and z axes while the platform can move in the z-axis [258].

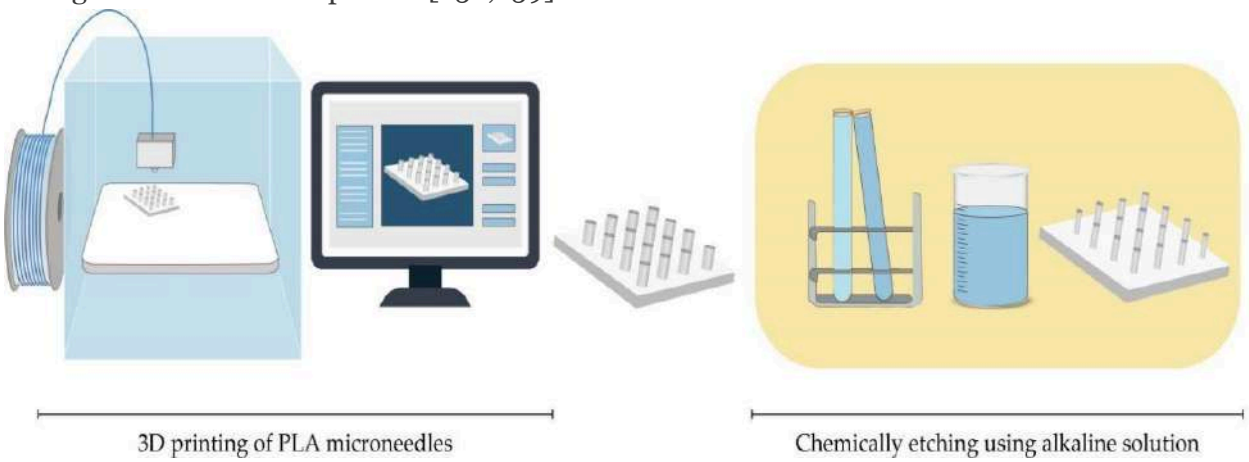

Figure 13: Mns Are Fabricated using Fused Deposition Modeling (Fdm) Techniques and Then Etched in an Alkalinesolution [216,217]

A variety of standard filaments are used in FDM printers, including nylon, acrylonitrile butadiene styrene (ABS), PLA, PVA, high-impact polystyrene (HIPS), and polyethylene terephthalate glycol-modified (PET-G). The dimensions of the filaments used in commercial print heads range from 1.75 mm to 2.85–3 mm [256].

Processing factors such as nozzle diameter, feed rate, building plate and nozzle temperatures, printing speed, layer heights, and part-created orientation should all be tuned during an FDM process [257,259]. FDM is a flexible and affordable way to manufacture MNs, but its primary drawback is its poor print quality. For the first time, Luzuriaga et al. described combining FDM with a post-fabrication etching phase to produce needles with the perfect size and form [217]. FDM was also effectively employed by Camovic et al. to print MNs, which were then coated [216] (Figure 13).

3.3.3 Digital Light Processing (DLP)

Another method based on photopolymerization is DLP, which uses light projections to polymerize photosensitive polymers. Using a high-resolution projector to flash the object's whole cross-section at once in the form of volumetric pixels, this approach is quicker thanStereolithography(SLA) [254]. Gittard et al. reported that DLP may be applied to the creation of MNs. In their work, they effectively used DLP to print solid MN array structures for wound healing applications in a variety of geometries using an acrylate-based polymer [267]. A desktop DLP 3D printer was also effectively utilized by El-Sayed et al. to create MN molds for the distribution of nanoparticles [268]. Using microstereolithographic (DLP) equipment,

Lu et al. created drug-loaded MN arrays for transdermal administration of a chemotherapeutic medication.

3.3.4 Stereolithography (SLA)

SLA is the most widely utilized method for printing MNs because of its high resolution, precision, and perfect surface finish. The first publication on the creation of MN arrays for transdermal medication distribution using the lithography-based multiphoton polymerization 3D printing approach came from Ovsianikov et al. [179]. The photopolymerization of liquid resin using photo-active monomers under UV light is the foundation of this technique. MNs are created by successive resin layers solidifying in the presence of intense light, such as a UV laser beam directed by scanner mirrors [256]. A laser beam applied to a resin's surface produces an MN pattern that gives the material a distinct depth. MNs are cured in the UV chamber after being cleaned in an alcohol bath to get rid of any unpolymerized resin residues [228,262].

SLA is a rather slow, costly, and constrained printing process due to its limited choice of printing materials (lack of biocompatibility) while producing high-quality components at a fine resolution (of up to 10 μm) [269]. This photopolymerization-based method was reported to be used by several research groups to produce solid MNs, hollow MNs, and MN molds [226, 260]. Using a Class 1 biocompatible resin that had exceptional mechanical strength and was coated with insulin-sugar films, Pere et al. and Economidou et al. created MN arrays using SLA [228,262].

3.4 Methods of Microneedle Coating

3.4.1 Gas-Jet Drying

Using a gas-jet applicator, the medication suspended in a coating solution is dried using a process known as "gas-jet drying" (Figure 14) [270]. It works particularly well for curved MNs because dip-coating's lengthy drying time is inconvenient in these circumstances. The liquid used for wet coating on the MNs' surface may migrate and alter in thickness, which might affect the dosing accuracy. Additionally, short (less than 90 microns in length) and tightly spaced (less than 20,000 cm 2) MNs can be used with this approach [271].

A tiny coating of gold was applied to solid silicon microprojections. The whole length of the microprojection is coated with the solution, which contains methylcellulose, surfactant, and model medication and has the perfect surface tension and viscosity. In order to guide the coating liquid onto the MNs and away from the base, the drying process began with a gas jet operating at 6–8 m/s at an incidence angle of 20° horizontally. The microprojections' coated layer had a thickness of 5 μm and grew quickly to prevent the coated material from moving on the base substrate and to allow it to cure. The uniform distribution and quick drying of the coating solution, the ability to remove excess coating solution from the base substrate, and the relatively constant viscosity of the bottom layer of the solution are only a few benefits of this technology [272].

It is possible to enhance the transport of big vaccine molecules via the SC by altering the gas jet technique used to coat MNs. The homogeneity and displacement of the drug from the whole MNs to the tips were guaranteed by rotating the patches, eliminating the patch edge, and raising the incidence angle from 20 to 70 degrees. The protective immunological response was produced at far lower levels than with the intramuscular injection. Additionally, these MN patches enhanced and prolonged the stability of the vaccination [273].

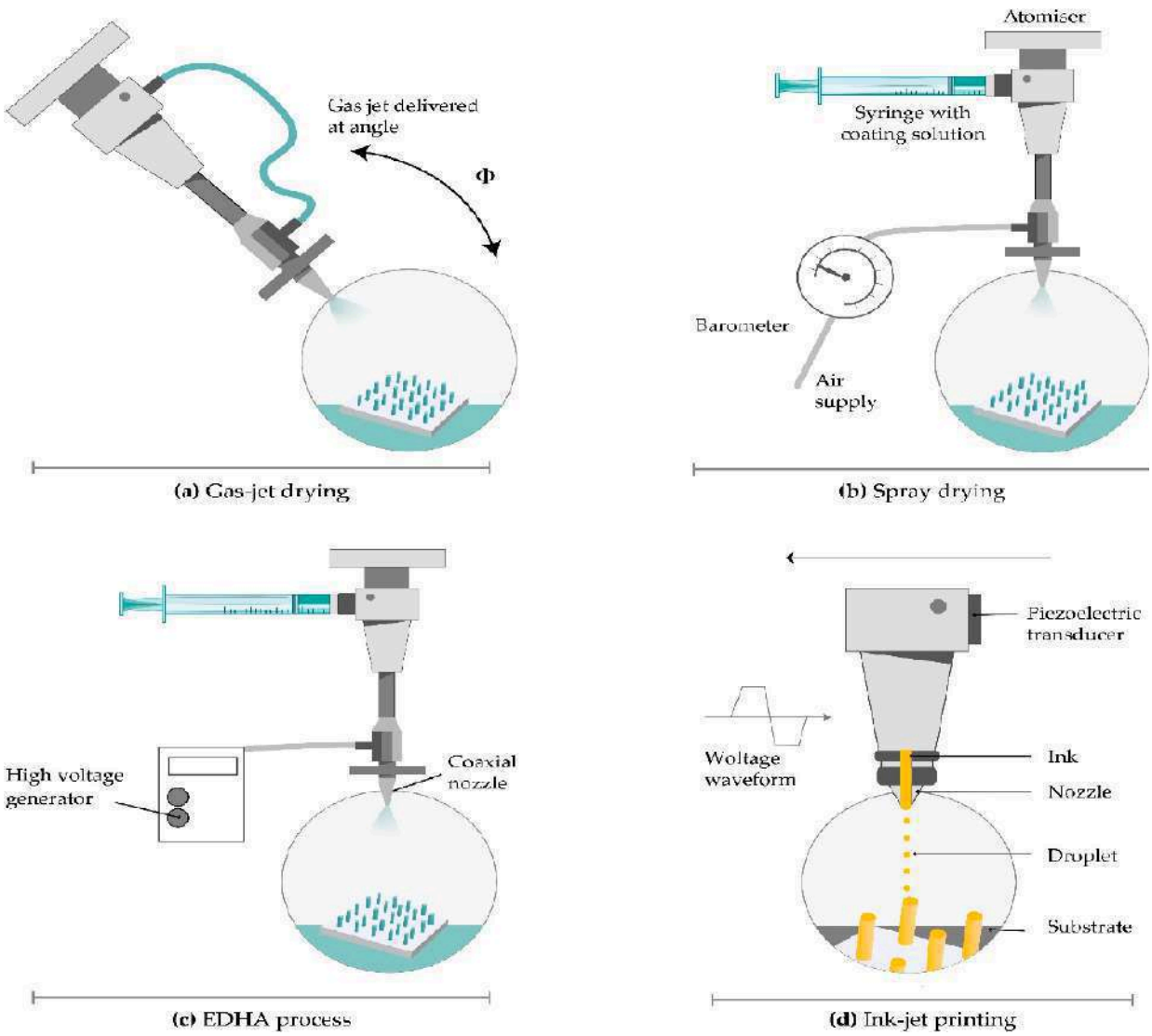

Figure 14: Strategies for Coating MNs. (a) Gas-jet Drying, (b) Spray Drying, (c) Electrohydrodynamic Atomization (EHDA) Procedures, and (d) ink-jet Printing are the Four Methods Mentioned above Image from [230]

3.4.2 Electrohydrodynamic Atomization (EDHA)

An electrical field creates charge inside the droplets during the process of electrohydrodynamic atomization (EHDA), which produces atomized droplets by moving a liquid. Droplets of liquid shoot out of a nozzle when the critical voltage is reached. Subsequently, it is placed onto a grounded collector situated beneath the tip of the nozzle (Figure 14) [274]. Drugs, polymers, and solvents are all present in the coating liquid. EHDA can produce fibers (electrospinning) and particles (electro spraying). Because of the insulating polymeric masks, this approach only coats the MN tips and leaves the base substrate uncovered. However, a significant amount of drug waste occurs on the mask over the basic substrate [275].

The EHDA technique is available in three different configurations: coaxial (two or more immiscible liquids are injected into separate nozzles), multiplexed (formulation is injected into a single or coaxial nozzle array), and single-needled (one nozzle is filled with formulation using a syringe pump). The coaxial method permits prolonged and regulated drug release while shielding the medication from direct environmental exposure [271]. Particle size, size distribution, porosity, shape, and surface charge

are significantly influenced by the following factors: solution viscosity, surface tension, flow velocity, voltage, and distance between the nozzle and collecting platform. Jet stability is affected by the properties of the material. The low electrical conductivity of the solvent is the primary need for the EHDA process [275].

This technique is used to the administration of delicate biomolecules such as proteins and peptides that become unstable when administered orally, as well as insulin, folic acid, gold utilized in gene transfer, and titanium dioxide as an antibacterial agent [275,276]. Ali et al. used the EHDA method to coat MNs with fibers and particles. The researchers concluded that MNs coated with PVP in ethanol released more quickly than MNs coated with polycaprolactone in dichloromethane, which displayed a sustained release profile. The skin was effectively penetrated by both varieties of MN, and the electrospun MN covering released a significant quantity of the medication after 6 hours [277].

3.4.3 Spray Coating

Spray coating refers to the process of creating droplets using fluid pressure. Fine droplets (less than 280 μm) are deposited onto an MN array, outspread, and combine to create an unbroken film coat. Atomization is the initial stage that produces tiny droplets (Figure 9). Subsequently, droplets cling to one another and deposit, crashing on the surface. Droplets coalesce on the substrate in the last stage to create an unbroken film covering [278].

The droplet size is determined by the nozzle design, concentration, input ray, viscosity, surface tension, and density of the coating solution, as well as processing parameters like the air-to-liquid mass ratio, spraying duration, atomization air pressure, gun-to-surface distance, and air cap setting. Spray density and spray velocity control the amount of droplets that land on the surface [278]. In addition to producing dissolved MNs, the spray coating technique may effectively apply an entire, micron-sized film-coating on silicon MN arrays (see Section 3.2.5).

McGrath et al. produced an atomized spray by connecting a nozzle to a supply of compressed air and a coating solution. They employed tape to secure silicon MN patches to the adjustable stage, and a peristaltic pump and syringe driver were used to regulate the liquid input rate. Fast film-forming and improved droplet coalescence on the MN surface were achieved with a coating solution consisting of HPMC, CMC, and surfactant [278].

3.4.4 Dip-Coating

By dipping MNs in drug formulation, the technique known as "dip-coating" selectively coatings the MN shaft while preventing contamination of the MN array's base substrate. You can employ different molten liquids, organic solvent-based solutions, or aqueous solutions. On the MN surface, dipping causes a liquid film to develop; drying then turns the adhering liquid film into a solid coating [279,280]. To stop the coating solution from rising when the MN shaft touches the base substrate, the viscosity and surface tension of the coating solution should be properly regulated. Either thin-film dip-coating or masked dip-coating can be used to selectively coat the MN shaft. In order to prevent the coating solution from flowing through to the base substrate, masked dip-coating requires the employment of a masking plate [282]. By ensuring that the coating solution's thickness is less than the MN's height, thin-film dip-coating eliminates the possibility of coating solution and base substrate contact by ensuring the coating solution's little capillary rise [279].

The thickness of the coating on the MN shaft directly affects the amount of medication coated on the MNs. By increasing the rate at which MNs leave the coating solution, improving solution viscosity, and increasing the number of dips, it is possible to obtain a larger thickness and drug mass. Surfactants lower the solution's surface tension and provide a homogeneous, integrated coating. The thickness of the coating is also affected by the drying period in between dips [281].

Dip-coating is a particularly practical technology for MN production because of its low cost and simple fabrication procedure. Upgrading the procedure with a roller, a fixture, a limit, and a dam board can result in optimal medication delivery [283]. This method's primary flaw is its long drying process, which might result in the loss of drug dispersion from MN surfaces. Also, if the MNs are tightly spaced apart, surface tension may prevent them from coating uniformly [279].

Stainless steel was used to create solid MNs by electropolishing and laser cutting. Then, with micron-scale control over the length of the coated shaft, appropriate quantities of CMC and Lutrol F-68 NF were utilized to improve viscosity, decrease surface tension of the coating solution, and prevent contamination of the base. Vitamin B, calcein, bovine serum albumin, plasmid DNA, and viruses were all coated on the MNs [204]. When recombinant human growth hormone was dip-coated onto titanium MNs, the absolute bioavailability was comparable to that of commercial subcutaneous injections. The authors concluded that MN patches could eventually take the place of these injections due to their simplicity of use and absence of discomfort [220].

Vaccine-coated MNs should be directed toward skin immune cells, where maintaining protein integrity is crucial since alterations in protein structure might affect immunological response and vaccination efficiency [290]. Heparin, a pH-responsive copolymer, and a combination of DNA vaccines were coated on MN bases. Electrostatic repulsion between the co-polymer and heparin allowed for the release of vaccinations [284]. Intracellularly encoded antigens, given to necessary effector cells directly for cytolytic action, are the basis of DNA vaccines. MNs enable the delivery of DNA vaccines to the dermal antigen-presenting cells by penetrating the skin's epidermis. Additionally, by using polyelectrolyte multilayers with adjuvant components, they facilitate the intracellular co-delivery of DNA vaccines [285]. The primary drawback of MNs coated with DNA vaccines is their low immunogenicity and coating efficiency. By increasing stainless steels affinity for plasmid DNA, nano-patterned MNs boosted vaccination effectiveness and immunological response. Because of their more hydrophilic surface, nano-patterned MNs demonstrated superior DNA vaccine loading capacity and dip-coating efficiency. Increased cell proliferation indicated improved cytocompatibility. The most significant difference was that their cellular immune responses were stronger [286].

When the influenza vaccine is coated on MNs, antigen activity may be reduced. In addition to increasing viscosity, CMC caused viral particle aggregation, which resulted in a reduction in vaccination activity. Trehalose was substituted for CMC to ensure that the antigen and its activity were protected since it prevented particle aggregation and had improved heat stability [287].

Antigen activity may be decreased on MNs coated with the influenza vaccination. CMC increased viscosity and also led to the agglomeration of virus particles, which decreased vaccination efficacy. Trehalose, which had better heat stability and inhibited particle aggregation, was used in place of CMC to preserve the antigen and its activity [288].

Another variation of the dip-coating technique is dropping coating. It means that the MN array should be dropped into the coating solution rather than dipped into it. A non-uniform coating of the MNs and the base, liquid segregation from the MN tip, and substrate buildup between MNs are caused by slow solvent evaporation. It proceeds to the point where the base is the region that is primarily covered. By heating the patch or vacuum-drying it, these disadvantages can be overcome [289].

IV. DELIVERY SYSTEM'S CHALLENGES USING MICRONEEDLES

In the foreseeable future, approving the transfer of MNs from research labs to pertinent businesses is a thrilling but challenging process. Some important concerns and obstacles should be taken into consideration as soon as possible in order to transition this revolutionary technology from the lab bench to viable goods in the relevant markets.

The future of the area and its commercial uses may be determined by the obstacles and proactive approaches to overcome them that we will examine in the following sections. The next sections address the primary challenges and concerns about the creation of a delivery system based on microneedles, which are summarized in Figure 15.

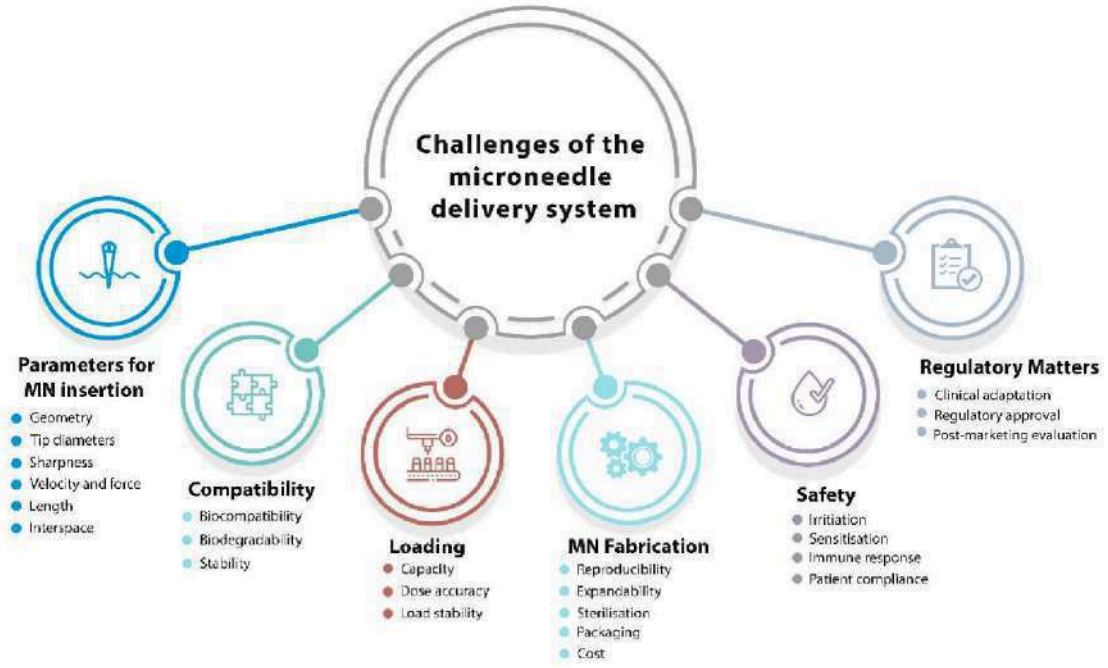

Figure 15: Factors Influencing the Delivery Technique based on Microneedles [365]

4.1 Parameters Affecting MN Insertion

One essential necessity for MN patches is that they must be able to pierce the skin enough. The properties of the skin, which might differ from person to person and across the body, should also be considered while handling this issue. A number of factors, including shape, base and tip diameters, length, and interspace (centre-to-centre spacing), significantly influence how MNs enter and penetrate the skin to overcome its elasticity [291,292]. For any MN application, a "one-size-fits-all" strategy cannot be considered during the design or development phases. The shape of individual MNs and the array, MN materials, the MN management strategy, and the properties of skin tissue are all highly correlated with the infiltration and active delivery efficacy of MNs [293]. By altering the microneedle's composition and form, the mechanical strength, insertion depth, and drug release profile may be precisely adjusted to suit certain medications and purposes.

4.2 Biocompatibility, Biodegradability, and Stability

Biocompatibility is one of the safety features of MN systems used in clinical settings. A number of studies are necessary to assess the biocompatibility of MN products based on contact durations of less than 24 hours, between 24 and 30 hours, and more than 30 hours in order to guarantee that they are safe for human exposure. [294]. The comparable tests for the first two periods are the intracutaneous reactivity, cytotoxicity, sensitization, and irritation tests. For the later stages of usage, genotoxicity and subacute/subchronic systematic toxicity testing are also advised. Since biodegradable materials can be safely broken down and eliminated from the body, it is preferable to employ them in microneedle construction. As a result, efforts to fabricate MN utilizing biodegradable polymeric materials have been made recently. The capacity to incorporate medicine into the microneedle matrix for skin discharge via biodegradation or

dissolution in the skin's bodily fluid is the main advantage of polymeric microneedle systems.

4.3 Loading Capacity and Dosage Accuracy

Loading capacity: The maximum amount of medication that a coated microneedle device can bolus dose is around 1 mg. While hollow microneedles provide "asneeded/on-demand" dosage or continuous infusion, squeezed skin tissue following microneedle insertion may block central exits. MNs can penetrate the skin's barrier qualities, but their effectiveness is mostly reliant on the biological formulation's passive diffusion into the skin. Large doses may be challenging to deliver as a result, and a significant portion of the dose may be lost on the skin's surface. Because of this, there has been hesitation to employ this technology for some clinical applications due to the timing of application and the difficulty to monitor dosage administration. The delivery of vaccinations, for which dose consistency is essential, is one instance.Recent studies have shown that administering vaccines directly to the epidermis and dermis of the skin can generate immune responses with much smaller vaccine doses compared to the traditional method of injecting into the muscles. However, if only a tiny fraction of the given dose reaches the skin, the advantages of this approach may be reduced. While this obstacle can be overcome, vaccines require a minimum dosage to activate immunity, which may be more difficult to achieve through passive diffusion.

Dosage accuracy: It is important to pay careful attention to the dose accuracy of MN delivery systems in continuous medication administration. Various techniques utilizing separable microneedles have been suggested to reduce the duration of patch wear and expedite the extraction of formulation from the microneedles [295,296]. Protein medications, such as insulin, erythropoietin, glucagon, growth hormones, and parathyroid hormones, are difficult to store and administer because bio-macromolecules quickly degrade and become inactive. In addition to using stabilisers, the ideal way to address these issues would be to consider all of the variables involved in the manufacturing of MN, including polymer concentration, sterilization, packaging, and temperatures for both production and storage. As was previously mentioned, MNs may be produced using a variety of materials and kinds.Accurate management of medication delivery efficiency using solid MNs presents certain challenges. Because of its narrow coating surface area, coated MNs can effectively administer precise dosages of a medicine, but their drug loading capacity is restricted. If dissolvable microneedles are made predominantly of hydrophilic, biocompatible, and biodegradable materials and if the cargo can be released completely inside the skin's interstitial fluid without producing undesired debris, then it is conceivable to encapsulate pharmaceuticals in the matrices of MNs. Reservoir leakage can be avoided when transferring relatively high dosages and different medications with regulated release (slow or quick delivery). Dissolvable microneedles may be a useful tool for stabilizing and maintaining nanoscale compositions while enhancing the penetration of nanoparticles through the stratum corneum barrier.Numerous methods have been extensively researched, and a number of analytical techniques have been established for both in vitro and in vivo tracing and tracking the trip of nanomaterials with their important payloads [297,298].

4.4 Skin Irritation and Recovery

The skin is an extremely receptive organ to the MN administration of any medicinal substance due to its immunogenic nature. As a side effect, mild and transient erythema may appear based on the medication's size, composition, and kind. During clinical trials, skin irritation, sensitization, and immunological response need to be assessed as part of MN product safety evaluations. Before doing any clinical studies on humans, this safety problem must be assessed by animal testing. On the other hand, if other challenges have been adequately handled as previously mentioned, the skin's high level of immunological responsiveness may offer a chance for MN-based vaccine administration.

4.5 Cost of Microneedle Fabrication

To fully implement microchip-based microneedles into therapeutic applications, current microneedle manufacturing procedures must be enhanced to large-scale production. Although comprehensive economic evaluations of the technology have not yet been completed, it is easy to assume that, similar to any new technology, the clinical use of MNs may be relatively costly because of the intricate fabrication and storage processes as well as the drawn-out approval process [290].

V. MECHANICAL PROPERTIES OF MN

The mechanical properties of the MNs must be considered during the MN design process since they will be exposed to an applied force during epidural implantation. The MNs must be strong enough to prevent failure in the MN array in order to do this [303]. According to Lutton et al. [304], no one test can accurately replicate and monitor the mechanical characteristics of the needle and the implantation of the MN in vivo. As a result, the MN should be subjected to a variety of mechanical tests for characterization. Axial force, transverse force, base plate break, and insertion force are among the several mechanical test kinds performed on MNs. Furthermore, several studies have been conducted to examine the connection between MN production parameters and mechanical characterization [305].

5.1 Transverse Force

The transverse force test entails applying a force using the y-axis parallel to the MN base plate. The transverse fracture force measurement is crucial because the roughness of the skin surface may cause the MN to bend transversely [304]. Furthermore, the transverse force, in addition to the axial force, completes the whole picture of the mechanical characteristic of the MN and hence forecasts the MN's bending behavior after insertion [306]. This test's drawback is that it requires manual alignment of the metal probe with a predetermined MN length [304].

Using the TA.XT-plus Texture Analyzer (Stable Micro Systems, Surrey, UK), Donnelly, et al. determined the transverse failure force of MN arrays [307]. Park et al. conducted a second investigation using a force-displacement station and a microscope to quantify the transverse force [308]. A PDMS arrangement supported the MN vertically on a metal plate under perpendicular stress. After testing the transverse force until the MNs broke, it was shown that displacement rises linearly with an MN base diameter. A micromechanical tester (Instron® Model 5969; Instron, Norwood, MA, USA) was used by Demir et al. [306] to measure the transverse force of the MN (Figure 16B).

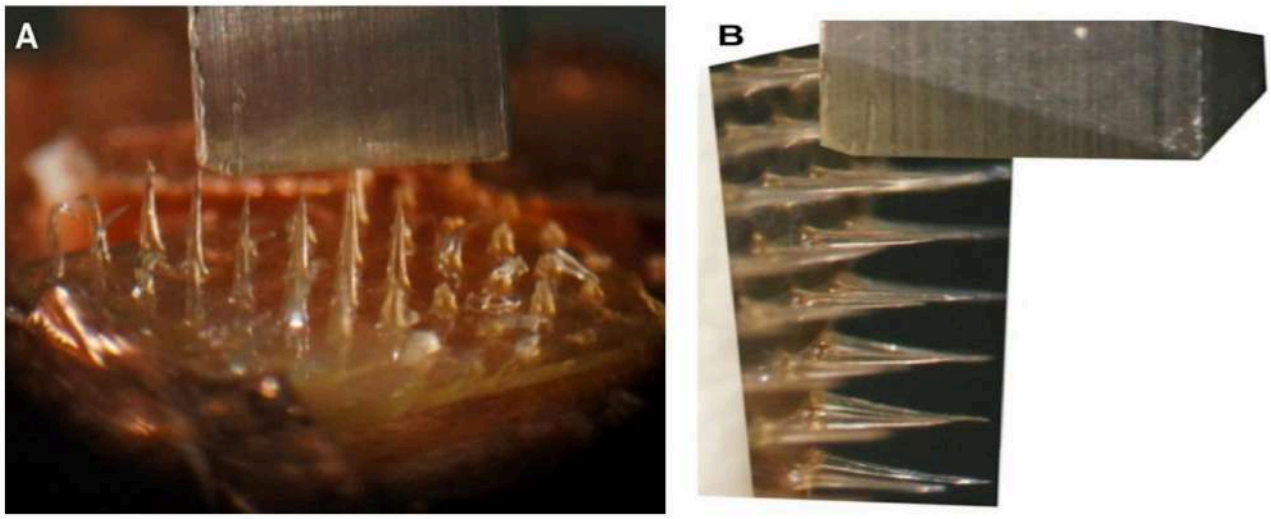

Figure 16: (A)Using the Instron® Model 5969 micromechanical tester, a digital image shows the SA MN placed up against the metal mill to detect the axial fracture force (Instron, Norwood, MA). (B) To evaluate the transverse fracture force using a micromechanical tester (Instron® Model 5969, Instron, Norwood, MA), MN shafts were transversely forced on the metal mill. [306]. Reproduced with permission from Characterization of Polymeric MN Arrays for Transdermal Drug Delivery by Demir et al., published in PLoS One (2013)

5.2 Axial Force

The most popular test is the axial force test, which involves exerting force on the MN array's base as well as the vertically oriented needle tips [307]. This mechanical test is crucial since it establishes the needles' failure force. Since it provides a rough range (expectation) of needle insertion force, knowing the needle failure force measurement is the most significant information, also known as the safety point [309].

Various tools and computation techniques have been used in several axial force investigations to ascertain the MN failure force. Davis et al. computed the force and displacement data [310] to measure the failure (ScopeTest1, EnduraTEC, Minnetonka, MN, USA). Additionally, Demir et al. used a universal testing apparatus (Instron® Model 5969, Instron, Norwood, MA, USA) (Figure 16A) [306] to evaluate the fracture force. Additionally, Khanna et al. used motorized actuators (Thorlabs Motorized Actuators, Morganville, New Jersey, USA) and a compression load cell (LCFA-500gF sensing capacity, Omega Co., Norwalk, CT, USA) to study the axial fracture tests [311]. Using a TA-XT2 Texture Analyzer (Stable Microsystems, Haslemere, UK) and a light microscope (GXMGE-5 digital microscope, Laboratory Analysis Ltd., Devon, UK), Donnelly et al. conducted compression mechanical tests [312]. Using a displacement-force test station (Model 921A, Tricor System, Elgin, IL, USA), Park and Prausnitz assessed the failure test [313].

5.3 Insertion Test

The axial force does not provide an exact measurement like the insertion test, which makes the insertion test more significant and distinct from the axial force. Additionally, this test was conducted on a variety of skin subjects, including humans, rats, and pigs (Figures 17 and 18). The ability to load and apply the medication to the skin is one benefit of utilizing an MN. Even if the fracture force of the needle is simulated by several mechanical tests, it's crucial to confirm the findings using real skin.

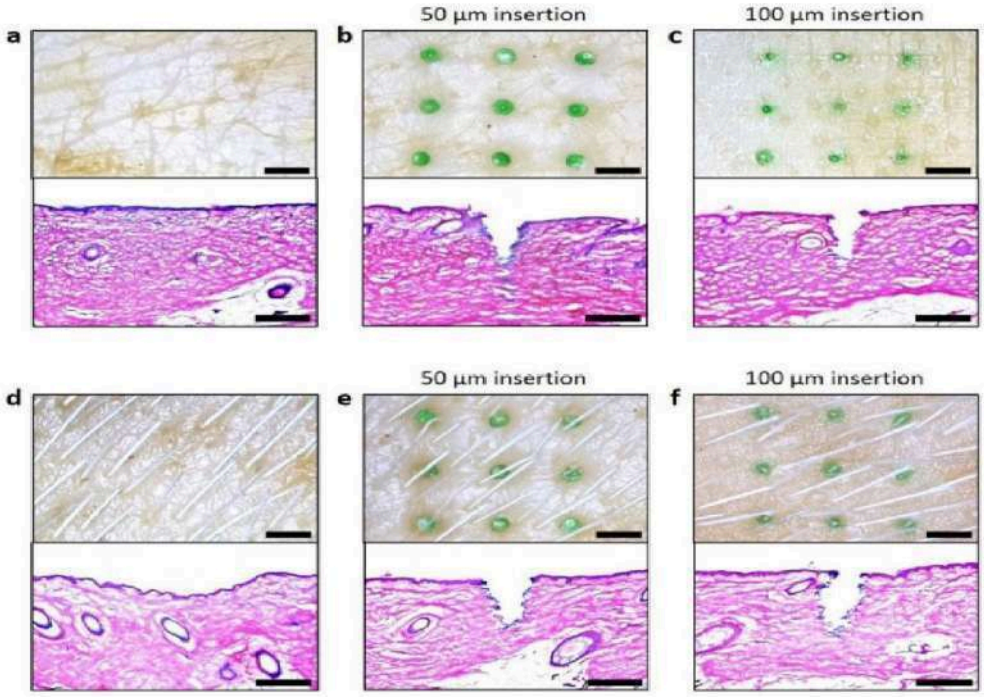

Figure 17: Histological analyses and microscopy pictures of hairy and hairless pig cadaver skin: (a) Skin of hairless pig cadaver before DMN implantation. (b) A 600 µm tall DMN is inserted every 50 µm. The depth of the DMN insertion into the skin was 650 µm. (c) Compared to DMNs implanted 50 µm deep, the base area of those placed 100 µm deep was less visible on the skin's surface. According to a histological analysis, the DMNs were implanted 700 µm deep in the skin. (d) The skin of a hairy pig cadaver before DMN injection. (e) DMNs placed 50 µm deep into hairy skin seemed identical to DMNs implanted into the skin of a hairless pig cadaver.(f) The hairy pig cadaver skin was pierced 700 µm deep by DMNs that were placed 100 µm deep. Scale bars: 500 µm for histology pictures; and 2 mm for microscopy images [314].Source: Shayan F. Lahiji et al., A patchless dissolving MN delivery system providing quick and effective transdermal medication administration; Springer Nature, 2015. Reproduced with permission [300,301]

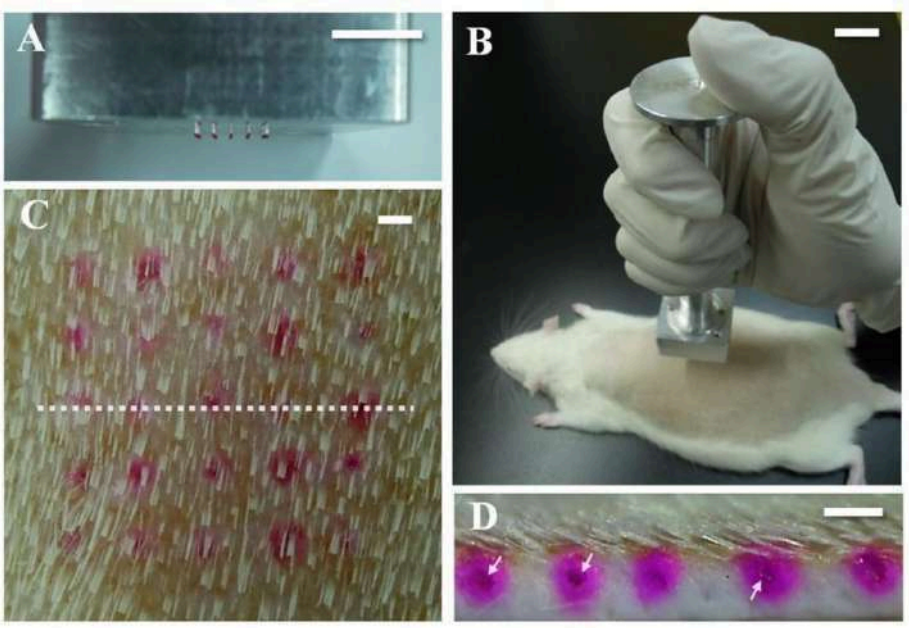

Figure 18: Investigation of in vivo skin penetration: (A) Troy MNs were arranged in an array (5 × 5) using an applicator. (B) The applicator was put on rat dorsal skin vertically by hand. (C) Skin image with Troy MNs added. The vertically sliced line utilized to extract sectional tissue is represented by the white dotted line, and the array of red dots depicts the place where rhodamine B-encapsulated Troy MNs were pierced. (D) Sectional view of the skin. Delivered rhodamine B is shown by red dots in the skin, while undissolved DMNs are indicated by a white arrow. 10 mm (A, B) and 1.0 mm (C, D) scale bars [315]. The Troy MN: A Rapidly Separating, Dissolving MN Formed by Cyclic Contact and Drying on the Pillar (CCDP), by Kim et al., is reproduced here with permission from PLoS One (2015) [301,302]

VI. FROM CLINICAL TRIALS TO COMMERCIAL DEVELOPMENT

MNs have so far been created from several materials utilizing a range of manufacturing techniques, and with a wide range of shapes, either with or without an MN application device. While MNs have been the subject of much research concerning transdermal drug administration and vaccine distribution, these systems may also be tailored to target delivery to other tissues, including hair follicles, the mucosa of the mouth and vagina, and the muscles that control the anal sphincter [315]. These days, MNs are also being investigated for the delivery of drugs to the cornea, sclera, and suprachoroidal region in the eyes [316]. MNs (Dermaroller®, Dermapen®) are already in the advanced stages of research and are being sold for cosmetic skincare. MNs have been studied recently as a component of the monitoring/diagnosis system to enable entirely painless transdermal bodily fluid sampling [317]. In order to demonstrate the effectiveness and safety of MN delivery systems over conventional administration methods, the bulk of these clinical trials employ MN injection systems and MN array-based patches.

For transdermal medication delivery to be effectively created and the finished product to have sufficient and repeatable penetration, the type of MNs and their shape must be carefully chosen. Typically, an MN application device—either impact-insertion or manual hand-held—is required to enable self-administration. A wide range of pharmaceutical firms and research facilities, such as 3M, Zosano Pharma, Alza Corporation, Becton-Dickinson Technologies, Valeritas, Vaxxas, Microneedle Therapy System, Nanopass Technologies Lohmann, Therapie-Systeme AG, and others, are involved in the development of Minnesota-based products.

Only a small number of MN devices are already on the market, and the majority are still in clinical studies. Becton-Dickinson Technologies created the first commercially available MN device, called Soluvia® (Figure 19A). However, some authors contend that this device actually uses very short hollow needles to successfully inject ID using a standard syringe barrel rather than true MN arrays [18]. 2009 saw the launch of Intanza® by Sanofi Pasteur, the first influenza vaccination to target the dermis [318]. The medicine Intanza is removed from use in the European Union in 2018 at the request of the holder of the marketing license, despite several clinical trials showing that the drug's advantages outweigh its hazards [319]. The FDA gave Nanopass Technologies' MicronJet® its approval in February 2010. This single-use MN device was used to administer insulin, lidocaine, and the influenza vaccination intradermally. It is made up of four hollow silicon needles that are less than 500 mm in length and are linked to a plastic device. The business finished a Phase 1 clinical research in 2009 to compare the insulin delivery system's pharmacokinetics and pharmacodynamics while using a standard needle with the Micronjet® [320]. The business created MicronJet600®, a new device version, to enhance device performance, particularly the insertion approach [321]. A clinical trial was conducted in 2019 by Yonsei University to examine the immunogenicity and safety of delivering Bacillus Calmette-Guerin (BCG) using a standard needle vs using the Micronjet600® device (Figure 19B) [322].

Figure 19: Current MN devices. (A) Soluvia®, (B) Micron Jet®600, © Microstructured Transdermal System®, (D) Qtrypta™, (E) SCSMicroinjector®, (F) Microinfusor®, (G)MicroCor®, (H) Bullfrog® Micro-Infusion Device. Image from [230]

VII. MN APPLICATIONS

Researchers, scientists, and industry players are all very interested in MNs. Numerous research has shown that MN has the potential and capacity to be administered in many domains. These include administering medications, administering vaccines, diagnosing illnesses, and applying cosmetics.

7.1 Disease Diagnosis

Several well-established bioassays that collect bodily fluid samples in order to evaluate and track medical conditions can be used to monitor disease diagnosis and treatment efficacy. The existing approaches cause discomfort and call for specific tools, skilled medical staff, and specialized methodologies [323]. On the other hand, bioassay solutions with straightforward installation and painless experience are provided by microneedle technology [323].

Numerous illnesses, including diabetes [324], Alzheimer's [325], and cancer [326] can be identified by a hollow MN. Another use for MNs is in patient health monitoring. To measure the glucose level, for instance, a hollow glass MN may be utilized [327]. Moreover, the MNs system for electrocardiography signal optimization was proposed by O'Mahony et al. [328]. To track alcohol levels in artificial interstitial fluid, an enzyme based on microneedles was functionalized [329]. Early-stage osteoarthritis biomarkers were identified using microneedles containing nanoparticles [208]. Hydrogen peroxide, lactate, dissolved oxygen, and glutamate were detected using microneedles [330].

7.2 Drug Delivery

In 1998, solid silicon MN was used for the first time to deliver drugs [331]. Human growth hormone was applied transdermally to the skin of hairless rats using a dissolvent MN patch [332]. An MN patch filled with caffeine that dissolves was able to regulate the weight of obese mice and function as an anti-obesity therapy [333]. Salmon calcitonin was administered using a coated MN patch [334]. A protein antigen (ovalbumin) was injected into the skin of hairless guinea pigs using a solid microneedle [335]. Insulin [336], BSA [337], and calcein [337] were all delivered using metal MNs and solid silicon MNs. Moreover, MNs have been employed in transdermal permeation of many medications, including paracetamol, ketoprofen, and ibuprofen [338]. Additional medications administered using microneedles include of glycerol, L-ascorbic acid, riboflavin, aspirin, docetaxel, pilocarpine, lidocaine, hydrochloride, and ketoprofen [330]. Some research has successfully achieved microneedle injection into chicken thigh [339], and brain tissue [340], even though the majority of studies employed microneedle array for drug delivery into mice, pigs, and human skin.

7.3 Cosmetic Application

MNs are frequently employed in cosmetic applications, including hair growth and skin therapy (Figure 20). A dissolvable MN patch based on hyaluronic acid was created by Kim et al. to provide ascorbic acid and retinyl retinoate intradermally [341]. Using a solid MN, Kumar et al. demonstrated an improvement in the local delivery of eflornithine (used to treat face hirsutism) both in vitro and in vivo [342]. Moreover, two alopecia areata patients were successfully treated with Minnesota technique [343]. Following therapy, hair growth was observed in these individuals. A MN has been used in successful clinical studies for hypertrophic burn scars [344], atrophic acne scars [345], and atrophic face scarring [346].

Figure 20: The Microneedling Treatment Group Showed Faster Hair Regrowth after One Week [215]. Image from [301,347]

7.4 Vaccine Delivery

One popular kind of MN used for vaccine administration is a dissolvable MN. In place of the conventional hypodermic injection needles used to provide vaccinations, the dissolvable MNs were employed. Dissolvable MNs are biocompatible, reliable, scalable, and do not produce biohazardous waste, in contrast to other forms of MN [348]. Vaccines against malaria, diphtheria [349], influenza [326], hepatitis B [350], HIV [351], and polio [352] were administered by soluble molecular nanoparticles (MNs).

Coated MNs arrays have been successfully employed for vaccination applications, while dissolvable MNs are the most often used form of MNs for vaccine administration [353]. Pigs' immune systems were strengthened in a trial by using a coated MN and the Bacillus Calmette-Guérin (BCG) vaccine, which was easy, safe, and compliant to give [354]. Hepatitis C virus protein was effectively encoded in a DNA vaccine coated on a microneedle in another investigation [355]. In mice, the microneedle was successfully primed for certain cytotoxic T lymphocytes (CTLs). In addition, a coated microneedle containing influenza viral antigen was used to vaccinate mice [356].

Rather than administering the anthrax recombinant protective antigen vaccine by injection, hollow MNs have been employed to do so [357]. In a mouse model, a hollow microneedle was tested as a vaccine against plaque [358]. When compared to intramuscular injection, the immune system responded similarly in a human clinical study employing hollow microneedle influenza vaccination [359].

Table 3: List of A Few Clinically Effective Microneedle Drug Delivery Devices that Can be used to Introduce Medication into Tte Bloodstream [364]

Drug	Microneedle type	Use	Reference
Donepezil HCL	Drug-coated microneedle	Alzheimer's disease	[360]
Sinomenine HCL	Dissolving microneedle	Analgesia, anti-cancer, anti-inflammatory	[361]
Meloxicam	Dissolving microneedle	Arthritis	[362]
5-aminolevulinic acid	Coated microneedle	Skin tumors	[363]

VIII. RESEARCH GAPS AND PROSPECTS FOR THE FUTURE

In contrast to alternative methods, this study presents the advantages of using MN for several applications. Furthermore, a number of studies recommend various materials, manufacturing processes, and needle kinds for the creation of an MN array. A large-scale clinical experiment was suggested for the use of MNs for various applications. Nonetheless, the field of MN array manufacturing still has deficiencies. We provide an overview for MNs in this part about the use of next-generation techniques, such as additive manufacturing, for COVID-19 testing and immunization, as well as the scaling up of manufacturing processes and predictive modeling of materials and manufacturing techniques.

8.1 Forecasting Model for MN Production

There is insufficient knowledge of the design parameters for the manufacture of MNs, which calls for more investigation. By examining the PDMS MN's dimensions with various laser power and scanning speed values, Chung and Tu expanded their research on producing the MN array to include merging CO2 laser processing and polymer molding [366]. The impact of hole width and pulse shot number on fabrication depth was investigated by Aoyagi et al. Additionally, they observed that sidewall smoothness was influenced by both hole diameter and repetition rate [367]. Nevertheless, no research has been done on methods of fabricating MNs arrays by process parameter adjustment. The performance of manufacturing processes has been improved in the literature using a variety of predictive model types [368–373], which may be expanded for MN creation. Previous research has shown that new manufacturing techniques combined with computer modeling [374–379] may produce complex biomolecules for use in biomedical applications. Moreover, a prediction model that connects manufacturing factors to drug elution characteristics and sensing applications is needed.

8.2 MN and Additive Manufacturing

A cheap cost, shorter fabrication time, and high-quality resolution are all provided by the promising technique known as additive manufacturing [380,381]. Compared to traditional MN manufacturing methods, the device size and formulation may be changed with few postprocessing steps, therefore fabricating an MN array with a 3D printer would be beneficial. Direct-write techniques [382–390] can also be applied to coat MNs with various biomolecules for effective medication release. Johnson and Procopio recently completed the first investigation in which they manufactured an MN structure using a commercial 3D printer [391]. To create tiny needles, they employed an Autodesk Ember printer with decreased layer height and enhanced antialiasing. An inexpensive SLA 3D printer was used in another recent work to manufacture MN arrays [392]. This investigation was expanded to evaluate the insertion of MN into the skin using a 30N force.

8.3 Scaling Up of Manufacturing Process

The possibility for large-scale MN manufacture is highly sought after given the recent rise in MN applications and the dearth of commercial MN goods (there are now just 13 MN items available)

[393]. More understanding of chemistry and manufacturing materials, according to Bhatnagar et al., would enable enterprises to meet their financial targets and realize higher profits and large-scale production [394]. To create a single MN array, the majority of existing MN manufacturing techniques need many phases [353]. By addressing this constraint, new research opportunities of the decrease or integration of the number of processes necessary for the fabrication of an MN become available.

8.4 Covid19 and MN

The MN strategy is a strong contender to combat the coronavirus (COVID-19) pandemic, as its effects are being felt globally. MN-based oropharyngeal swabs were presented by Chen et al. [395] to lower the number of false negative results in COVID-19 testing. This idea enables highly efficient viral capture, allowing medical professionals to distinguish between positive and negative samples. Since the COVID-19 vaccination is now accessible, those who are capable of self-administering the shot may receive it from MNs.

8.5 Next MN Generation

Several investigations have used synthetic MN to provide medications and vaccinations in vivo. Making an MN capable of delivering macromolecules with large molecular weights and high hydrophilicity, however, is an impending problem [396,397–399]. Irritation, skin allergies, and redness are other problems related to utilizing an MN for medication administration [400]. There are several MN devices on the market, such as the Dermaroller, however, no biodegradable polymer MN has yet to be released for sale [401]. Furthermore, no MN that may include protein products is available for purchase [402].

IX. CONCLUSION

Achieving effective MN mediates transdermal and intradermal distribution mostly depends on breaking through the stratum corneum barrier. MNs technology in the era of transdermal medication administration is summed up in this study. Because of its benefits, a lot of research and studies have been done on the creation of MNs. This study has provided illustrations of several MN design types, materials, and production techniques.

Many MN systems with unique delivery mechanisms have been created and deployed in the last few decades to deliver tiny or large compounds. As this thorough review highlights, recent studies have demonstrated that transdermal transport efficiency of small molecules, salt forms, excipients, and other formulation parameters is improved by transiently disrupting the skin microchannel lifespan. The synergistic impact of coupled enhancement in addition to MN therapy, vaccinations, and intradermal and transdermal distribution of macromolecules, including therapeutic peptides and proteins, were discussed. Additionally, the literature examines MN mechanical testing and their characterisation.

In conclusion, this work highlights the research deficit related to MN manufacturing. Despite the fact that MNs are mediating a number of novel transdermal products, they have not yet realized their full potential. It is becoming more and more clear that there is a gap in permitting cost-effective manufacturing for large-volume manufacture of MNs as our understanding of MN- mediated grows.

Funding

This research received no external funding.

Conflicts of Interest

Regarding this work, the writers have no conflicts of interest to disclose.

REFERENCE

1. Scheuplein, R.J.; Blank, I.H. Permeability of the skin. *Physiol. Rev.* 1971, *51*, 702– 747. [CrossRef] [PubMed].
2. Morrow, D.I. J.; Mc Carron, P.A.; Woolfson, A.D.; Donnelly, R.F. Innovative Strategies for Enhancing Topical and Transdermal Drug Delivery. *Open Drug Deliv. J.* 2007, *1*,36–59. [CrossRef]

3. Bourget, L. Überdie Resorption der Salicylsäure durch die Hautunddie Behandlung des akuten Gelen krheum- atismus. *Ther. Monatsh.* 1893, *7*, 531–539.
4. Surber, C.; Smith, E.W. The mystical effects of dermatological vehicles. *Dermatology* 2005, *210*,157–168. [CrossRef]
5. Blank, I.H. Further observations on factors which influence the water content of the stratumcorneum. *J. Investig. Dermatol.* 1953, *21*,259–271. [CrossRef]
6. Scheuplein, R.J. Mechanism of percutaneous absorption.II. Transient diffusion and the relative importance of various routes of skin penetration .*J. Invest. Dermatol.*1967, *48*, 79– 88. [CrossRef]
7. Thomas, B.J.; Finnin, B.C. The transdermal revolution. *Drug Discov. Today* 2004, *9*,697–703. [CrossRef]
8. Yousef, H., Alhajj, M., & Sharma, S., 2019. Anatomy, skin (integument), epidermis.
9. Boer, M.; Duchnik, E.; Maleszka, R.; Marchlewicz, M. Structural and Biophysical Characteristics of Human Skin in Maintaining Proper Epidermal Barrier Function. Adv. Dermatol. Allergol. 2016, 33, 1–5. [CrossRef] [PubMed]
10. Kolarsick, P.A.J.; Kolarsick, M.A.; Goodwin, C. Anatomy and Physiology of the Skin. J. Dermatol. Nurses Assoc. 2011, 3, 203–213. [CrossRef]
11. Roberts, M.S.; Cheruvu, H.S.; Mangion, S.E.; Alinaghi, A.; Benson, H.A.E.; Mohammed, Y.; Holmes, A.; van der Hoek, J.; Pastore, M.; Grice, J.E. Topical Drug Delivery: History, Percutaneous Absorption, and Product Development. Adv. Drug Deliv. Rev. 2021, 177, 113929. [CrossRef] [PubMed]
12. Ingrole, R.S.; Azizoglu, E.; Dul, M.; Birchall, J.C.; Gill, H.S.; Prausnitz, M.R. Trends of Microneedle Technology in the Scientific Literature, Patents, Clinical Trials and Internet Activity. Biomaterials 2021, 267, 120491. [CrossRef] [PubMed]
13. Sharma, G.; Alle, M.; Chakraborty, C.; Kim, J.-C. Strategies for Transdermal Drug Delivery against Bone Disorders: A Preclinical and Clinical Update. J. Control. Release 2021, 336, 375–395. [CrossRef] [PubMed]
14. Zaid Alkilani, A.; McCrudden, M.T.; Donnelly, R.F. Transdermal Drug Delivery: Innovative Pharmaceutical Developments Based on Disruption of the Barrier Properties of the Stratum Corneum. Pharmaceutics 2015, 7, 438–470. [CrossRef] [PubMed]
15. Donnelly, R.F.; Singh, T.R.R.; Larrañeta, E.; McCrudden, M.T. Microneedles for Drug and Vaccine Delivery and Patient Monitoring; John Wiley & Sons: Hoboken, NJ, USA, 2018.
16. Ramadon, D.; McCrudden, M.T.C.; Courtenay, A.J.; Donnelly, R.F. Enhancement Strategies for Transdermal Drug Delivery Systems: Current Trends and Applications. Drug Deliv. Transl. Res. 2022, 12, 758–791. [CrossRef]
17. Mahmood, S., Taher, M., Mandal, U.K., 2014. Experimental design and optimization of raloxifene hydrochloride loaded nano-transfersomes for transdermal application. Int. J. Nanomed. 9, 4331–4346.
18. Rai, V.K., Mishra, N., Yadav, K.S., Yadav, N.P., 2018. Nanoemulsion as pharmaceutical carrier for dermal and transdermal drug delivery: formulation development, stability issues, basic considerations and applications. J. Control. Release 270, 203–225.
19. Hathout, R.M., Woodman, T.J., Mansour, S., Mortada, N.D., Geneidi, A.S., Guy, R.H., 2010. Microemulsion formulations for the transdermal delivery of testosterone. Eur. J. Pharm. Sci. 40 (3), 188–196.
20. Tajbakhsh, M., Saeedi, M., Akbari, J., Morteza-Semnani, K., Nokhodchi, A., Hedaya- tizadeh-Omran, A., 2020. An investigation on parameters affecting the optimization of testosterone enanthate loaded solid nanoparticles for enhanced trans dermal delivery. Physicochem. Eng. Aspects Colloids Surf. A 124437.
21. Mittapally, S., Taranum, R., Parveen, S., 2018. Microneedles-a potential transdermal drug delivery. Int. J. Pharma. Res. Health Sci. 6 (3), 2579–2585.
22. Mahmood, S., Mandal, U.K., Chatterjee, B., 2018. Transdermal delivery of raloxifene HCl via ethosomal system: formulation, advanced characterizations and pharmacokinetic evaluation. Int. J. Pharm. 542 (1–2), 36–46.

23. Haque, T., Talukder, M.M.U., 2018. Chemical enhancer: a simplistic way to modulate barrier function of the stratum corneum. Adv. Pharm. Bull. 8 (2), 169.
24. Ye, Y., Yu, J., Wen, D., Kahkoska, A.R., Gu, Z., 2018. Polymeric microneedles for trans dermal protein delivery. Adv. Drug Deliv. Rev. 127, 106–118.
25. Alyautdin, R., Khalin, I., Nafeeza, M.I., Haron, M.H., Kuznetsov, D., 2014. Nanoscale drug delivery systems and the blood–brain barrier. Int. J. Nanomed. 9, 795–811.
26. Iqbal, N., Vitorino, C., Taylor, K.M., 2017. How can lipid nanocarriers improve trans dermal delivery of olanzapine? Pharm. Dev. Technol. 22 (4), 587–596.
27. Donnelly, R.F., Singh, T.R.R., Garland, M.J., Migalska, K., Majithiya, R., McCrudden, C.M., Woolfson, A.D., 2012a. Hydrogel-forming microneedle arrays for enhanced transdermal drug delivery. Adv. Funct. Mater. 22 (23), 4879–4890.
28. Guy, R.H. &Hadgraft, J. (eds.) Transdermal Drug Delivery (Marcel Dekker, New York; 2003).
29. Williams, A. Transdermal and Topical Drug Delivery (Pharmaceutical Press, London; 2003).
30. Prausnitz, M.R., Mitragotri, S. & Langer, R. Current status and future potential of trans dermal drug delivery. Nat. Rev. Drug Discov. 3, 115–124 (2004).
31. Bronaugh, R.L. & Maibach, H.I. (eds.) Percutaneous Absorption, edn. 4 (Marcel Dekker, New York; 2005).
32. Foldvari, M., Babiuk, S. & Badea, I. DNA delivery for vaccination and therapeutics through the skin. Curr. Drug Deliv. 3, 17–28 (2006).
33. Kshirsagar NA. Drug delivery systems. Indian J Pharmacol, 2000; 32(4):S54–61.
34. Patel D, Chaudhary SA, Parmar B, Bhura N. Transdermal drug delivery system: a review. Pharma Innov, 2012; 1(4):66–75.
35. Chetkowski RJ, Meldrum DR, Steingold KA, Randle D, Lu JK, Eggena P, Hershman JM, Alkjaersig NK, Fletcher AP, Judd HL. Biologic effects of transdermal estradiol. N Engl J Med, 1986; 314(25):1615–20.
36. Banerjee S, Chattopadhyay P, Ghosh A, Datta P, Veer V. Aspect of adhesives in transdermal drug delivery systems. Int J AdhesAdhes, 2014; 50:70–84.
37. Rayment CM, Kaul AF, Garfield JM. Comparative acceptance of three transdermal nitroglycerin placebo patches. Am J Hosp Pharm, 1985; 42:1362–5.
38. Kesarwani A, Yadav AK, Singh S, Gautam H, Singh HN, Sharma A, Yadav C. Theoretical aspects of transdermal drug delivery system. Bull Pharm Res, 2013; 3(2):78–89.
39. Wiedersberg S, Guy RH. Transdermal drug delivery: 30+ years of war and still fighting! J Control Release, 2014; 190:150–6.
40. Peng, S.; Cheng, L.; Wu, Q.; Li, Y.; Ran, L.; Wang, W.; Huang, K.; Zhu, R.; Xue, S.; Zhou, C.; et al. A Modified Hyaluronic Acid-Based Dissolving Microneedle Loaded With Daphnetin Improved the Treatment of Psoriasis. Front. Bioeng. Biotechnol. 2022, 10, 900274. [CrossRef]
41. Ingrole, R.S.; Azizoglu, E.; Dul, M.; Birchall, J.C.; Gill, H.S.; Prausnitz, M.R. Trends of Microneedle Technology in the Scientific Literature, Patents, Clinical Trials and Internet Activity. Biomaterials 2021, 267, 120491. [CrossRef] [PubMed]
42. Makvandi, P.; Jamaledin, R.; Chen, G.; Baghbantaraghdari, Z.; Zare, E.N.; Di Natale, C.; Onesto, V.; Vecchione, R.; Lee, J.; Tay, F.R.; et al. Stimuli-Responsive Transdermal Microneedle Patches. Mater. Today 2021, 47, 206–222. [CrossRef]
43. Hu,X.; Zhang, H.; Wang, Z.; Shiu, C.Y.A.; Gu, Z. Microneedle Array Patches Integrated with Nanoparticles for Therapy and Diagnosis. Small Struct. 2021, 2, 2000097. [CrossRef]
44. Makvandi, P.; Kirkby, M.; Hutton, A.R.; Shabani, M.; Yiu, C.K.; Baghbantaraghdari, Z.; Jamaledin, R.; Carlotti, M.; Mazzolai, B.; Mattoli, V. Engineering Microneedle Patches for Improved Penetration: Analysis, Skin Models and Factors Affecting Needle Insertion. Nano-Micro Lett. 2021, 13, 1–41. [CrossRef]
45. Yang, Y.; Song, W.; Wang, N.; Ren, Y.; Liu, H. Tip- Concentrated Microneedle Patch Delivering Everolimus for Therapy of Multiple

Sclerosis. Biomater. Adv. 2022, 135, 212729. [CrossRef]
46. Donnelly, R.F.; Raj Singh, T.R.; Woolfson, A.D. Microneedle-Based Drug Delivery Systems: Microfabrication, Drug Delivery, and Safety. Drug Deliv. 2010, 17, 187–207. [Cross Ref]
47. VanderMaaden, K.; Jiskoot, W.; Bouwstra, J. Microneedle Technologies for (Trans)Dermal Drug and Vaccine Delivery. J. Control. Release 2012, 161, 645–655. [CrossRef]
48. Tuan-Mahmood, T.-M.; McCrudden, M.T.; Torrisi, B.M.; McAlister, E.; Garland, M.J.; Singh, T.R.R.; Donnelly, R.F. Microneedles for Intradermal and Transdermal Drug Delivery. Eur. J. Pharm. Sci. 2013, 50, 623–637. [Cross Ref]
49. Pierre, M.B.R.; Rossetti, F.C. Microneedle-Based Drug Delivery Systems for Transdermal Route. Curr. Drug Targets 2014, 15, 281–291. [CrossRef]
50. Yadav, P.R.; Han, T.; Olatunji, O.; Pattanayek, S.K.; Das, D.B. Mathematical Modelling, Simulation and Optimisation of Microneedles for Transdermal Drug Delivery: Trends and Progress. Pharmaceutics 2020, 12, 693. [CrossRef]
51. Nguyen, T.T.; Nguyen, T.T.D.; Van Vo, G. Advances of Microneedles in Hormone Delivery. Biomed. Pharmacother. 2022, 145, 112393. [CrossRef]
52. Ali, M.; Namjoshi, S.; Benson, H.A.E.; Kumeria, T.; Mohammed, Y. Skin Biomechanics: Breaking the Dermal Barriers with Microneedles. Nano TransMed 2022, 1, e9130002. [CrossRef]
53. Kearney, M.-C.; Caffarel-Salvador, E.; Fallows, S.J.; McCarthy, H.O.; Donnelly, R.F. Microneedle-Mediated Delivery of Donepezil: Potential for Improved Treatment Options in Alzheimer's Disease. Eur. J. Pharm. Biopharm. 2016, 103, 43–50. [CrossRef]
54. McCrudden, M.T.C.; Alkilani, A.Z.; McCrudden, C.M.; McAlister, E.; McCarthy, H.O.; Woolfson, A.D.; Donnelly, R.F. Design and Physicochemical Characterisation of Novel Dissolving Polymeric Microneedle Arrays for Transdermal Delivery of HighQ Dose, LowMolecular Weight Drugs. J. Control. Release 2014, 180, 71–80. [CrossRef]
55. Chen, X.; Wang, L.; Yu, H.; Li, C.; Feng, J.; Haq, F.; Khan, A.; Khan, R.U. Preparation, Properties and Challenges of the Microneedles-Based Insulin Delivery System. J. Control. Release 2018, 288, 173–188. [CrossRef]
56. Liu, T.; Chen, M.; Fu, J.; Sun, Y.; Lu, C.; Quan, G.; Pan, X.; Wu, C. Recent Advances in Microneedles-Mediated Transdermal Delivery of Protein and Peptide Drugs. Acta Pharm. Sin. B 2021, 11, 2326–2343. [CrossRef]
57. Stinson, J.A.; Boopathy, A.V.; Cieslewicz, B.M.; Zhang, Y.; Hartman, N.W.; Miller, D.P.; Dirckx, M.; Hurst, B.L.; Tarbet, E.B.; Kluge, J.A. Enhancing Influenza Vaccine Immunogenicity and Efficacy through Infection Mimicry Using Silk Microneedles. Vaccine 2021, 39, 5410–5421. [CrossRef]
58. Yin, Y.; Su, W.; Zhang, J.; Huang, W.; Li, X.; Ma, H.; Tan, M.; Song, H.; Cao, G.; Yu, S. Separable Microneedle Patch to Protect and Deliver DNA Nanovaccines against COVID-19. ACS Nano 2021, 15, 14347–14359. [CrossRef]
59. Choi, S.Y.; Kwon, H.J.; Ahn, G.R.; Ko, E.J.; Yoo, K.H.; Kim, B.J.; Lee, C.; Kim, D. Hyaluronic Acid Microneedle Patch for the Improvement of Crow's Feet Wrinkles. Dermatol. Ther. 2017, 30, e12546. [CrossRef]
60. Mohammed, Y.H.; Yamada, M.; Lin, L.L.; Grice, J.E.; Roberts, M.S.; Raphael, A.P.; Benson, H.A.E.; Prow, T.W. Microneedle Enhanced Delivery of Cosmeceutically Relevant Peptides in Human Skin. PLoS ONE 2014, 9, e101956. [CrossRef] [PubMed]
61. Park, Y.; Park, J.; Chu, G.S.; Kim, K.S.; Sung, J.H.; Kim, B. Transdermal Delivery of Cosmetic Ingredients Using Dissolving Polymer Microneedle Arrays. Biotechnol. Bioprocess Eng. 2015, 20, 543–549. [CrossRef]
62. Niu, L.; Chu, L.Y.; Burton, S.A.; Hansen, K.J.; Panyam, J.Intradermal Delivery of Vaccine Nanoparticles Using HollowMicroneedle Array Generates Enhanced and Balanced Immune Response. J. Control. Release 2019, 294, 268–278. [CrossRef]

63. Peng, K.; Vora, L.K.; Tekko, I.A.; Permana, A.D.; Domínguez-Robles, J.; Ramadon, D.; Chambers, P.; McCarthy, H.O.; Larrañeta, E.; Donnelly, R.F. Dissolving Microneedle Patches Loaded with Amphotericin B Microparticles for Localised and Sustained Intradermal Delivery: Potential for Enhanced Treatment of Cutaneous Fungal Infections. J. Control. Release 2021, 339, 361–380. [CrossRef]
64. Zhang, D.; Das, D.B.; Rielly, C.D. An Experimental Study of Microneedle-Assisted Microparticle Delivery. J. Pharm. Sci. 2013, 102, 3632–3644. [CrossRef] [PubMed]
65. Roth, G.A.; Picece, V.C.T.M.; Ou, B.S.; Luo, W.; Pulendran, B.; Appel, E.A. Designing Spatial and Temporal Control of Vaccine Responses. Nat. Rev. Mater. 2022, 7, 174–195. [CrossRef] [PubMed]
66. Saha, I.; Rai, V.K. Hyaluronic Acid Based Microneedle Array: Recent Applications in Drug Delivery and Cosmetology. Carbohydr. Polym. 2021, 267, 118168. [CrossRef]
67. Kuwentrai, C.; Yu, J.; Rong, L.; Zhang, B.-Z.; Hu, Y.-F.; Gong, H.-R.; Dou, Y.; Deng, J.; Huang, J.-D.; Xu, C. Intradermal Delivery of Receptor-Binding Domain of SARS-CoV-2 Spike Protein with Dissolvable Microneedles to Induce Humoral and Cellular Responses in Mice. Bioeng. Transl. Med. 2021, 6, e10202. [CrossRef]
68. Ali, M.; Namjoshi, S.; Benson, H.A.; Mohammed, Y.; Kumeria, T. Dissolvable Polymer Microneedles for Drug Delivery and Diagnostics. J. Control. Release 2022, 347, 561–589. [CrossRef]
69. Naveen, N.R.; Goudanavar, P.S.; Ramesh, B.; Kumar, G.K. Prospection of Fabrication Techniques and Material Selection of Microneedles for Transdermal Drug Delivery: An Update on Clinical Trials. Mater. Today Proc. 2022, 69, 187–192.
70. Rajput, A.; Kulkarni, M.; Deshmukh, P.; Pingale, P.; Garkal, A.; Gandhi, S.; Butani, S. A Key Role by Polymers in Microneedle Technology: A New Era. Drug Dev. Ind. Pharm. 2022, 47, 1713–1732. [CrossRef]
71. Dabholkar, N.; Gorantla, S.; Waghule, T.; Rapalli, V.K.; Kothuru, A.; Goel, S.; Singhvi, G. Biodegradable Microneedles Fabricated with Carbohydrates and Proteins: Revolutionary Approach for Transdermal Drug Delivery. Int. J. Biol. Macromol. 2021, 170, 602–621. [CrossRef]
72. Zhou,P.; Zhao, S.; Huang, C.; Qu, Y.; Zhang, C. Bletilla Striata Polysaccharide Microneedle for Effective Transdermal Administration of Model Protein Antigen. Int. J. Biol. Macromol. 2022, 205, 511–519. [CrossRef]
73. Damiri, F.; Kommineni, N.; Ebhodaghe, S.O.; Bulusu, R.; Jyothi, V.G.S.; Sayed, A.A.; Awaji, A.A.; Germoush, M.O.; Al-Malky, H.S.; Nasrullah, M.Z. Microneedle-Based Natural Polysaccharide for Drug Delivery Systems (DDS): Progress and Challenges. Pharmaceuticals 2022, 15, 190. [CrossRef]
74. Dharadhar, S.; Majumdar, A.; Dhoble, S.; Patravale, V. Microneedles for Transdermal Drug Delivery: A Systematic Review. Drug Dev. Ind. Pharm. 2019, 45, 188–201. [CrossRef]
75. Permana, A.D.; Anjani, Q.K.; Sartini; Utomo, E.; Volpe-Zanutto, F.; Paredes, A.J.; Evary, Y.M.; Mardikasari, S.A.; Pratama, M.R.; Tuany, I.N.; et al. Selective Delivery of Silver Nanoparticles for Improved Treatment of Biofilm Skin Infection Using Bacteria-Responsive Microparticles Loaded into Dissolving Microneedles. Mater. Sci. Eng. C 2021, 120, 111786. [CrossRef]
76. Caudill, C.; Perry, J.L.; Iliadis, K.; Tessema, A.T.; Lee, B.J.; Mecham, B.S.; Tian, S.; DeSimone, J.M. Transdermal Vaccination via 3D-Printed Microneedles Induces Potent Humoral and Cellular Immunity. Proc. Natl. Acad. Sci. USA 2021, 118, e2102595118. [CrossRef]
77. Economidou, S.N.; Pissinato Pere, C.P.; Okereke, M.; Douroumis, D. Optimisation of Design and Manufacturing Parameters of 3D Printed Solid Microneedles for Improved Strength, Sharpness, and Drug Delivery. Micromachines 2021, 12, 117. [CrossRef]
78. Chen,Z.; Wu, H.; Zhao, S.; Chen, X.; Wei, T.; Peng, H.; Chen, Z. 3D-Printed Integrated Ultrasonic Microneedle Array for Rapid Transdermal Drug Delivery. Mol. Pharm. 2022, 19, 3314–3322. [CrossRef] [PubMed]

79. Nguyen, H.X.; Bozorg, B.D.; Kim, Y.; Wieber, A.; Birk, G.; Lubda, D.; Banga, A.K. Poly (Vinyl Alcohol) Microneedles: Fabrication, Characterization, and Application for Transdermal Drug Delivery of Doxorubicin. Eur. J. Pharm. Biopharm. 2018, 129, 88–103. [CrossRef] [PubMed]
80. Nguyen, H.X.; Banga, A.K. Delivery of Methotrexate and Characterization of Skin Treated by Fabricated PLGA Microneedles and Fractional Ablative Laser. Pharm. Res. 2018, 35, 1–20. [CrossRef]
81. Kalluri, H.; Banga, A.K. Formation and Closure of Microchannels in Skin Following Microporation. Pharm. Res. 2011, 28, 82–94. [CrossRef] [PubMed]
82. Brogden, N.K.; Banks, S.L.; Crofford, L.J.; Stinchcomb, A.L. Diclofenac Enables Unprecedented Week-Long Microneedle-Enhanced Delivery of a Skin Impermeable Medication in Humans. Pharm. Res. 2013, 30, 1947–1955. [CrossRef] [PubMed]
83. Gupta, J.; Gill, H.S.; Andrews, S.N.; Prausnitz, M.R. Kinetics of Skin Resealing after Insertion of Microneedles in Human Subjects. J. Control. Release 2011, 154, 148–155. [CrossRef]
84. Brogden, N.K.; Milewski, M.; Ghosh, P.; Hardi, L.; Crofford, L.J.; Stinchcomb, A.L. Diclofenac Delays Micropore Closure Following Microneedle Treatment in Human Subjects. J. Control. Release 2012, 163, 220–229. [CrossRef]
85. Haridass, I.N.; Wei, J.C.; Mohammed, Y.H.; Crichton, M.L.; Anderson, C.D.; Henricson, J.; Sanchez, W.Y.; Meliga, S.C.; Grice, J.E.; Benson, H.A. Cellular Metabolism and Pore Lifetime of Human Skin Following Microprojection Array Mediation. J. Control. Release 2019, 306, 59–68.
86. Avcil, M.; Çelik, A. Microneedles in Drug Delivery: Progress and Challenges. Micromachines 2021, 12, 1321. [CrossRef]
87. Chen, M.-C.; Huang, S.-F.; Lai, K.-Y.; Ling, M.-H. Fully Embeddable Chitosan Microneedles as a Sustained Release Depot for Intradermal Vaccination. Biomaterials 2013, 34, 3077–3086. [CrossRef]
88. Kim, Y.-C.; Park, J.-H.; Prausnitz, M.R. Microneedles for Drug and Vaccine Delivery. Adv. Drug Deliv. Rev. 2012, 64, 1547–1568. [CrossRef] [PubMed]
89. Nguyen, H.X.; Banga, A.K. Fabrication, Characterization and Application of Sugar Microneedles for Transdermal Drug Delivery. Ther. Deliv. 2017, 8, 249–264. [CrossRef]
90. Nguyen, H.X.; Banga, A.K. Enhanced Skin Delivery of Vismodegib by Microneedle Treatment. Drug Deliv. Transl. Res. 2015, 5, 407–423. [CrossRef]
91. Cheung, K.; Han, T.; Das, D.B. Effect of Force of Microneedle Insertion on the Permeability of Insulin in Skin. J. Diabetes Sci. Technol. 2014, 8, 444–452. [CrossRef]
92. Yan, G.; Warner, K.S.; Zhang, J.; Sharma, S.; Gale, B.K. Evaluation Needle Length and Density of Microneedle Arrays in the Pretreatment of Skin for Transdermal Drug Delivery. Int. J. Pharm. 2010, 391, 7–12. [CrossRef]
93. Kumar, A.; Li, X.; Sandoval, M.A.; Rodriguez, B.L.; Sloat, B.R.; Cui, Z. Permeation of Antigen Protein-Conjugated Nanoparticles and Live Bacteria through Microneedle-Treated Mouse Skin. Int. J. Nanomed. 2011, 6, 1253–1264. [CrossRef]
94. Li, G.; Badkar, A.; Kalluri, H.; Banga, A.K. Microchannels Created by Sugar and Metal Microneedles: Characterization by Microscopy, Macromolecular Flux and Other Techniques. J. Pharm. Sci. 2010, 99, 1931–1941. [CrossRef] [PubMed]
95. Zhang, S.; Qiu, Y.; Gao, Y. Enhanced Delivery of Hydrophilic Peptides in Vitro by Transdermal Microneedle Pretreatment. Acta Pharm. Sin. B 2014, 4, 100–104. [CrossRef] [PubMed]
96. Wu, Y.; Gao, Y.; Qin, G.; Zhang, S.; Qiu, Y.; Li, F.; Xu, B. Sustained Release of Insulin through Skin by Intradermal Microdelivery System. Biomed. Microdevices 2010, 12, 665–671. [CrossRef] [PubMed]
97. Li, Q.Y.; Zhang, J.N.; Chen, B.Z.; Wang, Q.L.; Guo, X.D. A Solid Polymer Microneedle Patch Pretreatment Enhances the Permeation of

Drug Molecules into the Skin. RSC Adv. 2017, 7, 15408–15415. [CrossRef]
98. Martanto, W.; Davis, S.P.; Holiday, N.R.; Wang, J.; Gill, H.S.; Prausnitz, M.R. Transdermal Delivery of Insulin Using Microneedles in Vivo. Pharm. Res. 2004, 21, 947–952. [CrossRef]
99. Qiu,Y.; Qin, G.; Zhang, S.; Wu, Y.; Xu, B.; Gao, Y. Novel Lyophilized Hydrogel Patches for Convenient and Effective Administration of Microneedle- Mediated Insulin Delivery. *Int.J. Pharm.*2012,*437*,51–56.[CrossRef]
100. Shrestha, P.; Stoeber, B. Fluid Absorption by Skin Tissue during Intradermal Injections through Hollow Microneedles. Sci. Rep. 2018, 8, 1–13. [CrossRef] [PubMed]
101. Donnelly, R.F.; Singh, T.R.R.; Larrañeta, E.; McCrudden, M.T. Microneedles for Drug and Vaccine Delivery and Patient Monitoring; John Wiley & Sons: Hoboken, NJ, USA, 2018.
102. Zaid Alkilani, A.; McCrudden, M.T.; Donnelly, R.F. Transdermal Drug Delivery: Innovative Pharmaceutical Developments Based on Disruption of the Barrier Properties of the Stratum Corneum. Pharmaceutics 2015, 7, 438–470. [CrossRef] [PubMed]
103. Terashima, S.; Tatsukawa, C.; Takahashi, T.; Suzuki, M.; Aoyagi, S. Fabrication of Hyaluronic Acid Hollow Microneedle Array. Jpn. J. Appl. Phys. 2020, 59, SIIJ03. [CrossRef]
104. Migalska, K.; Morrow, D.I.J.; Garland, M.J.; Thakur, R.; Woolfson, A.D.; Donnelly, R.F. Laser-Engineered Dissolving Microneedle Arrays for Transdermal Macromolecular Drug Delivery. Pharm. Res. 2011, 28, 1919– 1930. [CrossRef]
105. Harvey, A.J.; Kaestner, S.A.; Sutter, D.E.; Harvey, N.G.; Mikszta, J.A.; Pettis, R.J. Microneedle-Based Intradermal Delivery Enables Rapid Lymphatic Uptake and Distribution of Protein Drugs. Pharm. Res. 2011, 28, 107–116. [CrossRef] [PubMed]
106. McVey, E.; Hirsch, L.; Sutter, D.E.; Kapitza, C.; Dellweg, S.; Clair, J.; Rebrin, K.; Judge, K.; Pettis, R.J. Pharmacokinetics and Postprandial Glycemic Excursions Following Insulin Lispro Delivered by Intradermal Microneedle or Subcutaneous Infusion. J. Diabetes Sci. Technol. 2012, 6, 743–754. [CrossRef] [PubMed]
107. Gupta, J.; Felner, E.I.; Prausnitz, M.R. Rapid Pharmacokinetics of Intradermal Insulin Administered Using Microneedles in Type 1 Diabetes Subjects. Diabetes Technol. Ther. 2011, 13, 451–456. [CrossRef]
108. McAllister, D.V.; Wang, P.M.; Davis, S.P.; Park, J.-H.; Canatella, P.J.; Allen, M.G.; Prausnitz, M.R. Microfabricated Needles for Transdermal Delivery of Macromolecules and Nanoparticles: Fabrication Methods and Transport Studies. Proc. Natl. Acad. Sci. USA2003, 100, 13755–13760. [CrossRef]
109. Xenikakis, I.; Tsongas, K.; Tzimtzimis, E.K.; Katsamenis, O.L.; Demiri, E.; Zacharis, C.K.; Georgiou, D.; Kalogianni, E.P.; Tzetzis, D.; Fatouros, D.G. Transdermal Delivery of Insulin across Human Skin in Vitro with 3D Printed Hollow Microneedles. J. Drug Deliv. Sci. Technol. 2022, 67, 102891. [CrossRef]
110. Torrisi, B.M.; Zarnitsyn, V.; Prausnitz, M.R.; Anstey, A.; Gateley, C.; Birchall, J.C.; Coulman, S.A. Pocketed Microneedles for Rapid Delivery of a Liquid-State Botulinum Toxin A Formulation into Human Skin. J. Control. Release 2013, 165, 146–152. [CrossRef]
111. Golombek, S.; Pilz, M.; Steinle, H.; Kochba, E.; Levin, Y.; Lunter, D.; Schlensak, C.; Wendel, H.P.; Avci-Adali, M. Intradermal Delivery of Synthetic MRNA Using Hollow Microneedles for Efficient and Rapid Production of Exogenous Proteins in Skin. Mol. Ther.-Nucleic Acids 2018, 11, 382–392. [CrossRef]
112. Valla, V. Therapeutics of Diabetes Mellitus: Focus on Insulin Analogues and Insulin Pumps. Exp. Diabetes Res. 2010, 2010, 178372. [CrossRef]
113. Burton, S.A.; Ng, C.-Y.; Simmers, R.; Moeckly, C.; Brandwein, D.; Gilbert, T.; Johnson, N.; Brown, K.; Alston, T.; Prochnow, G.; et al. Rapid Intradermal Delivery of Liquid Formulations Using a Hollow Microstructured Array. Pharm. Res. 2011,28,31–40. [CrossRef]
114. Van der Maaden K, Jiskoot W, Bouwstra J. Microneedle technologies for (trans)dermal

a Novel Transdermal Microprojection Delivery System. Pharm. Res. 2009, 26, 2454–2463. [CrossRef]
129. Sathyan, G.; Sun, Y.N.; Weyers, R.; Daddona, P.; Staehr, P.; Gupta, S. Macroflux® Desmopressin Transdermal Delivery System: Pharmacokinetics and Pharmacodynamic Evaluation in Healthy Volunteers. AAPS J. 2004, 6, 665.
130. An, M.; Liu, H. Dissolving Microneedle Arrays for Transdermal Delivery of Amphiphilic Vaccines. Small 2017, 13, 1700164. [CrossRef]
131. Hong, X.; Wei, L.; Wu, F.; Wu, Z.; Chen, L.; Liu, Z.; Yuan, W. Dissolving and Biodegradable Microneedle Technologies for Transdermal Sustained Delivery of Drug and Vaccine. Drug Des. Devel. Ther. 2013, 7, 945–952. [CrossRef]
132. Tran, K.; Gavitt, T.D.; Farrell, N.J.; Curry, E.J.; Mara, A.B.; Patel, A.; Brown, L.; Kilpatrick, S.; Piotrowska, R.; Mishra, N. Transdermal Microneedles for the Programmable Burst Release of Multiple Vaccine Payloads. Nat. Biomed. Eng. 2021, 5, 998–1007. [CrossRef]
133. Lopez-Ramirez, M.A.; Kupor, D.; Marchiori, L.; Soto, F.; Rueda, R.; Reynoso, M.; Narra, L.R.; Chakravarthy, K.; Wang, J. Combinatorial Microneedle Patch with Tunable Release Kinetics and Dual Fast-Deep/Sustained Release Capabilities. J. Mater. Chem. B 2021, 9, 2189–2199. [CrossRef]
134. Amani, H.; Shahbazi, M.-A.; D'Amico, C.; Fontana, F.; Abbaszadeh, S.; Santos, H.A. Microneedles for Painless Transdermal Immunotherapeutic Applications. J. Control. Release 2021, 330, 185–217. [CrossRef]
135. Dardano, P.; De Martino, S.; Battisti, M.; Miranda, B.; Rea, I.; De Stefano, L. One-Shot Fabrication of Polymeric Hollow Microneedles by Standard Photolithography. Polymers 2021, 13, 520. [CrossRef]
136. Chang, H.; Chew, S.W.T.; Zheng, M.; Lio, D.C.S.; Wiraja, C.; Mei, Y.; Ning, X.; Cui, M.; Than, A.; Shi, P.; et al. Cryomicroneedles for Transdermal Cell Delivery. Nat. Biomed. Eng. 2021, 5, 1008–1018. [CrossRef]
137. Yang, J.; Zhang, H.; Hu, T.; Xu, C.; Jiang, L.; Shrike Zhang, Y.; Xie, M. Recent Advances of Microneedles Used towards Stimuli Responsive Drug Delivery, Disease Theranostics, and Bioinspired Applications. Chem. Eng. J. 2021, 426, 130561. [CrossRef]
138. Vora, L.K.; Moffatt, K.; Tekko, I.A.; Paredes, A.J.; Volpe-Zanutto, F.; Mishra, D.; Peng, K.; Raj Singh Thakur, R.; Donnelly, R.F. Microneedle Array Systems for Long-Acting Drug Delivery. Eur. J. Pharm. Biopharm. 2021, 159, 44–76. [CrossRef]
139. Ohn, J.; Jang, M.; Kang, B.M.; Yang, H.; Hong, J.T.; Kim, K.H.; Kwon, O.; Jung, H. Dissolving Candlelit Microneedle for Chronic Inflammatory Skin Diseases. Adv. Sci. 2021, 8, 2004873. [CrossRef] [PubMed]
140. Yu, J.; Zhang, Y.; Ye, Y.; DiSanto, R.; Sun, W.; Ranson, D.; Ligler, F.S.; Buse, J.B.; Gu, Z. Microneedle-Array Patches Loaded with Hypoxia-Sensitive Vesicles Provide Fast Glucose-Responsive Insulin Delivery. Proc. Natl. Acad. Sci. USA 2015, 112, 8260–8265. [CrossRef]
141. Lee, K.; Lee, C.Y.; Jung, H. Dissolving Microneedles for Transdermal Drug Administration Prepared by Stepwise Controlled Drawing of Maltose. Biomaterials 2011, 32, 3134–3140. [CrossRef] [PubMed]
142. Chen, M.-C.; Ling, M.-H.; Lai, K.-Y.; Pramudityo, E. Chitosan Microneedle Patches for Sustained Transdermal Delivery of Macromolecules. Biomacromolecules 2012, 13, 4022–4031. [CrossRef] [PubMed]
143. Yi, X.; Wang, C.; Yu, X.; Su, W.; Yuan, Z. Chitosan/Zinc Nitrate Microneedles for Bacterial Biofilm Eradication. J. Biomed. Mater. Res. B Appl. Biomater. 2021, 109, 911–920. [CrossRef]
144. Chu, L.Y.; Choi, S.-O.; Prausnitz, M.R. Fabrication of Dissolving Polymer Microneedles for Controlled Drug Encapsulation and Delivery: Bubble and Pedestal Microneedle Designs. J. Pharm. Sci. 2010, 99, 4228–4238. [CrossRef]
145. Moga, K.A.; Bickford, L.R.; Geil, R.D.; Dunn, S.S.; Pandya, A.A.; Wang, Y.; Fain, J.H.; Archuleta, C.F.; O'Neill, A.T.; Desimone, J.M. Rapidly-Dissolvable Microneedle Patches via a Highly Scalable and Reproducible Soft

drug and vaccine delivery. J Control Release. 2012;161:645–55.
115. Chen, X.; Kask, A.S.; Crichton, M.L.; McNeilly, C.; Yukiko, S.; Dong, L.; Marshak, J.O.; Jarrahian, C.; Fernando, G.J.; Chen, D. Improved DNAVaccination by Skin-Targeted Delivery using Dry-Coated Densely-PackedMicroprojection Arrays. J. Control. Release 2010, 148, 327–333. [CrossRef]
116. Ma, Y.; Gill, H.S. Coating Solid Dispersions on Microneedles via a Molten Dip-Coating Method: Development and in Vitro Evaluation for Transdermal Delivery of a Water-Insoluble Drug. J. Pharm. Sci. 2014, 103, 3621–3630. [CrossRef]
117. Waghule, T.; Singhvi, G.; Dubey, S.K.; Pandey, M.M.; Gupta, G.; Singh, M.; Dua, K. Microneedles: A Smart Approach and Increasing Potential for Transdermal Drug Delivery System. Biomed. Pharmacother. 2019, 109, 1249–1258. [CrossRef]
118. Ameri, M.; Kadkhodayan, M.; Nguyen, J.; Bravo, J.A.; Su, R.; Chan, K.; Samiee, A.; Daddona, P.E. Human Growth Hormone Delivery with a Microneedle Transdermal System: Preclinical Formulation, Stability, Delivery and PK of Therapeutically Relevant Doses. Pharmaceutics 2014, 6, 220–234. [CrossRef]
119. Kusamori, K.; Katsumi, H.; Sakai, R.; Hayashi, R.; Hirai, Y.; Tanaka, Y.; Hitomi, K.; Quan, Y.; Kamiyama, F.; Yamada, K. DevelopmentofaDrug-CoatedMicroneedleArrayandItsApplicationforTransdermalDeliveryofInterferonAlpha. Biofabrication 2016, 8, 015006. [CrossRef]
120. Caudill, C.L.; Perry, J.L.; Tian, S.; Luft, J.C.; DeSimone, J.M. Spatially Controlled Coating of Continuous Liquid Interface Production Microneedles for Transdermal Protein Delivery. J. Control. Release 2018, 284, 122–132. [CrossRef]
121. Daddona, P.E.; Matriano, J.A.; Mandema, J.; Maa, Y.-F. Parathyroid Hormone (1-34)-Coated Microneedle Patch System: Clinical Pharmacokinetics and Pharmacodynamics for Treatment of Osteoporosis. Pharm. Res. 2011, 28, 159–165. [CrossRef]
122. Kapoor, Y.; Milewski, M.; Dick, L.; Zhang, J.; Bothe, J.R.; Gehrt, M.; Manser, K.; Nissley, B.; Petrescu, I.; Johnson, P. Coated Microneedles for Transdermal Delivery of a Potent Pharmaceutical Peptide. Biomed. Microdevices 2020, 22, 7. [CrossRef]
123. Peters, E.E.; Ameri, M.; Wang, X.; Maa, Y.-F.; Daddona, P.E. Erythropoietin-Coated ZP-Microneedle Transdermal System: Preclinical Formulation, Stability, and Delivery. Pharm. Res. 2012, 29, 1618–1626. [CrossRef]
124. Ross, S.; Scoutaris, N.; Lamprou, D.; Mallinson, D.; Douroumis, D. Inkjet Printing of Insulin Microneedles for Transdermal Delivery. Drug Deliv. Transl. Res. 2015, 5, 451–461. [CrossRef]
125. Saurer, E.M.; Flessner, R.M.; Sullivan, S.P.; Prausnitz, M.R.; Lynn, D.M. Layer-by-Layer Assembly of DNA-and Protein-Containing Films on Microneedles for Drug Delivery to the Skin. Biomacromolecules 2010, 11, 3136–3143. [CrossRef]
126. Zhao, X.; Coulman, S.A.; Hanna, S.J.; Wong, F.S.; Dayan, C.M.; Birchall, J.C. Formulation of Hydrophobic Peptides for Skin Delivery via Coated Microneedles. J. Control. Release 2017, 265, 2–13. [CrossRef]
127. Li, S.; Li, W.; Prausnitz, M. Individually Coated Microneedles for Co-Delivery of Multiple Compounds with Different Properties. Drug Deliv. Transl. Res. 2018, 8, 1043–1052. [CrossRef]
128. Ameri, M.; Daddona, P.E.; Maa, Y.-F. Demonstrated Solid-State Stability of Parathyroid Hormone PTH (1–34) Coated on a Novel Transdermal Microprojection Delivery System. Pharm. Res. 2009, 26, 2454–2463. [CrossRef]
129. Sathyan, G.; Sun, Y.N.; Weyers, R.; Daddona, P.; Staehr, P.; Gupta, S. Macroflux® Desmopressin Transdermal Delivery System: Pharmacokinetics and Pharmacodynamic Evaluation in Healthy Volunteers. AAPS J. 2004, 6, 665.
130. An, M.; Liu, H. Dissolving Microneedle Arrays for Transdermal Delivery of Amphiphilic Vaccines. Small 2017, 13, 1700164. [CrossRef]
131. Hong, X.; Wei, L.; Wu, F.; Wu, Z.; Chen, L.; Liu, Z.; Yuan, W. Dissolving and

Biodegradable Microneedle Technologies for Transdermal Sustained Delivery of Drug and Vaccine. Drug Des. Devel. Ther. 2013, 7, 945–952. [CrossRef]
132. Tran, K.; Gavitt, T.D.; Farrell, N.J.; Curry, E.J.; Mara, A.B.; Patel, A.; Brown, L.; Kilpatrick, S.; Piotrowska, R.; Mishra, N. Transdermal Microneedles for the Programmable Burst Release of Multiple Vaccine Payloads. Nat. Biomed. Eng. 2021, 5, 998–1007. [CrossRef]
133. Lopez-Ramirez, M.A.; Kupor, D.; Marchiori, L.; Soto, F.; Rueda, R.; Reynoso, M.; Narra, L.R.; Chakravarthy, K.; Wang, J. Combinatorial Microneedle Patch with Tunable Release Kinetics and Dual Fast-Deep/Sustained Release Capabilities. J. Mater. Chem. B 2021, 9, 2189–2199. [CrossRef]
134. Amani, H.; Shahbazi, M.-A.; D'Amico, C.; Fontana, F.; Abbaszadeh, S.; Santos, H.A. Microneedles for Painless Transdermal Immunotherapeutic Applications. J. Control. Release 2021, 330, 185–217. [CrossRef]
135. Dardano, P.; De Martino, S.; Battisti, M.; Miranda, B.; Rea, I.; De Stefano, L. One-Shot Fabrication of Polymeric Hollow Microneedles by Standard Photolithography. Polymers 2021, 13, 520. [CrossRef]
136. Chang, H.; Chew, S.W.T.; Zheng, M.; Lio, D.C.S.; Wiraja, C.; Mei, Y.; Ning, X.; Cui, M.; Than, A.; Shi, P.; et al. Cryomicroneedles for Transdermal Cell Delivery. Nat. Biomed. Eng. 2021, 5, 1008–1018. [CrossRef]
137. Yang, J.; Zhang, H.; Hu, T.; Xu, C.; Jiang, L.; Shrike Zhang, Y.; Xie, M. Recent Advances of Microneedles Used towards Stimuli Responsive Drug Delivery, Disease Theranostics, and Bioinspired Applications. Chem. Eng. J. 2021, 426, 130561. [CrossRef]
138. Vora, L.K.; Moffatt, K.; Tekko, I.A.; Paredes, A.J.; Volpe-Zanutto, F.; Mishra, D.; Peng, K.; Raj Singh Thakur, R.; Donnelly, R.F. Microneedle Array Systems for Long-Acting Drug Delivery. Eur. J. Pharm. Biopharm. 2021, 159, 44–76. [CrossRef]
139. Ohn, J.; Jang, M.; Kang, B.M.; Yang, H.; Hong, J.T.; Kim, K.H.; Kwon, O.; Jung, H. Dissolving Candlelit Microneedle for Chronic Inflammatory Skin Diseases. Adv. Sci. 2021, 8, 2004873. [CrossRef] [PubMed]
140. Yu, J.; Zhang, Y.; Ye, Y.; DiSanto, R.; Sun, W.; Ranson, D.; Ligler, F.S.; Buse, J.B.; Gu, Z. Microneedle-Array Patches Loaded with Hypoxia-Sensitive Vesicles Provide Fast Glucose-Responsive Insulin Delivery. Proc. Natl. Acad. Sci. USA 2015, 112, 8260–8265. [CrossRef]
141. Lee, K.; Lee, C.Y.; Jung, H. Dissolving Microneedles for Transdermal Drug Administration Prepared by Stepwise Controlled Drawing of Maltose. Biomaterials 2011, 32, 3134–3140. [CrossRef] [PubMed]
142. Chen, M.-C.; Ling, M.-H.; Lai, K.-Y.; Pramudityo, E. Chitosan Microneedle Patches for Sustained Transdermal Delivery of Macromolecules. Biomacromolecules 2012, 13, 4022–4031. [CrossRef] [PubMed]
143. Yi, X.; Wang, C.; Yu, X.; Su, W.; Yuan, Z. Chitosan/Zinc Nitrate Microneedles for Bacterial Biofilm Eradication. J. Biomed. Mater. Res. B Appl. Biomater. 2021, 109, 911–920. [CrossRef]
144. Chu, L.Y.; Choi, S.-O.; Prausnitz, M.R. Fabrication of Dissolving Polymer Microneedles for Controlled Drug Encapsulation and Delivery: Bubble and Pedestal Microneedle Designs. J. Pharm. Sci. 2010, 99, 4228–4238. [CrossRef]
145. Moga, K.A.; Bickford, L.R.; Geil, R.D.; Dunn, S.S.; Pandya, A.A.; Wang, Y.; Fain, J.H.; Archuleta, C.F.; O'Neill, A.T.; Desimone, J.M. Rapidly-Dissolvable Microneedle Patches via a Highly Scalable and Reproducible Soft Lithography Approach. Adv. Mater. 2013, 25, 5060–5066. [CrossRef]
146. Fukushima, K.; Yamazaki, T.; Hasegawa, R.; Ito, Y.; Sugioka, N.; Takada, K. Pharmacokinetic and Pharmacodynamic Evaluation of Insulin Dissolving Microneedles in Dogs. Diabetes Technol. Ther. 2010, 12, 465–474. [CrossRef]
147. Ito, Y.; Yamazaki, T.; Sugioka, N.; Takada, K. Self-Dissolving Micropile Array Tips for Percutaneous Administration of Insulin. J. Mater. Sci. Mater. Med. 2010, 21, 835–841. [CrossRef]

148. Shen, D.; Yu, H.; Wang, L.; Chen, X.; Feng, J.; Zhang, Q.; Xiong, W.; Pan, J.; Han, Y.; Liu, X. Biodegradable Phenylboronic Acid- Modified-Polylysine for Glucose-Responsive Insulin Delivery via Transdermal Micro- needles. J. Mater. Chem. B 2021, 9, 6017–6028. [CrossRef]
149. Zhang, Y.; Wu, M.; Tan, D.; Liu, Q.; Xia, R.; Chen, M.; Liu, Y.; Xue, L.; Lei, Y. A Dissolving and Glucose-Responsive Insulin Releasing Microneedle Patch for Type 1 Diabetes Therapy. J. Mater. Chem. B 2021, 9, 648–657. [CrossRef]
150. Chen, M.-C.; Ling, M.-H.; Kusuma, S.J. Poly--Glutamic Acid Microneedles with a Supporting Structure Design as a Potential Tool for Transdermal Delivery of Insulin. Acta Biomater. 2015, 24, 106–116. [CrossRef]
151. Ling, M.-H.; Chen, M.-C. Dissolving Polymer Microneedle Patches for Rapid and Efficient Transdermal Delivery of Insulin to Diabetic Rats. Acta Biomater. 2013, 9, 8952–8961. [CrossRef]
152. Kim, J.D.; Kim, M.; Yang, H.; Lee, K.; Jung, H. Droplet-Born Air Blowing: Novel Dissolving Microneedle Fabrication. J. Control. Release 2013, 170, 430–436. [CrossRef]
153. Yu, J.; Zhang, Y.; Ye, Y.; DiSanto, R.; Sun, W.; Ranson, D.; Ligler, F.S.; Buse, J.B.; Gu, Z. Microneedle-Array Patches Loaded with Hypoxia-Sensitive Vesicles Provide Fast Glucose-Responsive Insulin Delivery. Proc. Natl. Acad. Sci. USA 2015, 112, 8260–8265. [CrossRef]
154. Yang, C.; Sheng, T.; Hou, W.; Zhang, J.; Cheng, L.; Wang, H.; Liu, W.; Wang, S.; Yu, X.; Zhang, Y. Glucose-Responsive Microneedle Patch for Closed-Loop Dual-Hormone Delivery in Mice and Pigs. Sci. Adv. 2022, 8, eadd3197. [CrossRef]
155. Demir, B.; Rosselle, L.; Voronova, A.; Pagneux, Q.; Quenon, A.; Gmyr, V.; Jary, D.; Hennuyer, N.; Staels, B.; Hubert, T. Innovative Transdermal Delivery of Insulin Using Gelatin Methacrylate-Based Microneedle Patches in Mice and Mini-Pigs. Nanoscale Horiz. 2022, 7, 174–184. [CrossRef]
156. Mönkäre, J.; Reza Nejadnik, M.; Baccouche, K.; Romeijn, S.; Jiskoot, W.; Bouwstra, J.A. IgG-Loaded Hyaluronan-Based Dissolving Microneedles for Intradermal Protein Delivery. J. Control. Release 2015, 218, 53–62. [CrossRef]
157. Jeong, H.-R.; Kim, J.-Y.; Kim, S.-N.; Park, J.-H. Local Dermal Delivery of Cyclosporin A, a Hydrophobic and High Molecular Weight Drug, Using Dissolving Microneedles. Eur. J. Pharm. Biopharm. 2018, 127, 237–243. [CrossRef]
158. Liu, S.; Jin, M.; Quan, Y.; Kamiyama, F.; Kusamori, K.; Katsumi, H.; Sakane, T.; Yamamoto, A. Transdermal Delivery of Relatively High Molecular Weight Drugs Using Novel Self-Dissolving Microneedle Arrays Fabricated from Hyaluronic Acid and Their Characteristics and Safety after Application to the Skin. Eur. J. Pharm. Biopharm. 2014, 86, 267–276. [CrossRef]
159. Chen, J.; Qiu, Y.; Zhang, S.; Gao, Y. Dissolving Microneedle-Based Intradermal Delivery of Interferon--2b. Drug Dev. Ind. Pharm. 2016, 42, 890–896. [CrossRef]
160. Dillon, C.; Hughes, H.; O'Reilly, N.J.; McLoughlin, P. Formulation and Characterisation of Dissolving Microneedles for the Transdermal Delivery of Therapeutic Peptides. Int. J. Pharm. 2017, 526, 125–136. [CrossRef]
161. FakhraeiLahiji, S.; Jang, Y.; Huh, I.; Yang, H.; Jang, M.; Jung, H. Exendin- 4–Encapsulated Dissolving Microneedle Arrays for Efficient Treatment of Type 2 Diabetes. Sci. Rep. 2018, 8, 1–9. [CrossRef]
162. Lahiji, S.F.; Jang, Y.; Ma, Y.; Dangol, M.; Yang, H.; Jang, M.; Jung, H. Effects of Dissolving Microneedle Fabrication Parameters on the Activity of Encapsulated Lysozyme. Eur. J. Pharm. Sci. 2018, 117, 290–296. [CrossRef]
163. Vora, L.K.; Courtenay, A.J.; Tekko, I.A.; Larrañeta, E.; Donnelly, R.F. Pullulan-Based Dissolving Microneedle Arrays for Enhanced Transdermal Delivery of Small and Large Biomolecules. Int. J. Biol. Macromol. 2020, 146, 290–298. [CrossRef] [PubMed]

164. GhavamiNejad, A.; Li, J.; Lu, B.; Zhou, L.; Lam, L.; Giacca, A.; Wu, X.Y. Glucose-Responsive Composite Microneedle Patch for Hypoglycemia-Triggered Delivery of Native Glucagon. Adv. Mater. 2019, 31, 1901051. [CrossRef] [PubMed]
165. Naito, C.; Katsumi, H.; Suzuki, T.; Quan, Y.; Kamiyama, F.; Sakane, T.; Yamamoto, A. Self-Dissolving Microneedle Arrays for Transdermal Absorption Enhancement of Human Parathyroid Hormone (1-34). Pharmaceutics 2018, 10, 215. [CrossRef]
166. Chi, J.; Zhang, X.; Chen, C.; Shao, C.; Zhao, Y.; Wang, Y. Antibacterial and Angiogenic Chitosan Microneedle Array Patch for Promoting Wound Healing. Bioact. Mater. 2020, 5, 253–259. [CrossRef] [PubMed]
167. Fukushima, K.; Ise, A.; Morita, H.; Hasegawa, R.; Ito, Y.; Sugioka, N.; Takada, K. Two-Layered Dissolving Microneedles for Percutaneous Delivery of Peptide/Protein Drugs in Rats. Pharm. Res. 2011, 28, 7–21. [CrossRef] [PubMed]
168. Ito, Y.; Murano, H.; Hamasaki, N.; Fukushima, K.; Takada, K. Incidence of Low Bioavailability of Leuprolide Acetate after Percutaneous Administration to Rats by Dissolving Microneedles. Int. J. Pharm. 2011, 407, 126–131. [CrossRef]
169. FakhraeiLahiji, S.; Kim, Y.; Kang, G.; Kim, S.; Lee, S.; Jung, H. Tissue Interlocking Dissolving Microneedles for Accurate and Efficient Transdermal Delivery of Biomolecules. Sci. Rep. 2019, 9, 7886. [CrossRef]
170. Henry S, McAllister DV, Allen MG, Prausnitz MR. Microfabricated microneedles: a novel approach to transdermal drug delivery. J Pharma Sci, 1998; 87(8):922–5.
171. Bal S, Kruithof AC, Liebl H, Tomerius M, Bouwstra J, Lademann J, Meinke M. In vivo visualization of microneedle conduits in human skin using laser scanning microscopy. Laser Phys Lett, 2010; 7(3):242–6.
172. McGrath MG, Vrdoljak A, O'Mahony C, Oliveira JC, Moore AC, Crean AM. Determination of parameters for successful spray coating of silicon microneedle arrays. Int J Pharm, 2011; 415(1–2):140–9
173. Cheng MC, Huang SF, inventors; National Cheng Kung University, assignee. Embeddable micro-needle patch for transdermal drug delivery and method of manufacturing the same. United States patent US 9,675,789, 2017 Jun 13.
174. Ita, K. Transdermal delivery of drugs with microneedles—potential and challenges. Pharmaceutics 2015, 7, 90–105. [CrossRef]
175. Bariya, S.H.; Gohel, M.C.; Mehta, T.A.; Sharma, O.P. Microneedles: An emerging transdermal drug. J. Pharm. Pharmacol. 2012, 64, 11–29. [CrossRef] [PubMed
176. Henry, S.; McAllister, D.V.; Allen, M.G.; Prausnitz, M.R. Microfabricated microneedles: A novel approach to transdermal drug delivery. J. Pharm. Sci. 1998, 87, 922–925. [CrossRef] [PubMed]
177. Wang, P.M.; Cornwell, M.; Prausnitz, M.R. Minimally invasive extraction of dermal interstitial fluid for glucose monitoring using microneedles. Diabetes Technol. Ther. 2005, 7, 131–141. [CrossRef]
178. Gupta, J.; Felner, E.I.; Prausnitz, M.R. Minimally invasive insulin delivery in subjects with type 1 diabetes using hollow microneedles. Diabetes Technol. Ther. 2009, 11, 329–337. [CrossRef]
179. Ovsianikov, A.; Chichkov, B.; Mente, P.; Monteiro-Riviere, N.A.; Doraiswamy, A.; Narayan, R.J. Two photon polymerization of polymer-ceramic hybridmaterialsfo transdermal drug delivery. Int. J.Appl. Ceram. Technol. 2007, 4, 22–29. [CrossRef]
180. Gill, H.S.; Prausnitz, M.R. Coated microneedles for transdermal delivery. J. Control. Release 2007, 117, 227–237. [CrossRef] [PubMed]
181. Kaur, M.; Ita, K.B.; Popova, I.E.; Parikh, S.J.; Bair, D.A. Microneedle-assisted delivery of verapamil hydrochloride and amlodipine besylate. Eur. J. Pharm. Biopharm. 2014, 86, 284–291. [CrossRef]
182. Gupta, J.; Gill, H.S.; Andrews, S.N.; Prausnitz, M.R. Kinetics of skin resealing after insertion of microneedles in human subjects. J. Control. Release 2011, 154, 148–155. [CrossRef]

183. Cheung, K.; Das, D.B. Microneedles for drug delivery: Trends and progress. Drug Deliv. 2016, 23, 2338–2354. [CrossRef]
184. Park, J.H.; Allen, M.G.; Prausnitz, M.R. Biodegradable polymer microneedles: Fabrication, mechanics and transdermal drug delivery. J. Control. Release 2005, 104, 51–66. [CrossRef]
185. Tu, J.; Reeves, N. Feasibility Study of Microneedle Fabrication from a thin Nitinol Wire Using a CW Single-Mode Fiber Laser. Open Eng. 2019, 9, 167–177. [CrossRef]
186. Park, J.H.; Allen, M.G.; Prausnitz, M.R. Polymer micro needles for controlled- release drug delivery. Pharm.Res. 2006, 23, 1008–1019. [CrossRef] [PubMed]
187. McAllister, D.V.; Wang, P.M.; Davis, S.P.; Park, J.H.; Canatella, P.J.; Allen, M.G.; Prausnitz, M.R.M icrofabricated needles for transdermal delivery of macromolecules and nanoparticles: Fabrication methods and transport studies. Proc. Natl. Acad. Sci. USA 2003, 100, 13755–13760. [CrossRef]
188. Pérennès, F.; Marmiroli, B.; Matteucci, M.; Tormen, M.; Vaccari, L.; Di Fabrizio, E. Sharp beveled tip hollow microneedle arrays fabricated by LIGA and 3D soft lithography with polyvinyl alcohol. J. Micromechanics Microengineering 2006, 16, 473–479. [CrossRef]
189. Park, J.H.; Choi, S.O.; Seo, S.; Choy, Y.B.; Prausnitz, M.R. A microneedle roller for transdermal drug delivery. Eur. J. Pharm. Biopharm. 2010, 76, 282–289. [CrossRef]
190. Kolli, C.S.; Banga, A.K. Characterization of solid maltose microneedles and their use for transdermal delivery. Pharm. Res. 2008, 25, 104–113. [CrossRef] [PubMed]
191. Camovi´c, M.; Biš ˇcevi´c, A.; Br ˇci´c, I.; Bor ˇcak, K.; Bušatli´c, S.; ´ Cenanovi´c, N.; Dedovi´c, A.; Mulali´c, A.; Sirbubalo, M.; Tucak, A.; et al. Acid-resistant capsules with sugar microneedles for oral delivery of ascorbic acid. In Proceedings of the CMBEBIH 2019, IFMBE Proceedings, Banja Luka, Bosnia and Herzegovina, 16–18 May 2019; Springer: Cham, Switzerland, 2019; pp. 749–753.
192. Ito, Y.; Hagiwara, E.; Saeki, A.; Sugioka, N.; Takada, K. Feasibility of microneedles for percutaneous absorption of insulin. Eur. J. Pharm. Sci. 2006, 29, 82–88. [CrossRef]
193. Kim, Y.C.; Park, J.H.; Prausnitz, M.R. Microneedles for drug and vaccine delivery. Adv. Drug Deliv. Rev. 2012, 64, 1547–1568. [CrossRef]
194. Kathuria, H.; Kang, K.; Cai, J.; Kang, L. Rapid micro needle fabrication by heating and photolithography. Int. J. Pharm. 2020, 575, 118992. [CrossRef]
195. Wilke, N.; Mulcahy, A.; Ye, S.R.; Morrissey, A. Process optimization and characterization of silicon microneedles fabricated by wet etch technology. Microelectronics J. 2005, 36, 650–656. [CrossRef]
196. Liu, Y.; Eng,P.F.; Guy, O.J.; Roberts, K.; Ashraf, H.; Knight, N. Advanced deep reactive-ion etching technology for hollow microneedles for transdermal blood sampling and drug delivery. IET Nanobiotechnology 2013, 7, 59–62. [CrossRef]
197. Paik, S.J.; Byun, S.; Lim, J.M.; Park, Y.; Lee, A.; Chung, S.; Chang, J.; Chun, K.; Cho, D. In-plane single-crystal-silicon microneedles for minimally invasive microfluid systems. Sens. Actuators A Phys. 2004, 114, 276–284. [CrossRef]
198. Wang, P.C.; Wester, B.A.; Rajaraman, S.; Paik, S.J.; Kim, S.H.; Allen, M.G. Hollow polymer microneedle array fabricated by photolithography process combined with micromolding technique. In Proceedings of the 31st Annual International Conference of the IEEE Engineering in Medicine and Biology Society: Engineering the Future of Biomedicine, Minneapolis, MN, USA, 3–6 September 2009; pp. 7026–7029.
199. Ma, B.; Liu, S.; Gan, Z.; Liu, G.; Cai, X.; Zhang, H.; Yang, Z. A PZT insulin pump integrated with a silicon microneedle array for transdermal drug delivery. Microfluid. Nanofluidics 2006, 2, 417–423. [CrossRef]
200. Tu, J.; Du, G.; Reza Nejadnik, M.; Mönkäre, J.; van der Maaden, K.; Bomans, P.H.H.; Sommerdijk, N.A.J.M.; Slütter, B.; Jiskoot, W.; Bouwstra, J.A.; et al. Mesoporous Silica Nanoparticle-Coated Microneedle Arrays for

Intradermal Antigen Delivery. Pharm. Res. 2017, 34, 1693–1706. [CrossRef] [PubMed]
201. Doraiswamy, A.; Jin, C.; Narayan, R.J.; Mageswaran, P.; Mente, P.; Modi, R.; Auyeung, R.; Chrisey, D.B.; Ovsianikov, A.; Chichkov, B. Two photon induced polymerization of organic-inorganic hybrid biomaterials for microstructured medical devices. Acta Biomater. 2006, 2, 267–275. [CrossRef] [PubMed]
202. Norman, J.J.; Choi, S.O.; Tong, N.T.; Aiyar, A.R.; Patel, S.R.; Prausnitz, M.R.; Allen, M.G. Hollow microneedles for intradermal injection fabricated by sacrificial micromolding and selective electro-deposition. Biomed. Microdevices 2013, 15, 203–210. [CrossRef] [PubMed]
203. Jung, P.; Lee, T.; Oh, D.; Hwang, S.; Jung, I.; Lee, S.; Ko, J. Nickel microneedles fabricated by sequential copper and nickel electroless plating and copper chemical wet etching. Sens. Mater. 2008, 20, 45–53.
204. Gill, H.S.; Prausnitz, M.R. Coated microneedles for transdermal delivery. J. Control. Release 2007, 117, 227–237. [CrossRef] [PubMed]
205. Martanto, W.; Davis, S.P.; Holiday, N.R.; Wang, J.; Gill, H.S.; Prausnitz, M.R. Transdermal delivery of insulin using microneedles in vivo. Pharm. Res. 2004, 21, 947–952. [CrossRef] [PubMed]
206. Gill, H.S.; Prausnitz, M.R. Coating formulations for microneedles. Pharm. Res. 2007,24,1369–1380. [CrossRef] [PubMed]
207. Gill, H.S.; Denson, D.D.; Burris, B.A.; Prausnitz, M.R. E ect of microneedle design on pain in human subjects. Clin. J. Pain 2008, 24, 585–594. [CrossRef]
208. Indermun, S.; Luttge, R.; Choonara, Y.E.; Kumar, P.; Du Toit, L.C.; Modi, G.; Pillay, V. Current advances in the fabrication of microneedles for transdermal delivery. J. Control. Release 2014, 185, 130–138. [CrossRef]
209. Nagarkar, R.; Singh, M.; Nguyen, H.X.; Jonnalagadda, S. A review of recent advances in microneedle technology for transdermal drug delivery. J. Drug Deliv. Sci. Technol. 2020, 59, 101923. [CrossRef]
210. Omatsu, T.; Chujo, K.; Miyamoto, K.; Okida, M.; Nakamura, K.; Aoki, N.; Morita, R. Metal microneedle fabrication using twisted light with spin. Opt. Express 2010, 18, 7616–7622. [CrossRef]
211. Evens, T.; Malek, O.; Castagne, S.; Seveno, D.; Van Bael, A. A novel method for producing solid polymer microneedles using laser ablated moulds in an injection moulding process. Manuf. Lett. 2020, 24, 29–32. [CrossRef]
212. Martanto, W.; Moore, J.S.; Kashlan, O.; Kamath, R.; Wang, P.M.; O'Neal, J.M.; Prausnitz, M.R. Microinfusion using hollow microneedles. Pharm. Res. 2006, 23, 104–113. [CrossRef]
213. Mahadevan, G.; Sheardown, H.; Selvaganapathy, P. PDMS embedded microneedles as a controlled release system for the eye. J. Biomater. Appl. 2013, 28, 20–27. [CrossRef] [PubMed]
214. Gittard, S.D.; Ovsianikov, A.; Chichkov, B.N.; Doraiswamy, A.; Narayan, R.J. Two-photon polymerization of microneedles for transdermal drug delivery. Expert Opin. Drug Deliv. 2010, 7, 513–533. [CrossRef] [PubMed]
215. Ling, M.H.; Chen, M.C. Dissolving polymer microneedle patches for rapid and e cient transdermal delivery of insulin to diabetic rats. Acta Biomater. 2013, 9, 8952–8961. [CrossRef]
216. Camovi´c, M.; Bišˇcevi´c, A.; Brˇci´c, I.; Borˇcak, K.; Bušatli´c, S.; ´ Cenanovi´c, N.; Dedovi´c, A.; Mulali´c, A.; Osmanli´c, M.; Sirbubalo, M.; et al. Coated 3D printed PLA microneedles as transdermal drug delivery systems. In Proceedings of the CMBEBIH 2019, IFMBE Proceedings, Banja Luka, Bosnia and Herzegovina, 16–18 May 2019; Springer: Cham, Switzerland, 2019; pp. 735–742.
217. Luzuriaga, M.A.; Berry, D.R.; Reagan, J.C.; Smaldone, R.A.; Gassensmitha, J.J. Biodegradable 3D Printed Polymer Microneedles for Transdermal Drug Delivery. Lab Chip 2018, 18, 1223–1230. [CrossRef]
218. Aoyagi, S.; Izumi, H.; Isono, Y.; Fukuda, M.; Ogawa, H. Laser fabrication of high aspect ratio thin holes on biodegradable polymer and

its application to a microneedle. Sens. Actuators A Phys. 2007, 139, 293–302. [CrossRef]
219. Parker, E.R.; Rao, M.P.; Turner, K.L.; Meinhart, C.D.; MacDonald, N.C. Bulk micromachined titanium microneedles. J. Microelectromech. Syst. 2007, 16, 289–295. [CrossRef]
220. Ameri, M.; Kadkhodayan, M.; Nguyen, J.; Bravo, J.A.; Su, R.; Chan, K.; Samiee, A.; Daddona, P.E. Humangrowth hormone delivery with a microneedle transdermal system: Preclinical formulation, stability, delivery and PK of therapeutically relevant doses. Pharmaceutics 2014, 6, 220–234. [CrossRef]
221. Guillot, A.J.; Cordeiro, A.S.; Donnelly, R.F.; Montesinos, M.C.; Garrigues, T.M.; Melero, A. Microneedle-based delivery: An overview of current applications and trends. Pharmaceutics 2020, 12, 569. [CrossRef]
222. Lutton, R.E.M.; Larrañeta, E.; Kearney, M.C.; Boyd, P.; Woolfson, A.D.; Donnelly, R.F. A novel scalable manufacturing process for the production of hydrogel-forming microneedle arrays. Int. J. Pharm. 2015, 494, 417–429. [CrossRef] [PubMed]
223. Kim, J.D.; Kim, M.; Yang, H.; Lee, K.; Jung, H. Droplet-born air blowing: Novel dissolving microneedle fabrication. J. Control. Release 2013, 170, 430–436. [CrossRef]
224. Zahn, J.D.; Talbot, N.H.; Liepmann, D.; Pisano, A.P. Microfabricated polysilicon microneedles for minimally invasive biomedical devices. Biomed. Microdevices 2000, 2, 295–303. [CrossRef]
225. Trotta, M.; Debernardi, F.; Caputo, O.; Charcosset, C.; El-Harati, A.; Fessi, H.; Mishra, V.; Bansal, K.K.; Verma, A.; Yadav, N.; et al. Cationic solid lipid nanoparticles reconstituted from low density lipoprotein components for delivery of siRNA. Int. J. Pharm. 2012, 68, 268–273.
226. Yeung, C.; Chen, S.; King, B.; Lin, H.; King, K.; Akhtar, F.; Diaz, G.; Wang, B.; Zhu, J.; Sun, W.; etal. A3D-printed microfluidic-enabled hollow microneedle architecture for transdermal drug delivery. Biomicrofluidics 2019, 13, 064125. [CrossRef]
227. Uddin, M.J.; Scoutaris, N.; Economidou, S.N.; Giraud, C.; Chowdhry, B.Z.; Donnelly, R.F.; Douroumis, D. 3D printed microneedles for anticancer therapy of skin tumours. Mater. Sci. Eng. C 2020, 107, 110248. [CrossRef] [PubMed]
228. Economidou, S.N.; Pere, C.P.P.; Reid, A.; Uddin, M.J.; Windmill, J.F.C.; Lamprou, D.A.; Douroumis, D. 3Dprinted microneedle patches using stereolithography (SLA)for intradermal insulin delivery. Mater. Sci. Eng. C 2019, 102, 743–755. [CrossRef]
229. Cordeiro, A.S.; Tekko, I.A.; Jomaa, M.H.; Vora, L.; Mcalister, E.; Volpe-zanutto, F.; Nethery, M.; Baine, P.T.; Mitchell, N.; Mcneill, D.W.; et al. Two-Photon Polymerisation 3D Printing of Microneedle Array Templates with Versatile Designs: Application in the Development of Polymeric Drug Delivery Systems. Pharm. Res. 2020, 37, 1–15. [CrossRef] [PubMed]
230. Tucak A, Sirbubalo M, Hindija L, Rahić O, Hadžiabdić J, Muhamedagić K, Čekić A, Vranić E. Microneedles: Characteristics, Materials, Production Methods and Commercial Development. Micromachines (Basel). 2020 Oct 27; 11(11): 961. doi: 10.3390/mi11110961. PMID: 33121041; PMCID: PMC7694032.
231. Albarahmieh, E.; AbuAmmouneh, L.; Kaddoura, Z.; AbuHantash, F.; Alkhalidi, B.A.; Al-Halhouli, A. Fabrication of Dissolvable Microneedle Patches Using an Innovative Laser-Cut Mould Design to Shortlist Potentially Transungual Delivery Systems: In Vitro Evaluation. AAPS PharmSciTech 2019, 20, 1–14. [CrossRef] [PubMed]
232. Kim, Y.C.; Park, J.H.; Prausnitz, M.R. Microneedles for drug and vaccine delivery. Adv. Drug Deliv. Rev. 2012, 64, 1547–1568.
233. Bariya, S.H.; Gohel, M.C.; Mehta, T.A.; Sharma, O.P. Microneedles: An emerging transdermal drug. J. Pharm. Pharmacol. 2012, 64, 11–29.
234. Roxhed, N. A Fully Integrated Microneedle-Based Transdermal Drug Delivery System; KTH-Royal Institute of Technology: Stockholm, Sweden, 2007.

235. Razali, A.R.; Qin, Y. A review on micro-manufacturing, micro-forming and their key issues. Procedia Eng. 2013, 53, 665–672.
236. Nuxoll, E. BioMEMS in drug delivery. Adv. Drug Deliv. Rev. 2013, 65, 1611–1625.
237. Kathuria, H.; Kang, K.; Cai, J.; Kang, L. Rapid microneedle fabrication by heating and photolithography. Int. J. Pharm. 2020, 575, 118992.
238. Pérennès, F.; Marmiroli, B.; Matteucci, M.; Tormen, M.; Vaccari, L.; Di Fabrizio, E. Sharp beveled tip hollow microneedle arrays fabricated by LIGA and 3D soft lithography with polyvinyl alcohol. J. Micromechanics Microengineering 2006, 16, 473–479.
239. Madou, M. Fundamentals of Microfabrication and Nanotechnology, 1st ed.; CRC Press: Boca Raton, FL, USA, 2012.
240. Ita, K. Transdermal delivery of drugs with microneedles: Strategies and outcomes. J. Drug Deliv. Sci. Technol. 2015, 29, 16–23.
241. Larrañeta, E.; Lutton, R.E.M.; Woolfson, A.D.; Donnelly, R.F. Microneedle arrays as transdermal and intradermal drug delivery systems: Materials science, manufacture and commercial development. Mater. Sci. Eng. R Rep. 2016, 104, 1–32.
242. Wilke, N.; Mulcahy, A.; Ye, S.R.; Morrissey, A. Process optimization and characterization of silicon microneedles fabricated by wet etch technology. Microelectronics J. 2005, 36, 650–656.
243. Liu, Y.; Eng, P.F.; Guy, O.J.; Roberts, K.; Ashraf, H.; Knight, N. Advanced deep reactive-ion etching technology for hollow microneedles for transdermal blood sampling and drug delivery. IET Nanobiotechnology 2013, 7, 59–62.
244. Kim, Y.C.; Park, J.H.; Prausnitz, M.R. Microneedles for drug and vaccine delivery. Adv. Drug Deliv. Rev. 2012, 64, 1547–1568.
245. Roxhed, N.; Gasser, T.C.; Griss, P.; Holzapfel, G.A.; Stemme, G. Penetration-enhanced ultrasharp microneedles and prediction on skin interaction for efficient transdermal drug delivery. J. Microelectromech. Syst. 2007, 16, 1429–1440.
246. Donnelly, R.F.; Majithiya, R.; Singh, T.R.R.; Morrow, D.I.J.; Garland, M.J.; Demir, Y.K.; Migalska, K.; Ryan, E.; Gillen, D.; Scott, C.J.; et al. Design, optimization and characterisation of polymeric microneedle arrays prepared by a novel laser-based micro-moulding technique. Pharm. Res. 2011, 28, 41–57. [CrossRef]
247. McCrudden, M.T.C.; Alkilani, A.Z.; McCrudden, C.M.; McAlister, E.; McCarthy, H.O.; Woolfson, A.D.; Donnelly, R.F. Design and physicochemical characterisation of novel dissolving polymeric microneedle arrays for transdermal delivery of high dose, low molecular weight drugs. J. Control. Release 2014, 180, 71–80. [CrossRef]
248. Larrañeta, E.; Lutton, R.E.M.; Woolfson, A.D.; Donnelly, R.F. Microneedle arrays as transdermal and intradermal drug delivery systems: Materials science, manufacture and commercial development. Mater. Sci. Eng. R Rep. 2016, 104, 1–32. [CrossRef]
249. Prausnitz, M.R. Microneedles for transdermal drug delivery. Adv. Drug Deliv. Rev. 2004, 56, 581–587. [CrossRef]
250. McGrath, M.G.; Vucen, S.; Vrdoljak, A.; Kelly, A.; O'Mahony, C.; Crean, A.M.; Moore, A. Production of dissolvable microneedles using an atomised spray process: E ect of microneedle composition on skin penetration. Eur. J. Pharm. Biopharm. 2014, 86, 200–211. [CrossRef] [PubMed]
251. Wu, L.; Takama, N.; Park, J.; Kim, B.; Kim, J.; Jeong, D. Shadow mask assisted droplet-born air-blowing method for fabrication of dissoluble microneedle. In Proceedings of the 12th International Conference on Nano/Micro Engineered and Molecular Systems, Los Angeles, CA, USA, 9–12 April 2017; pp. 456–459.
252. Kim, J.D.; Bae, J.H.; Kim, H.K.; Jeong, D.H. Droplet-born Air Blowing(DAB) technology for the industrialization of dissolving microneedle. In Proceedings of the World Congress on Recent Advances in Nanotechnology, Prague, Czech Republic, 1–2 April 2016.
253. Huh, I.; Kim, S.; Yang, H.; Jang, M.; Kang, G.; Jung, H. E ects of two droplet-based dissolving microneedle manufacturing methods on the activity of encapsulated

epidermal growth factor and ascorbic acid. Eur. J. Pharm. Sci. 2018, 114, 285–292. [CrossRef]
254. Economidou, S.N.; Lamprou, D.A.; Douroumis, D. 3D printing applications for transdermal drug delivery. Int. J. Pharm. 2018, 544, 415–424. [CrossRef] [PubMed]
255. Alhnan, M.A.; Okwuosa, T.C.; Sadia, M.; Wan, K.W.; Ahmed, W.; Arafat, B. Emergence of 3D Printed Dosage Forms: Opportunities and Challenges. Pharm. Res. 2016, 33, 1817–1832. [CrossRef] [PubMed]
256. Jamróz, W.; Szafraniec, J.; Kurek, M.; Jachowicz, R. 3D Printing in Pharmaceutical and Medical Applications—Recent Achievements and Challenges. Pharm. Res. 2018, 35, 176. [CrossRef]
257. Prasad, L.K.; Smyth, H. 3D Printing technologies for drug delivery: A review. Drug Dev. Ind. Pharm. 2016, 42, 1019–1031. [CrossRef] [PubMed]
258. Lim, S.H.; Kathuria, H.; Tan, J.J.Y.; Kang, L. 3D printed drug delivery and testing systems—A passing fad or the future? Adv. Drug Deliv. Rev. 2018, 132, 139–168. [CrossRef]
259. Goole, J.; Amighi, K. 3D printing in pharmaceutics: A new tool for designing customized drug delivery systems. Int. J. Pharm. 2016, 499, 376–394. [CrossRef] 130. Awad, A.; Trenfield, S.J.; Gaisford, S.; Basit, A.W. 3D printed medicines: A new branch of digital healthcare. Int. J. Pharm. 2018, 548, 586–596. [CrossRef]
260. Krieger, K.J.; Bertollo, N.; Dangol, M.; Sheridan, J.T.; Lowery, M.M.; O'Cearbhaill, E.D. Simple and customizable method for fabrication of high-aspect ratio microneedle molds using low-cost 3D printing. Microsyst. Nanoeng. 2019, 5. [CrossRef]
261. Farias, C.; Lyman, R.; Hemingway, C.; Chau, H.; Mahacek, A.; Bouzos, E.; Mobed-Miremadi, M. Three-dimensional (3D) printed microneedles for microencapsulated cell extrusion. Bioengineering 2018, 5. [CrossRef]
262. Pere, C.P.P.; Economidou, S.N.; Lall, G.; Ziraud, C.; Boateng, J.S.; Alexander, B.D.; Lamprou, D.A.; Douroumis, D. 3D printed microneedles for insulin skin delivery. Int. J. Pharm. 2018, 544, 425–432. [CrossRef]
263. Xenikakis, I.; Tzimtzimis, M.; Tsongas, K.; Andreadis, D.; Demiri, E.; Tzetzis, D.; Fatouros, D.G. Fabrication and finite element analysis of stereolithographic 3D printed microneedles for transdermal delivery of model dyes across human skin in vitro. Eur. J. Pharm. Sci. 2019, 137, 104976. [CrossRef] [PubMed]
264. Trautmann, A.; Roth, G.L.; Nujiqi, B.; Walther, T.; Hellmann, R. Towards a versatile point-of-care system combining femtosecond laser generated microfluidic channels and direct laser written microneedle arrays. Microsyst. Nanoeng. 2019, 5. [CrossRef] [PubMed]
265. Aksit, A.; Arteaga, D.N.; Arriaga, M.; Wang, X.; Watanabe, H.; Kasza, K.E.; Lalwani, A.K.; Kysar, J.W. In-vitro perforation of the round window membrane via direct 3-D printed microneedles. Biomed. Microdevices 2018, 20. [CrossRef]
266. Wu, M.; Zhang, Y.; Huang, H.; Li, J.; Liu, H.; Guo, Z.; Xue, L.; Liu, S.; Lei, Y. Assisted 3D printing of microneedle patches for minimally invasive glucose control in diabetes. Mater. Sci. Eng. C 2020, 117, 111299. [CrossRef] [PubMed]
267. Gittard,S.D.; Miller,P.R.; Jin, C.; Martin,T.N.; Boehm,R.D.; Chisholm,B.J.; Stafslien,S.J.; Daniels,J.W.; Cilz, N.; Monteiro-Riviere, N.A.; et al. Deposition of antimicrobial coatings on microstereolithography-fabricated microneedles. Jom 2011, 63, 59–68. [CrossRef]
268. El-Sayed, N.; Vaut, L.; Schneider, M. Customized fast-separable microneedles prepared with the aid of 3D printing for nanoparticle delivery. Eur. J. Pharm. Biopharm. 2020, 154, 166–174. [CrossRef] [PubMed]
269. Ngo, T.D.; Kashani, A.; Imbalzano, G.; Nguyen, K.T.Q.; Hui, D. Additive manufacturing (3D printing): Areview of materials, methods, applications and challenges. Compos. Part B 2018, 143, 172–196. [CrossRef]

270. Lim, D.J.; Vines, J.B.; Park, H.; Lee, S.H. Microneedles: A versatile strategy for transdermal delivery of biological molecules. Int. J. Biol. Macromol. 2018, 110, 30–38. [CrossRef]
271. Haj-Ahmad, R.; Khan, H.; Arshad, M.S.; Rasekh, M.; Hussain, A.; Walsh, S.; Li, X.; Chang, M.W.; Ahmad, Z. Microneedle coating techniques for transdermal drug delivery. Pharmaceutics 2015, 7, 486–502. [CrossRef]
272. Chen, X.; Prow, T.W.; Crichton, M.L.; Jenkins, D.W.K.; Roberts, M.S.; Frazer, I.H.; Fernando, G.J.P.; Kendall, M.A.F. Dry-coated microprojection array patches for targeted delivery of immunotherapeutics to the skin. J. Control. Release 2009, 139, 212–220. [CrossRef]
273. Chen, X.; Fernando, G.J.P.; Crichton, M.L.; Flaim, C.; Yukiko, S.R.; Fairmaid, E.J.; Corbett, H.J.; Primiero, C.A.; Ansaldo, A.B.; Frazer, I.H.; et al. Improving the reach of vaccines to low-resource regions, with a needle-free vaccine delivery device and long-term thermostabilization. J. Control. Release 2011, 152, 349–355. [CrossRef]
274. Nikolaou, M.; Krasia-Christoforou, T. Electrohydrodynamic methods for the development of pulmonary drug delivery systems. Eur. J. Pharm. Sci. 2018, 113, 29–40. [CrossRef]
275. Haj-Ahmad, R.; Rasekh, M.; Nazari, K.; Li, Y.; Fu, Y.; Li, B.; Zhang, Q.; Xia, Z.; Liu, H.; Gu, T.; et al. EHDA Spraying: A Multi-Material Nano-Engineering Route. Curr. Pharm. Des. 2015, 21, 3239–3247. [CrossRef] [PubMed]
276. Khan, H.; Mehta, P.; Msallam, H.; Armitage, D.; Ahmad, Z. Smart microneedle coatings for controlled delivery and biomedical analysis. J. Drug Target. 2014, 22, 790–795. [CrossRef]
277. Ali, R.; Mehta, P.; Kyriaki Monou, P.; Arshad, M.S.; Panteris, E.; Rasekh, M.; Singh, N.; Qutachi, O.; Wilson, P.; Tzetzis, D.; et al. Electrospinning/electrospraying coatings for metal microneedles: A design of experiments (DOE) and quality by design (QbD) approach. Eur. J. Pharm. Biopharm. 2020, 156, 20–39. [CrossRef] [PubMed]
278. McGrath, M.G.; Vrdoljak, A.; O'Mahony, C.; Oliveira, J.C.; Moore, A.C.; Crean, A.M. Determination of parameters for successful spray coating of silicon microneedle arrays. Int. J. Pharm. 2011, 415, 140–149. [CrossRef]
279. Ita, K. Transdermal delivery of drugs with microneedles: Strategies and outcomes. J. Drug Deliv. Sci. Technol. 2015, 29, 16–23. [CrossRef]
280. Duarah,S.; Sharma,M.; Wen, J. European Journal of Pharmaceutics and Biopharmaceutics Recent advancesin microneedle-baseddrugdelivery: Special emphasis on its use in paediatric population. Eur. J. Pharm.Biopharm. 2019, 136, 48–69. [CrossRef] [PubMed]
281. Ingrole, R.S.J.; Gill, H.S. Microneedle coating methods: A review with a perspective. J. Pharmacol. Exp. Ther. 2019, 370, 555–569. [CrossRef]
282. Caudill, C.L.; Perry, J.L.; Tian, S.; Luft, J.C. Spatially controlled coating of continuous liquid interface production microneedles for transdermal protein delivery. J. Control. Release 2018, 284, 122–132. [CrossRef] [PubMed]
283. Liang, L.; Chen, Y.; Zhang, B.L.; Zhang, X.P.; Liu, J.L.; Shen, C.B.; Cui, Y.; Guo, X.D. Optimization of dip-coating methods for the fabrication of coated microneedles for drug delivery. J. Drug Deliv. Sci. Technol. 2020, 55, 101464. [CrossRef]
284. Duong, H.T.T.; Kim, N.W.; Thambi, T.; Giang Phan, V.H.; Lee, M.S.; Yin, Y.; Jeong, J.H.; Lee, D.S. Microneedle arrays coated with charge reversal pH-sensitive copolymers improve antigen presenting cells-homing DNA vaccine delivery and immune responses. J. Control. Release 2018, 269, 225–234. [CrossRef]
285. Farris, E.; Brown, D.M.; Ramer-Tait, A.E.; Pannier, A.K. Micro- and nanoparticulates for DNA vaccine delivery. Exp. Biol. Med. 2016, 241, 919–929. [CrossRef] [PubMed]
286. Jung, D.; Rejinold, N.S.; Kwak, J.E.; Park, S.H.; Kim, Y.C. Nano-patterning of a stainless steel microneedle surface to improve the dip-coating e ciency of a DNA vaccine and its immune response. Colloids Surfaces B Biointerfaces 2017, 159, 54–61. [CrossRef]

287. Kim, Y.C.; Quan, F.S.; Compans, R.W.; Kang, S.M.; Prausnitz, M.R. Formulation and coating of microneedles with inactivated influenza virus to improve vaccine stability and immunogenicity. J. Control. Release 2010, 142, 187–195. [CrossRef] [PubMed]
288. Van Der Maaden, K.; Sekerdag, E.; Schipper, P.; Kersten, G.; Jiskoot, W.; Bouwstra, J. Layer- by-LayerAssembly of Inactivated Poliovirus and N-Trimethyl Chitosan on pH-Sensitive Microneedles for Dermal Vaccination. Langmuir 2015, 31, 8654–8660. [CrossRef] [PubMed]
289. Vrdoljak, A.; McGrath, M.G.; Carey, J.B.; Draper, S.J.; Hill, A.V.S.; O'Mahony, C.; Crean, A.M.; Moore, A.C. Coated microneedle arrays for transcutaneous delivery of live virus vaccines. J. Control. Release 2012, 159, 34–42. [CrossRef] [PubMed]
290. Van Der Maaden, K.; Jiskoot, W.; Bouwstra, J. Microneedle technologies for (trans)dermal drug and vaccine delivery. J. Control. Release 2012, 161, 645–655. [CrossRef]
291. Sirbubalo, M.; Tucak, A.; Muhamedagic, K.; Hindija, L.; Rahi´ c, O.; Hadžiabdi´ c, J.; Cekic, A.; Begic-Hajdarevic, D.; Cohodar Husic, M.; Derviševi´ c, A.; et al. 3D Printing-A "Touch-Button" Approach to Manufacture Microneedles for Transdermal Drug Delivery. Pharmaceutics 2021, 13, 924. [CrossRef]
292. Kjar, A.; Huang, Y. Application of Micro-Scale 3D Printing in Pharmaceutics. Pharmaceutics 2019, 11, 390. [CrossRef]
293. Prausnitz, M.R. Engineering Microneedle Patches for Vaccination and Drug Delivery to Skin. Annu. Rev. Chem. Biomol. Eng. 2017, 8, 177–200. [CrossRef]
294. FDA.FDAGuidance. Use of International Standards. ISO 10993-1. Biological Evaluation of Medical Devices—Part 1:Evaluation and Testing within a Risk Management Process; FDA: Silver Spring, MD, USA, 2016.
295. Choi, I.J.; Kang, A.; Ahn, M.H.; Jun, H.; Baek, S.K.; Park, J.H.; Na, W.; Choi, S.O. Insertion-responsive microneedles for rapid intradermal delivery of canine influenza vaccine. J. Control. Release Off. J. Control. Release Soc. 2018, 286, 460–466. [CrossRef]
296. Li,W.; Terry, R.N.; Tang, J.; Feng, M.R.; Schwendeman, S.P.; Prausnitz, M.R. Rapidly separable microneedle patch for the sustained release of a contraceptive. Nat. Biomed. Eng. 2019, 3, 220–229. [CrossRef] [PubMed]
297. Permana, A.D.; Nainu, F.; Moffatt, K.; Larrañeta, E.; Donnelly, R.F. Recent advances in combination of microneedles and nanomedicines for lymphatic targeted drug delivery. Wiley Interdiscip. Rev. Nanomed. Nanobiotechnology 2021, 13, e1690. [CrossRef]
298. Sully, R.E.; Moore, C.J.; Garelick, H.; Loizidou, E.; Podoleanu, A.G.; Gubala, V. Nanomedicines and microneedles: A guide to their analysis and application. Anal. Methods Adv. Methods Appl. 2021, 13, 3326–3347. [CrossRef]
299. Adhikari, B.B.; Goodson, J.L.; Chu, S.Y.; Rota, P.A.; Meltzer, M.I. Assessing the Potential Cost-Effectiveness of Microneedle Patches in Childhood Measles Vaccination Programs: The Case for Further Research and Development. Drugs RD 2016, 16, 327–338. [CrossRef]
300. Lahiji SF, Dangol M, Jung H. A patchless dissolving microneedle delivery system enabling rapid and efficient transdermal drug delivery. Sci Rep. 2015 Jan 21;5:7914. doi: 10.1038/srep07914. PMID: 25604728; PMCID: PMC4300505.
301. Aldawood FK, Andar A, Desai S. A Comprehensive Review of Microneedles: Types, Materials, Processes, Characterizations and Applications. Polymers (Basel). 2021 Aug 22;13(16):2815. doi: 10.3390/polym13162815. PMID: 34451353; PMCID: PMC8400269.
302. Kim M, Yang H, Kim S, Lee C, Jung H. The Troy Microneedle: A Rapidly Separating, Dissolving Microneedle Formed by Cyclic Contact and Drying on the Pillar (CCDP). PLoS One. 2015 Aug 26;10(8):e0136513. doi: 10.1371/journal.pone.0136513. PMID: 26308945; PMCID: PMC4550382.
303. Khanna, P.; Silva, H.; Bhansali, S. Variation in microneedle geometry to increase shear strength. Procedia Eng. 2010, 5, 977–980. [CrossRef]

304. Lutton, R.E.M.; Moore, J.; Larrañeta, E.; Ligett, S.; Woolfson, A.D.; Donnelly, R.F. Microneedle characterisation: The need for universal acceptance criteria and GMP specifications when moving towards commercialisation. Drug Deliv. Transl. Res. 2015, 5, 313–331. [CrossRef]
305. Gittard, S.D.; Chen, B.; Xu, H.; Ovsianikov, A.; Chichkov, B.; Monteiro-Riviere, N.; Narayan, R.J. The effects of geometry on skin penetration and failure of polymer microneedles. J. Adhes. Sci. Technol. 2013, 27, 227–243. [CrossRef] [PubMed]
306. Demir, Y.K.; Akan, Z.; Kerimoglu, O. Characterization of Polymeric Microneedle Arrays for Transdermal Drug Delivery. PLoS ONE2013, 8, e77289. [CrossRef]
307. Donnelly, R.F.; Majithiya, R.; Singh, R.R.T.; Morrow, D.I.J.; Garland, M.J.; Demir, Y.K.; Migalska, K.; Ryan, E.; Gillen, D.; Scott, C.J.; et al. Design, Optimization and Characterisation of Polymeric Microneedle Arrays Prepared by a Novel Laser-Based Micromoulding Technique. Pharm. Res. 2011, 28, 41–57. [CrossRef] [PubMed]
308. Park, J.-H.; Yoon, Y.-K.; Choi, S.-O.; Prausnitz, M.R.; Allen, M.G. Tapered Conical Polymer Microneedles Fabricated Using an Integrated Lens Technique for Transdermal Drug Delivery. IEEE Trans. Biomed. Eng. 2007, 54, 903–913. [CrossRef]
309. Park, J.-H.; Allen, M.G.; Prausnitz, M.R. Biodegradable polymer microneedles Fabrication, mechanics andtransdermal drug delivery. J. Control. Release 2005, 104, 51–66. [CrossRef]
310. Davis, S.P.; Landis, B.J.; Adams, Z.H.; Allen, M.G.; Prausnitz, M.R. Insertion of microneedles into skin: Measurement and prediction of insertion force and needle fracture force. J. Biomech. 2004, 37, 1155–1163. [CrossRef] [PubMed]
311. Khanna, P.; Luongo, K.; Strom, J.A.; Bhansali, S. Axial and shear fracture strength evaluation of silicon microneedles. Microsyst. Technol. 2010, 16, 973–978. [CrossRef]
312. Maelíosa, R.F.D.; McCrudden, T.C.; Alkilani, A.Z.; McCrudden, C.M.; McAlister, E.; McCarthy, H.O.; Woolfson, A.D. Design and physicochemical characterisation of novel dissolvingpolymeric microneedle arrays for transdermal delivery of high dose, low molecular weight drugs. J. Control. Release 2014, 180, 71–80.
313. Park, J.-H.; Prausnitz, M.R. Analysis of mechanical failure of polymer microneedles by axial force. J. Korean Phys. Soc. 2010, 56, 1223–1227. [CrossRef] [PubMed]
314. Kim, M.; Yang, H.; Kim, S.; Lee, C.; Jung, H. The Troy Microneedle: A Rapidly Separating, Dissolving Microneedle Formed by Cyclic Contact and Drying on the Pillar (CCDP). PLoS ONE 2015, 10, e0136513. [CrossRef]
315. Lee,J.W.; Prausnitz, M.R. Drugdelivery using microneedle patches: Notjust for skin. Expert Opin. Drug Deliv. 2018, 15, 541–543. [CrossRef] [PubMed]
316. Thakur, R.R.S.; Tekko, I.; McAvoy, K.; McMillan, H.; Jones, D.; Donnelly, R.F. Minimally invasive microneedles for ocular drug delivery. Expert Opin. Drug Deliv. 2017, 14, 525–537. [CrossRef]
317. Donnelly, R.F.; Mooney, K.; Ca arel- Salvador, E.; Torrisi, B.M.; Eltayib, E.; McElnay, J.C. Microneedle-mediated minimally invasive patient monitoring. Ther. Drug Monit. 2014, 36, 10–17. [CrossRef] [PubMed]
318. Laurent, P.E.; Bonnet, S.; Alchas, P.; Regolini, P.; Mikszta, J.A.; Pettis, R.; Harvey, N.G. Evaluation of the clinical performance of a new intradermal vaccine administration technique and associated delivery system. Vaccine 2007, 25, 8833–8842. [CrossRef]
319. Intanza | European Medicines Agency. Available online: https://www.ema.europa.eu/en/medicines/human/EPAR/intanza (accessed on 19 October 2020).
320. A Pilot Study to Assess the Safety, PK and PD of Insulin Injected via MicronJet or Conventional Needle. Available online: https://clinicaltrials.gov/ct2/show/study?term=microneedle&rank=13 (accessed on 29 August 2020).
321. Levin, Y.; Kochba, E.; Hung, I.; Kenney, R. Intradermal vaccination using the novel microneedle device MicronJet600: Past, present, and future. Hum. Vaccines Immunother. 2015, 11, 991–997. [CrossRef]

322. Clinical Study to Evaluate Safety and Immunogenicity of Bacillus Calmette-Guerin (BCG) Delivery via Novel Micronjet600 Device Compared to Those via Conventional Needle. Available online: https:// clinical-trials. gov/ct2/show/NCT04064554 (accessed on 24 September 2020).
323. Zhu, J.; Zhou, X.; Libanori, A.; Sun, W. Microneedle-based bioassays. Nanoscale Adv. 2020, 2, 4295–4304. [CrossRef]
324. Chang, H.; Zheng, M.; Yu, X.; Than, A.; Seeni, R.Z.; Kang, R.; Tian, J.; Khanh, D.P.; Liu, L.; Chen, P.; et al. A Swellable Microneedle Patch to Rapidly Extract Skin Interstitial Fluid for Timely Metabolic Analysis. Adv. Mater. 2017, 29, 1–8. [CrossRef]
325. Kim, J.-Y.; Han, M.-R.; Kim, Y.-H.; Shin, S.-W.; Nam, S.-Y.; Park, J.-H. Tip-loaded dissolving microneedles for transdermal delivery of donepezil hydrochloride for treatment of Alzheimer's disease. Eur. J. Pharm. Biopharm. 2016, 105, 148–155. [CrossRef] [PubMed]
326. Yang, J.; Liu, X.; Fu, Y.; Song, Y. Recent advances of microneedles for biomedicalapplications- drug delivery and beyond.pdf. Acta Pharm. Sin. B 2019, 9, 469–483. [CrossRef]
327. Wang, P.M.; Cornwell, M.; Prausnitz, M.R. Minimally Invasive Extraction of Dermal Interstitial Fluid for Glucose Monitoring Using Microneedles. Diabetes Technol. Ther. 2005, 7, 131–141. [CrossRef] [PubMed]
328. O'Mahony, C.; Pini, F.; Vereschagina, L.; Blake, A.; O'Brien, J.; Webster, C.; Galvin, P.; McCarthy, K.G. Skin insertion mechanisms of microneedle-based dry electrodes for physiological signal monitoring. In Proceedings of the 2013 IEEE Biomedical Circuits and Systems Conference (BioCAS), Rotterdam, The Netherlands, 31 October–2 November 2013; pp. 69–72.
329. Mohan, A.V.; Windmiller, J.R.; Mishra, R.K.; Wang, J. Continuous minimally-invasive alcohol monitoring using microneedle sensor arrays. Biosens. Bioelectron. 2017, 91, 574–579. [CrossRef] 208. Sharma, S.; Hatware, K.; Bhadane, P.; Sindhikar, S.; Mishra, D.K. Recent advances in microneedle composites for biomedical applications: Advanced drug delivery technologies. Mater. Sci. Eng. C 2019, 103, 109717. [CrossRef] [PubMed]
330. Nayak, S.; Suryawanshi, S.; Bhaskar, V. Microneedle Technology for Transdermal Drug Delivery: Applications and Combination With Other Enhancing Techniques. J. Drug Deliv. Ther. 2016, 6, 65–83. [CrossRef]
331. Henry, S.; McAllister, D.V.; Allen, M.G.; Prausnitz, M.R. Microfabricated Microneedles: A Novel Approach to Transdermal Drug Delivery. J. Pharm. Sci. 1998, 87, 922–925. [CrossRef]
332. Lee, J.W.; Choi, S.-O.; Felner, E.I.; Prausnitz, M.R. Dissolving Microneedle Patch for Transdermal Delivery of Human Growth Hormone. Small 2011, 7, 531–539. [CrossRef] [PubMed]
333. Dangol, M.; Kim, S.; Li, C.G.; Lahiji, S.F.; Jang, M.; Ma, Y.; Huh, I.; Jung, H. Anti-obesity effect of a novel caffeine-loaded dissolving microneedle patchin high-fat diet-induced obese C57BL:6J mice. J. Control. Release 2017, 265, 41–47. [CrossRef]
334. Tas, C.; Mansoor, S.; Kalluri, H.; Zarnitsyn, V.G.; Choi, S.-O.; Banga, A.K.; Prausnitz, M.R. Delivery of salmon calcitonin using a microneedle patch. Int. J. Pharm. 2012, 423, 257–263. [CrossRef] [PubMed]
335. Matriano, J.A.; Cormier, M.; Johnson, J.; Young, W.A.; Buttery, M.; Nyam, K.; Daddona, P.E. Macroflux®Microprojection Array Patch Technology: A New and Efficient Approach for Intracutaneous Immunization. Pharm. Res. 2002, 19, 63–70. [CrossRef]
336. McAllister, D.V.; Wang, P.M.; Davis, S.P.; Park, J.-H.; Canatella, P.J.; Allen, M.G.; Prausnitz, M.R. Microfabricated needles for transdermal delivery of macromolecules and nanoparticles: Fabrication methods and transport studies. Proc. Natl. Acad. Sci. USA2003, 100, 13755–13760. [CrossRef] [PubMed]
337. Donnelly, R.F.; Morrow, D.I.J.; McCarron, P.; Woolfson, A.D.; Morrissey, A.; Juzenas, P.; Juzeniene, A.; Iani, V.; McCarthy, H.; Moan, J. Microneedle Arrays Permit Enhanced Intradermal Delivery of a Preformed

Photosensitizer. Photochem. Photobiol. 2009, 85, 195–204. [CrossRef] [PubMed]
338. Stahl, J.; Wohlert, M.; Kietzmann, M. Microneedle pretreatment enhances the percutaneous permeation of hydrophilic compounds with high melting points. BMC Pharmacol. Toxicol. 2012, 13, 5. [CrossRef] [PubMed]
339. Stoeber, B.; Liepmann, D. Fluid injection through out-of-plane microneedles. In Proceedings of the 1st Annual International IEEE-EMBS Special Topic Conference on Microtechnologies in Medicine and Biology. Proceedings, Lyon, France, 12–14 October 2000; pp. 224–228.
340. Chen, J.; Wise, K.D.; Hetke, J.F.; Bledsoe, S.C. A multichannel neural probe for selective chemical delivery at the cellular level. IEEE Trans. Biomed. Eng. 1997, 44, 760–769. [CrossRef] [PubMed]
341. Park, Y.-H.; Ha, S.K.; Choi, I.; Kim, K.S.; Park, J.; Choi, N.; Kim, B.; Sung, J.H. Fabrication of degradable carboxymethyl cellulose (CMC) microneedle with laser writing and replica molding process for enhancement of transdermal drug delivery. Biotechnol. Bioprocess Eng. 2016, 21, 110–118. [CrossRef]
342. Kumar, A.; Naguib, Y.; Shi, Y.-C.; Cui, Z. A method to improve the efficacy of topical eflornithine hydrochloride cream. Drug Deliv. 2016, 23, 1495–1501. [CrossRef] [PubMed]
343. Mysore, V.; Chandrashekar, B.; Yepuri, V. Alopecia areata-successful outcome with microneedling and triamcinolone acetonide. J. Cutan. Aesthetic Surg. 2014, 7, 63–64. [CrossRef] [PubMed]
344. Aust, M.C.; Knobloch, K.; Reimers, K.; Redeker, J.; Ipaktchi, R.; Altintas, M.A.; Gohritz, A.; Schwaiger, N.; Vogt, P.M. Percutaneous collagen induction therapy: An alternative treatment for burn scars. Burns 2010, 36, 836–843. [CrossRef] [PubMed]
345. El-Domyati, M.; Barakat, M.; Awad, S.; Medhat, W.; El-Fakahany, H.; Farag, H. Microneedling therapy for atrophic acne scars an objective evaluation. J. Clin. Aesthet. Dermatol. 2015, 8, 36–42. [PubMed]
346. Majid, I. Microneedling therapy in atrophic facial scars: An objective assessment. J. Cutan. Aesthetic Surg. 2009, 2, 26–30. [CrossRef]
347. Dhurat R, Sukesh M, Avhad G, Dandale A, Pal A, Pund P. A randomized evaluator blinded study of effect of microneedling in androgenetic alopecia: a pilot study. Int J Trichology. 2013 Jan;5(1):6-11. doi: 10.4103/0974-7753.114700. PMID: 23960389; PM CID: PMC3746236.
348. Marshall, S.; Sahm, L.J.; Moore, A. The success of microneedle-mediated vaccine delivery into skin. Hum. Vaccines Immunother. 2016, 12, 2975–2983. [CrossRef]
349. Matsuo, K.; Hirobe, S.; Yokota, Y.; Ayabe, Y.; Seto, M.; Quan, Y.S.; Kamiyama, F.; Tougan, T.; Horii, T.; Mukai, Y.; et al. Transcutaneous immunization using a dissolving microneedle array protects against tetanus, diphtheria, malaria, and influenza. J. Control. Release 2012, 160, 495–501. [CrossRef]
350. Poirier, D.; Renaud, F.; Dewar, V.; Strodiot, L.; Wauters, F.; Janimak, J.; Shimada, T.; Nomura, T.; Kabata, K.; Kuruma, K.; et al. Hepatitis B surface antigen incorporated in dissolvable microneedle array patch is antigenic and thermostable. Biomaterials 2017, 145, 256–265. [CrossRef]
351. Pattani, A.; McKay, P.; Garland, M.J.; Curran, R.M.; Migalska, K.; Cassidy, C.M.; Malcolm, K.; Shattock, R.J.; McCarthy, H.; Donnelly, R.F. Microneedle mediated intradermal delivery of adjuvanted recombinant HIV-1 CN54gp140 effectively primes mucosal boost inoculations. J. Control. Release 2012, 162, 529–537. [CrossRef]
352. Edens, C.; Dybdahl-Sissoko, N.C.; Weldon, W.C.; Oberste, M.S.; Prausnitz, M.R. Inactivated polio vaccination using a microneedle patch is immunogenic in the rhesus macaque. Vaccine 2015, 33, 4683–4690. [CrossRef]
353. Larraneta, E.; Lutton, R.E.M.; Woolfson, A.D.; Donnelly, R.F. Microneedle Arrays As Transdermal and Intradermal Drug De livery Systems: Materials Science, Manufacture and Commercial Development; Elsevier:

Amsterdam, The Netherlands, 2016; Volume 104, pp. 1–32.
354. Hiraishi, Y.; Nandakumar, S.; Choi, S.-O.; Lee, J.W.; Kim, Y.-C.; Posey, J.E.; Sable, S.B.; Prausnitz, M.R. Bacillus Calmette-Guérin vaccination using a microneedle patch. Vaccine 2011, 29, 2626–2636. [CrossRef] [PubMed]
355. Gill, H.S.; Söderholm, J.; Prausnitz, M.R.; Sällberg, M. Cutaneous vaccination using microneedles coated with hepatitis C DNA vaccine. Gene Ther. 2010, 17, 811–814. [CrossRef]
356. Zhu, Q.; Zarnitsyn, V.G.; Ye, L.; Wen, Z.; Gao, Y.; Pan, L.; Skountzou, I.; Gill, H.S.; Prausnitz, M.R.; Yang, C.; et al. Immunization by vaccine-coated microneedle arrays protects against lethal influenza virus challenge. Proc. Natl. Acad. Sci. USA 2009, 106, 7968–79739. [CrossRef] [PubMed]
357. Mikszta, J.A.; Dekker, J.P.; Harvey, N.G.; Dean, C.H.; Brittingham, J.M.; Huang, J.; Sullivan, V.J.; Dyas, B.; Roy, C.; Ulrich, R.G. Microneedle-Based Intradermal Delivery of the Anthrax Recombinant Protective Antigen Vaccine. Infect. Immun. 2006, 74, 6806–6810. [CrossRef] [PubMed]
358. Huang, J.; D'Souza, A.J.; Alarcon, J.B.; Mikszta, J.A.; Ford, B.M.; Ferriter, M.S.; Evans, M.; Stewart, T.; Amemiya, K.; Ulrich, R.G.; et al. Protective Immunity in Mice Achieved with Dry Powder Formulation and Alternative Delivery of Plague F1-V Vaccine. Clin. Vaccine Immunol. 2009, 16, 719–725. [CrossRef]
359. Van Damme, P.; Oosterhuis-Kafeja, F.; van der Wielen, M.; Almagor, Y.; Sharon, O.; Levin, Y. Safety and efficacy of a novel microneedle device for dose sparing intradermal influenza vaccination in healthy adults. Vaccine 2009, 27, 454–459. [CrossRef]
360. Kearney MC, Caffarel-Salvador E, Fallows SJ, McCarthy HO, Donnelly RF. Microneedle-mediated delivery of donepezil: potential for improved treatment options in Alzheimer's disease. Eur J Pharma Biopharma, 2016; 103: 43–50.
361. Wu X, Chen Y, Gui S, Wu X, Chen L, Cao Y, Yin D, Ma P. Sinomenine hydrochloride-loaded dissolving microneedles enhanced its absorption in rabbits. Pharm Dev Technol, 2016; 21(7):787–93.
362. Amodwala S, Kumar P, Thakkar HP. Statistically optimized fast dissolving microneedle transdermal patch of meloxicam: a patient friendly approach to manage arthritis. Eur J Pharm Sci, 2017; 104:114–23.
363. Donnelly RF, Singh TR, Woolfson AD. Microneedle-based drug delivery systems: microfabrication, drug delivery, and safety. Drug Delivery, 2010; 17(4):187–207.
364. Bariya SH, Gohel MC, Mehta TA, Sharma OP. Microneedles: an emerging transdermal drug delivery system. J Pharm Pharmacol. 2012 Jan;64(1):11-29. doi: 10.1111/j.2042-7158.2011.01369.x.Epub 2011 Nov 4. PMID: 22150668.
365. Avcil M, Çelik A. Microneedles in Drug Delivery: Progress and Challenges. Micromachines (Basel). 2021 Oct 28; 12(11): 1321. doi: 10.3390/mi12111321. PMID: 34832-733; PMCID: PMC8623547.
366. Tu, K.T.; Chung, C.K. Rapid prototyping of biodegradable microneedle arrays by integrating CO2laser processing and polymer molding. J. Micromech. Microeng. 2016, 26, 65015. [CrossRef]
367. Aoyagi, S.; Izumi, H.; Isono, Y.; Fukuda, M.; Ogawa, H. Laser fabrication of high aspect ratio thin holes on biodegradable polymer and its application to a microneedle. Sensors Actuators A Phys. 2007, 139, 293–302. [CrossRef]
368. Akter, T.; Desai, S. Developing a predictive model for nanoimprint lithography using artificial neural networks. Mater. Des. 2018, 160, 836–848. [CrossRef]
369. Elhoone, H.; Zhang, T.; Anwar, M.; Desai, S. Cyber-based design for additive manufacturing using artificial neural networks for Industry 4.0. Int. J. Prod. Res. 2019, 58, 2841–2861. [CrossRef]
370. Almakaeel, H.; Albalawi, A.; Desai, S. Artificial neural network based framework for cyber nano manufacturing. Manuf. Lett. 2018, 15, 151–154. [CrossRef]

371. Desai, S.; Dean, C.; Desai, Y. Cyber-enabled concurrent material and process selection in a flexible design for manufacture paradigm. Int. J. Adv. Manuf. Technol. 2018, 97, 1719–1731. [CrossRef]
372. Desai, S.; Bidanda, B.; Lovell, M.R. Material and process selection in product design using decision-making technique (AHP). Eur. J. Ind. Eng. 2012, 6, 322–346. [CrossRef]
373. Desai, S.; Dean, C. Concurrent material and process selection in a flexible design for manufacture paradigm. In Proceedings of the 2007 Industrial Engineering Research Conference, Nashville, TN, USA, 19–23 May 2007; p. 764.
374. Cordeiro, J.; Desai, S. Process Parameter Studies of Molecular Dynamics Models to Control Substrate Wettability. In Proceedings of the ASME2015 International Manufacturing Science and Engineering Conference, Charlotte, NC, USA, 8–12 June 2015.
375. Aljohani, A.; Desai, S. 3D Printing of Porous Scaffolds for Medical Applications. Am. J. Eng. Appl. Sci. 2018, 11, 1076–1085. [CrossRef]
376. Cordeiro, J.; Desai, S. Exploring Nano Scale Design Space with Molecular Dynamics Simulations. In Proceedings of the 2015 Industrial and Systems Engineering Research Conference, Nashville, TN, USA, 30 May–2 June 2015; pp. 856–861.
377. Cordeiro, J.; Desai, S. The Leidenfrost Effect at the Nanoscale. J. Micro Nano Manuf. 2016, 4, 041001. [CrossRef]
378. Rodrigues, J.; Desai, S. The Effect of Water Droplet Size, Temperature and Impingement Velocity on Gold Wettability at the Nanoscale. J. Micro Nano Manuf. 2017, 5, 031008.
379. Marquetti, I.; Rodrigues, J.; Desai, S.S. Ecological Impact of Green Computing Using Graphical Processing Units in Molecular Dynamics Simulations. Int. J. Green Comput. 2018, 9, 35–48. [CrossRef]
380. Ogunsanya, M.; Isichei, J.; Parupelli, S.K.; Desai, S.; Cai, Y. In-situ Droplet Monitoring of Inkjet 3D Printing Process using Image Analysis and Machine Learning Models. Procedia Manuf. 2021, 53, 427–434. [CrossRef]
381. Tofail, S.A.M.; Koumoulos, E.P.; Bandyopadhyay, A.; Bose, S.; O'Donoghue, L.; Charitidis, C. Additive manufacturing: Scientific and technological challenges, market uptake and opportunities. Mater. Today 2018, 21, 22–37. [CrossRef]
382. Desai, S.; Lovell, M. CFD analysis of a continuous inkjet print head for direct write fabrication. In Proceedings of the ASME 2007 International Mechanical Engineering Congress and Exposition, Seattle, WA, USA, 11–15 November 2007; Volume 13. pp. 209–213.
383. Desai, S.; Desai, S.; Lovell, M. Statistical Optimization of Process Variables in A Continuous Inkjet Process—A Case Study. Int. J. Ind. Eng. Theory Appl. Pract. 2008, 15, 104–112.
384. Desai, S.; Lovell, M. Computational fluid dynamics analysis of a direct write manufacturing process. Int. J. Nanomanuf. 2009, 3, 171. [CrossRef]
385. Desai, S.; Lovell, M. Modeling fluid–structure interaction in a direct write manufacturing process. J. Mater. Process. Technol. 2012, 212, 2031–2040. [CrossRef]
386. Desai, S.; Lovell, M. Multiphysics modeling of A piezoelectric Bimorph disc in A Direct Write Fabrication Process. In Proceedings of the ASME 2005 International Mechanical Engineering Congress and Exposition, Orlando, FL, USA, 5–11 November 2005; Volume 100, pp. 437–442.
387. Desai, S.; Lovell, M.; Cordle, J. Coupled field analysis of a piezoelectric bimorph disc in a direct write process. Compos. Part B Eng. 2007, 38, 824–832. [CrossRef]
388. Chappell, C.; Desai, S.; Sankar, J. Computational Modeling of a Drop-on-Demand (DOD) Inkjet System for Understanding Microdroplet Behavior. ASME Early Career Tech. J. 2008, 6, 350–359.
389. Rodrigues, J.; Desai, S. The nanoscale Leidenfrost effect. Nanoscale 2019, 11, 12139–12151. [CrossRef]
390. Marquetti, I.; Desai, S. Molecular Modeling of Bone Morphogenetic Protein for Tissue

Engineering Applications. In Proceedings of the 2018 IISE Annual Conference, Orlando, FL, USA, 19–22 May 2018.
391. Johnson, A.R.; Procopio, A.T. Low cost additive manufacturing of microneedle masters. 3D Print. Med. 2019, 5, 2. [CrossRef]
392. Krieger, K.J.; Bertollo, N.; Dangol, M.; Sheridan, J.T.; Lowery, M.M.; O'Cearbhaill, E.D. Simple and customizable method for fabrication of high-aspect ratio microneedle molds using low-cost 3D printing. Microsyst. Nanoeng. 2019, 5, 42. [CrossRef]
393. Economidou, S.N.; Douroumis, D. 3D printing as a transformative tool for microneedle systems: Recent advances, manufacturing considerations and market potential. Adv. Drug Deliv. Rev. 2021, 173, 60–69. [CrossRef]
394. Bhatnagar, S.; Gadeela, P.R.; Thathireddy, P.; Venuganti, V.V.K. Microneedle-based drug delivery: Materials of construction. J. Chem. Sci. 2019, 131, 90. [CrossRef]
395. Chen, W.; Cai, B.; Geng, Z.; Chen, F.; Wang, Z.; Wang, L.; Chen, X. Reducing False Negatives in COVID-19 Testing by Using Microneedle-Based Oropharyngeal Swabs. Matter 2020, 3, 1589–1600. [CrossRef] [PubMed]
396. Ita, K. Transdermal Delivery of Drugs with Microneedles—Potential and Challenges. Pharmaceutics 2015, 7, 90–105. [CrossRef]
397. Marquetti, I.; Desai, S. Molecular modeling the adsorption behavior of bone morphogenetic protein-2 on hydrophobic and hydrophilic substrates. Chem. Phys. Lett. 2018, 706, 285–294.[CrossRef]
398. Marquetti, I.; Desai, S. Adsorption Behavior of Bone Morphogenetic Protein-2 on a Graphite Substrate for Biomedical Applications. Am. J. Eng. Appl. Sci. 2018, 11, 1037–1044. [CrossRef]
399. Desai, S.; Perkins, J.; Harrison, B.S.; Sankar, J. Understanding release kinetics of biopolymer drug delivery microcapsules for biomedical applications. Mater. Sci. Eng. B Solid-State Mater. Adv. Technol. 2010, 168, 127–131. [CrossRef]
400. Waghule, T.; Singhvi, G.; Dubey, S.K.; Pandey, M.M.; Gupta, G.; Singh, M.; Dua, K. Microneedles: A smart approach and increasing potential for transdermal drug delivery system. Biomed. Pharmacother. 2018, 109, 1249–1258. [CrossRef]
401. Li, Q.Y.; Zhang, J.N.; Chen, B.Z.; Wang, Q.L.; Guo, X.D. A solid polymer microneedle patch pretreatment enhances the permeation of drug molecules into the skin. RSC Adv. 2017, 7, 15408–15415. [CrossRef]
402. Al-Japairai, K.A.S.; Mahmood, S.; Almurisi, S.H.; Venugopal, J.R.; Hilles, A.R.; Azmana, M.; Raman, S. Current trends in polymer microneedle for transdermal drug delivery. Int. J. Pharm. 2020, 587, 119673. [CrossRef]

Optimization of Results in Necks with Obtuse Angles: Diagnosis and Treatment of Deep Planes

MD Pavani Juan, MD Lembo Saverio & MD Diaz Jimena

INTRODUCTION

Over time, neck lifting has undergone a notable evolution. Initially, techniques focused on treating the skin and subcutaneous cellular tissue (SCT), resulting in excessive tension on these structures, producing suboptimal results and unaesthetic scars.

Over time, techniques involving plication of the platysma muscle (PM) in its lateral and medial regions were introduced, aiming to reposition deep structures through compression and tension. However, these approaches had limitations as the results tended to deteriorate quickly due to the stretching of the platysma fascicles.

Keywords: NA

Classification: NLM Code: WO 600

Language: English

LJP Copyright ID: 392844

Great Britain Journals Press

London Journal of Medical & Health Research

Volume 24 | Issue 8 | Compilation 1.0

Optimization of Results in Necks with Obtuse Angles: Diagnosis and Treatment of Deep Planes

MD Pavani Juan[α], MD Lembo Saverio[σ] & MD Diaz Jimena[ρ]

Author α: Plastic Surgeon member SACPER, SCPBA, AACE.
σ: Head and Neck Surgeon.
ρ: Plastic Surgeon.

I. INTRODUCTION

Over time, neck lifting has undergone a notable evolution. Initially, techniques focused on treating the skin and subcutaneous cellular tissue (SCT), resulting in excessive tension on these structures, producing suboptimal results and unaesthetic scars.

Over time, techniques involving plication of the platysma muscle (PM) in its lateral and medial regions were introduced, aiming to reposition deep structures through compression and tension. However, these approaches had limitations as the results tended to deteriorate quickly due to the stretching of the platysma fascicles.

Today, a more advanced approach has been adopted in neck treatment, shifting from focusing on tension on the platysma to reducing deep structures. The deep neck lifting technique addresses the reduction of superficial and deep fat compartments, as well as the digastric muscles and the submandibular gland, avoiding excessive tension on the PM sutures. This methodology allows for more stable and long-lasting results over time.

Applied Anatomy

We can describe the anatomical structures in planes:

Plane 1: Skin

Plane 2: The SCT (superficial fat) contains adherent septa extending from the superficial face of the PM (perimysium) to the deep face of the dermis, forming a unit or combined layer with the skin. This plane can be separated by sharp dissection accompanied by dilation; however, a thin layer of fat remains firmly attached to the PM.

PM: platisma muscle
SCT: subcutaneos cellular tissue.
DAO: depressor anguli oris
DLI: Depressor labii inferioris.
SMG: submandibular gland.
ECM: esternocleidomastoideo. **ABDM**: anerior belly digastric muscle.
FN: facial nerve

Plane 3: Represented by the PM, which, in its natural aging process, undergoes gradual atrophy and descends from the zygoma, giving rise to the surgical plane called SMAS. At age 30, the PM is located at the level of the dental alveolar line.

The PM has 5 portions: 1. Preparotid; 2. ECM; 3. Modilolar; 4. Labial; 5. Mandibular. The fibers of the platysma have a longitudinal direction in its cervical and facial portions. In contrast, in the facial portion near the dental alveolar line and the modiolus, a change in direction to horizontal, parallel to the maxilla, can be observed. We believe that some of these fibers correspond to the risorius muscle (Figure 1). In its anterior portion, after passing the mentonian ligament, it is located below the depressor anguli oris (DAO) muscle and gives rise to the depressor labii inferioris (DLI). We can assert that the DLI is a continuation of the PM, sharing the same anatomical plane, fiber direction, and innervation from the cervical branches of the facial nerve.

In the midline, there are anatomical variations of decussation, which De Castro classified as:

- *Type I (75%):* PM separated in the suprahyoid region, with its junction 1-2 cm from the chin.
- *Type II (15%):* Fibers meet completely at the level of the thyroid cartilage, up to the chin.
- *Type III (10%):* Fibers fully separated, with subcutaneous insertion into the chin muscles.

In Type I and III cases, deep supra-hyoid fat herniation is often observed.

The PM in its lower part is attached to the clavicular and acromial adipose tissue, and superiorly it is fixed by the mentonian ligament and has firm attachments to the tail of the parotid gland posterolaterally.

Plane 4: An areolar space that can be separated, with the ceiling being the platysma and the floor being the superficial layer of the deep cervical aponeurosis.

Plane 5: Corresponds to the superficial layer of the deep cervical aponeurosis, which extends upward to the pre-masseteric-parotid fascia and posteriorly to the aponeurosis of the sternocleidomastoid muscle (ECM). All vascular and nerve elements run beneath this fascia, up to the anterior limit of the masseter, where the zygomatic, buccal, and marginal branches of the facial nerve (FN) emerge. In the neck region, at the posterior limit of the submandibular gland, the cervical branches of the FN perforate the aponeurosis and adhere vertically to the deep face of the PM.

In the anterior suprahyoid region, there is dense and fibrous deep fat attached to the cervical fascia, with significant lymphatic content. They can be differentiated into pre-digastric and inter-digastric. In the lateral portion, there is a triangle formed by the mandibular border and the digastric muscle with its two bellies. In this sector, the aponeurosis forms the capsule of the submandibular gland.

Plane 6: This plane involves the mylohyoid muscle and the anterior belly of the digastric muscle (ABDM) (Figure 2), which evolves with slight atrophy and a consequent descent of the buccal floor, and with it, a descent of the submandibular gland (SMG), which is sometimes accompanied by secondary hypertrophy due to fat deposits from aging or increased BMI. All these structures descend in the aging neck (Figure 3).

Function of the PM: It is a flat sheet that connects to the skin through perimysium and retinacula (lamination) and covers the deep structures. In facial expressions, it is responsible for the downward movement of the lower lip along with the DLI. During aging, this muscle tries to maintain its anatomy by supporting the lax deep structures, acquiring greater tonicity and shortening, leading to the formation of bands that are initially dynamic and later static, also contributing to the formation of a more obtuse, aged neck.

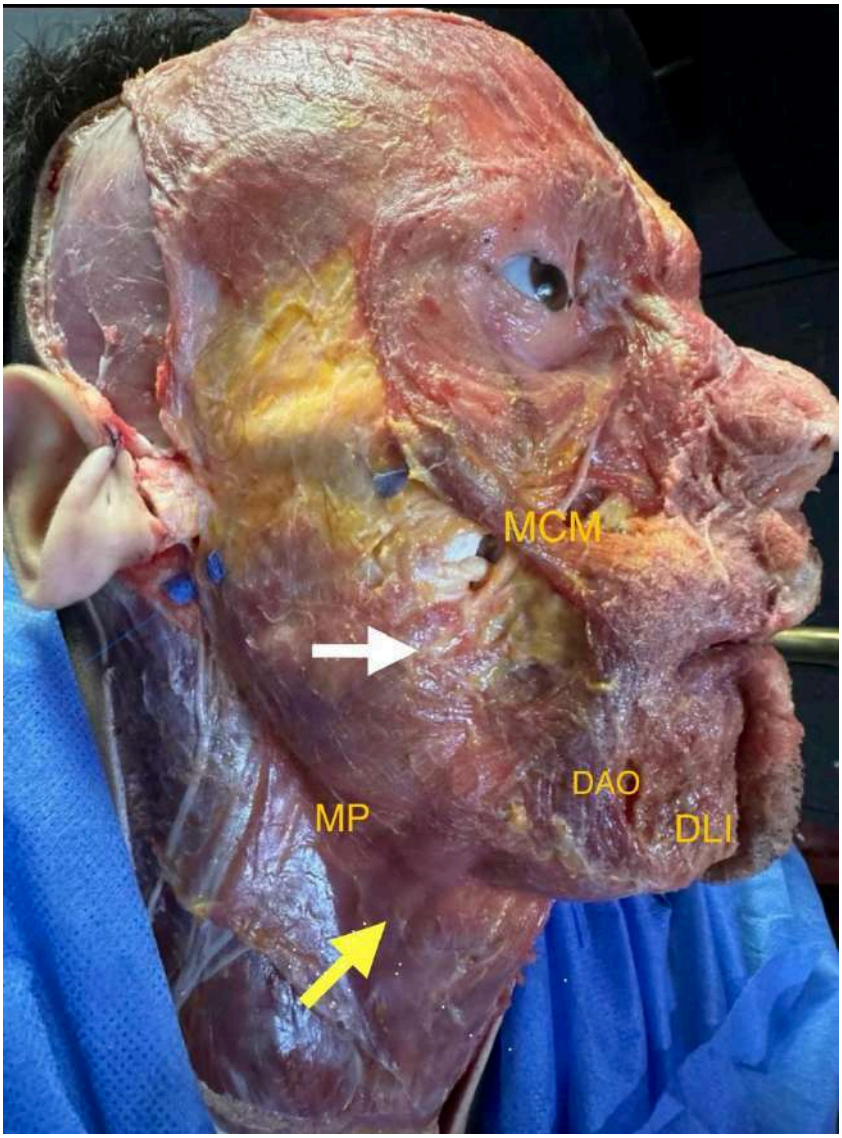

Figure 1: (young specimen): The platysma muscle can be seen with its cervical portion and longitudinal fibers (yellow arrow) and its superior facial portion near the zygoma, with horizontal fibers (white arrow), corresponding to the risorius muscle.

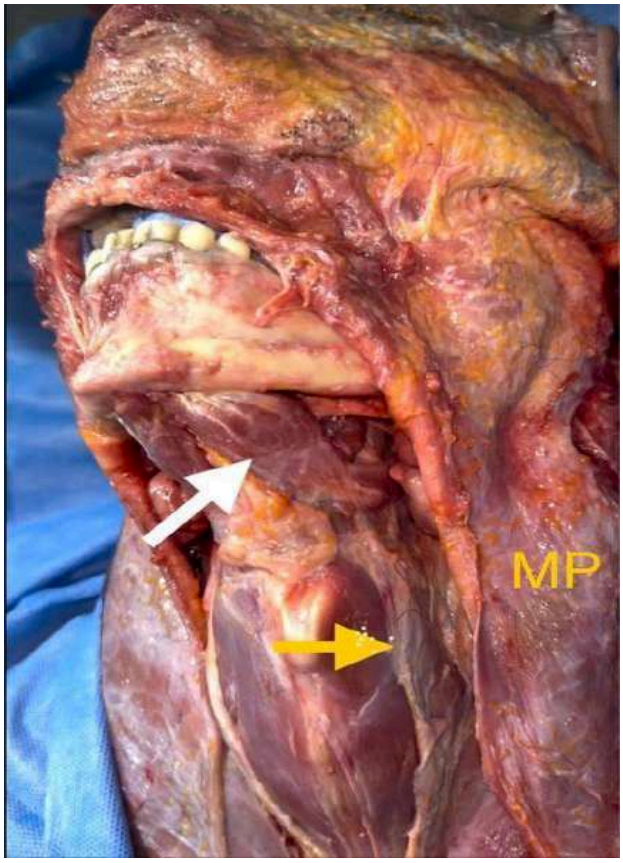

Figure 2: White arrow: ABDM (anterior belly of digastric muscle); yellow arrow: resected edge of the deep cervical aponeurosis, superficial layer

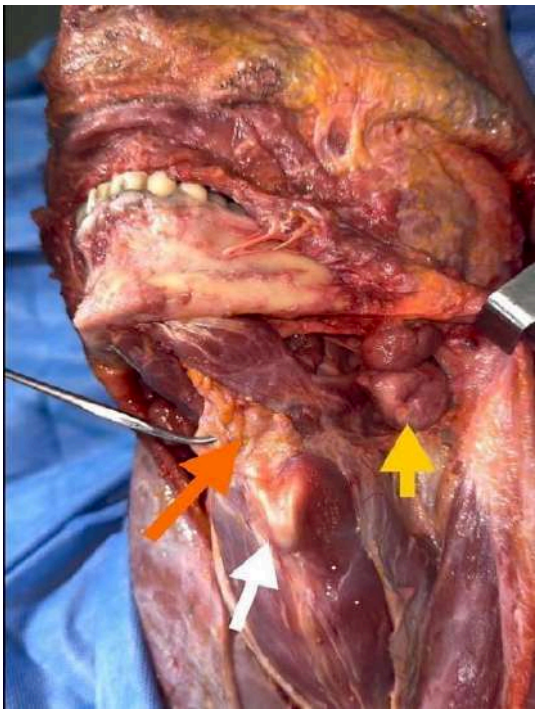

Figure 3: Yellow arrow: Ptosis of the SMG (submandibular gland), which is located below the mandibular border, reaching the level of the hyoid bone. White arrow: Thyroid cartilage. Orange arrow: Hyoid bone and deep interdigastric fat held with a Halsted clamp.

Figures 2 and 3: Dissection of a specimen with an obtuse neck where we can observe a ptotic ABDM (anterior belly of digastric muscle) protruding below the mandibular border, as well as a ptotic SMG (submandibular gland).

II. CERVICAL CLASSIFICATION

Aesthetic Neck: All authors describe it as having a cervicomental angle of 105 to 120 degrees, a defined mandibular border with some horizontal depth from the lower mandibular border to the neck, a slight visibility of the anterior edge of the sternocleidomastoid (ECM), a marked gonial angle, and a more visible thyroid cartilage in men.

Unaesthetic Neck: We further classify it as follows:

1. *Congenitally Obtuse:* This type of neck, with an angle greater than 120 degrees, is associated with retrognathia and poor positioning of the hyoid (more anterior and inferior). It is observed in young individuals (Figure 3.1).
2. *Lipodystrophic Obtuse:* Young patients with increased body mass index and/or ethnic variants with predominance of lipodystrophic necks, typically ranging in age from 20 to 35 years.
3. *Aged Obtuse Neck:* Begins with skin laxity and platysmal atrophy, generally starting from age 45, followed by ptosis of the buccal floor and observable fat redistribution starting from age 55, with the presence of jowls.

Grade I: Skin laxity with or without lipodystrophy in Plane 2.

Grade II: Addition of platysmal bands.

Grade III: Additional deep fat component.

Grade IV: Additional ptosis of the SMG (submandibular gland).

4. *Short Neck:* Excluding syndromes such as Klippel-Feil, Turner Syndrome, and necks that appear short due to morbid obesity.

Congenitally short necks are those where the ratio between the clavicular-menton distance represents less than 24% of the clavicular-vertex distance. These patients frequently present with ptosis and hypertrophy of the SMG, submental bulging due to deep fat and ABDM (anterior belly of digastric muscle), as well as laxity in the infrahyoids: sternothyroid muscles.

5. *Secondary Neck:* We can differentiate two types of secondary necks:

a) Secondary to Energy Treatments: E.g., radiofrequency, ultrasound, subcutaneous laser. In these cases, we observe reabsorption of fat tissue in Plane 2 as well as varying degrees of platysmal atrophy, which we believe are related to the number of sessions the patient undergoes.

b) Secondary to Previous Surgery: Liposuction, lifting, other procedures.

IV. PHYSICAL EXAMINATION

Performed with the patient seated, observing and palpating cervical structures.

- Static and dynamic platysmal bands.
- Chin ptosis.
- Skin laxity, thin skin with atrophy of the PM, visible deep structures.
- Superficial fat gives the appearance of a uniformly bulging full neck that obscures the contraction of the PM and does not move with swallowing.
- The deeper anterior fat, which is more compact and fibrous, moves with swallowing and is mostly distributed centrally and vertically. Laterally, the ABDM and then the SMG can be observed; while they can be examined, their final assessment is intraoperative.

V. TREATMENT

Once the diagnosis is made, we determine the type of neck we are dealing with. We can describe 5 types of procedures for neck treatment:

1. *Cervical Liposuction:* This technique, either alone or combined with energy devices, is suitable for lipodystrophic necks in patients under 35 years old who do not present with SMG ptosis, retrognathia, or jowls.
2. *Isolated Neck via Submental Approach:* Indicated for obtuse necks in young patients

with some degree of retrognathia, deep fat lipodystrophy, and mild hypertrophy and ptosis of the submandibular gland, with a present gonial angle and without jowls.

3. *Isolated Neck via Submental and Lateral Approach:* The same as the previous case but with a lack of definition of the mandibular angle (Figure 3.1).
4. *Cervicofacial Lift with Lateral Approach Without PM Delamination:* For patients with a good cervicomental angle, presence of jowls, mid-facial ptosis, some cervical skin laxity without bands, and De Castro Type I platysma decussation.
5. *Cervicofacial Lift with Lateral and Submental Approach, With or Without PM Delamination:* For patients with facial and cervical ptosis, obtuse neck, or short neck.

Figure 3.1: Pre and postoperative at 30 days. Congenital obtuse neck. Isolated submental and lateral treatment type III. Chin implant placement

Figure 3.2: Pre and postoperative at 2 months. Treatment type V with reduction of SMG (submandibular gla

VI. SURGICAL TECHNIQUE

We will describe the steps for the lateral and submental neck approaches:

Lateral Approach: Retroauricular incision: follows a line placed in the retroauricular groove, extending upward and horizontally across the mastoid when it becomes flat, then continuing towards the occipital area in a pre-pilose manner (Figure 7).

Dissection Limits:

- *Lateral Region:* Lower limit 6 cm below the gonion (subcutaneous dissection).
- *Central Region:* Lower limit at the upper border of the thyroid cartilage and upper limit at the mandibular margin (Figure 8).

Submental Approach: Make a slightly curvilinear incision at the posterior border of the mandibular bone at the submental level, 2.5 cm in length (Figure 4).

Separate the lower skin edge with a double hook, section Plane 1 and Plane 2 with a needle-tip electrocautery until the mentalis muscle fibers and PM (platysma muscle) are visible. Perform dilation and cutting with scissors laterally in Plane 2 above the PM, leaving a 5 mm layer of fatty tissue in the skin flap.

Finally, repeat this dissection in the central area. This allows for a uniform flap with even thickness of fat (Figure 5).

To achieve better visualization and working field, partially release the mandibular ligament subcutaneously laterally for about 2 cm. If the patient has significant submental skin laxity, a total release of the ligament is justified. This allows for better excursion and vertical traction from the SMAS (superficial musculoaponeurotic system) - facial platysma. Perform hemostasis of the area.

Incise along the midline with needle-tip electrocautery and dissect laterally below the PM, near its deep face, leaving the subplatysmal fat adhered to the deep plane. The limit is the external border of the ABDM (anterior belly of digastric muscle) and visualization of its tendon at the level of the hyoid bone.

Figure 4: Slightly Curved Submental Incision along the Posterior Border of the Mandibular Bone

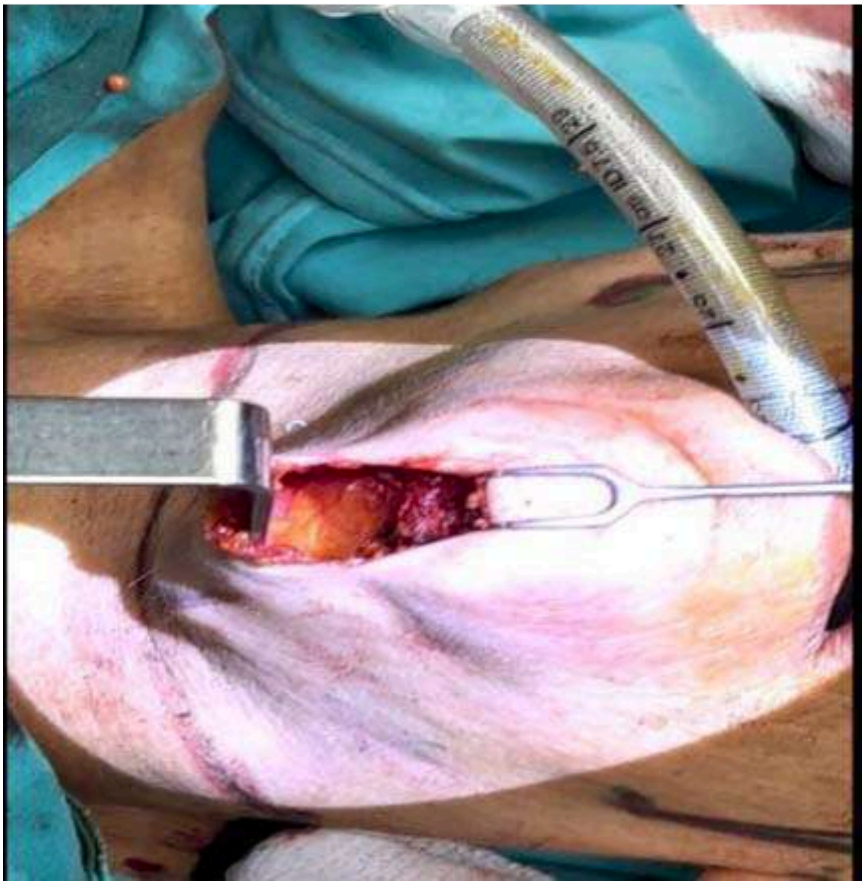

Figure 5: Anterior Cervical Dissection from the Submental Incision, Showing the Dermofat Flap

We now explain a series of steps that we believe provide better control in the uniform reduction of deep structures in obtuse necks:

1. *Resection of the Deep Fat:* Remove the deep fat located over the ABDM (anterior belly of digastric muscle).
2. Addressing SMG Hypertrophy and Ptosis: If there is hypertrophy and ptosis of the SMG (submandibular gland), locate these issues at the level of the digastric tendon by dissecting the deep face of the PM (platysma muscle) until reaching its capsule.
   - Infiltrate with lidocaine and adrenaline to prevent bleeding.
3. *Incision and Dissection of SMG Capsule:* Incise the SMG capsule on its inferointernal part with needle-tip electrocautery, then continue with intracapsular dissection using blunt maneuvers with a swab and hemostasis with needle-tip electrocautery.

Once the superficial pole is released, resect the portion below the mandibular border ("ptotic") with bipolar electrocautery (intensity 25), achieving progressive coagulation that gradually sections the gland.

Intermittently irrigate the area with saline to cool the tissues and prevent thermal injury to the cervical and marginal branches of the facial nerve (FN), which are close to the lateral surface of the glandular capsule.

4. *Resection and Reduction of ABDM:* Resect and reduce the ABDM tangentially. This provides two benefits: it reduces their volume and weakens them, aiding in the retraction and elevation of the hyoid bone.
5. *Resection of Interdigastric Fat:* Control the resection and reduction of interdigastric fat, leveling it with the remaining digastric bellies.
6. *Bring PM Flaps to the Midline:* Bring the PM flaps towards the midline and resect the excess that extends beyond it.
7. *Suture Medial Edges of PM:* Suture the medial edges of the PM in the midline, from the hyoid bone to the mental region.

Avoid infrahyoid suturing, as it can create resistance and affect the excursion and vectorization of the SMAS-platsima facial.

8. *Horizontal Myotomy of PM:* Perform a horizontal myotomy of the PM 1 cm below the hyoid bone, 2 cm in length, bilaterally to address platysmal bands and provide a hammock effect on the SMG during lateral traction.

Observations on the Technique:

- *Light Skin Laxity Only:* When the neck presents only slight skin laxity without platysmal bands, lateral traction of the PM (platysma muscle) alone is sufficient.
- *Presence of Bands or Significant Submental Skin Laxity:* When there are bands or noticeable submental skin laxity, a submental approach is necessary.
- *Neck Post-Surgery or Energy Therapy with PM Atrophy:* For necks secondary to previous surgery or energy therapies with PM atrophy, precise dissection of Plane 2 in the submental triangle is required to ensure the skin adapts to the new deep structure. In the lateral region, modify the technique by advancing in plane 2 to the anterior border of the ECM (sternocleidomastoid muscle), then entering plane 4 to visualize the SMG, creating a lateral composite cervical flap.

The goal is to obtain a PM not delaminated from the skin (Figure 9), which can be retracted without tearing the atrophic platysma, allowing it to be fixed to the mastoid aponeurosis (Figure 10).

This technique is described as the Face and Neck Lift Preservation technique by Dr. Mike Nayak.[1]

Special Considerations for Obtuse Neck:

- *Steps 2 and 3:* These are only performed when palpation and observation reveal a ptotic and/or hypertrophic SMG.
- *Resection of SMG Capsule:* Once the SMG capsule is opened, it must be resected;

[1] Limited Delamination Modifications to the Extended Deep Plane Rytidectomy:
An Anatomical Basis for Improved Outcomes
AQ: au Michael Roskies, MD, MSc, FRCSC,1,* Dominic Bray,2 Neil A. Gordon,3,4 Alessandro Gualdi,5 AQ: 1 L. Mike Nayak,6 and Ben Talei.

otherwise, secondary ptosis will occur due to weakening.

- *Step 5:* Avoid over-resection of the interdigastric fat to prevent a cosmetic complication known as "cobra neck."
- *Interdigastric Tendon Suturing:* Suturing the interdigastric tendons can help mobilize the hyoid bone backward and upward, improving the cervicomental angle. Note that if the SMG was not previously addressed, this maneuver will make it visible.
- *Deep Cervical Fascia Release:* Another approach is to release the deep cervical fascia at the superior border of the hyoid bone, allowing it to move posteriorly and superiorly, assisted by the posterior belly of the digastric muscle.
- *Step 8:* Ensure that the myotomy is performed lower than the hyoid bone (1 cm); otherwise, the hammock effect from the lateral tension of the platysma on its fixation to the mastoid will be lost

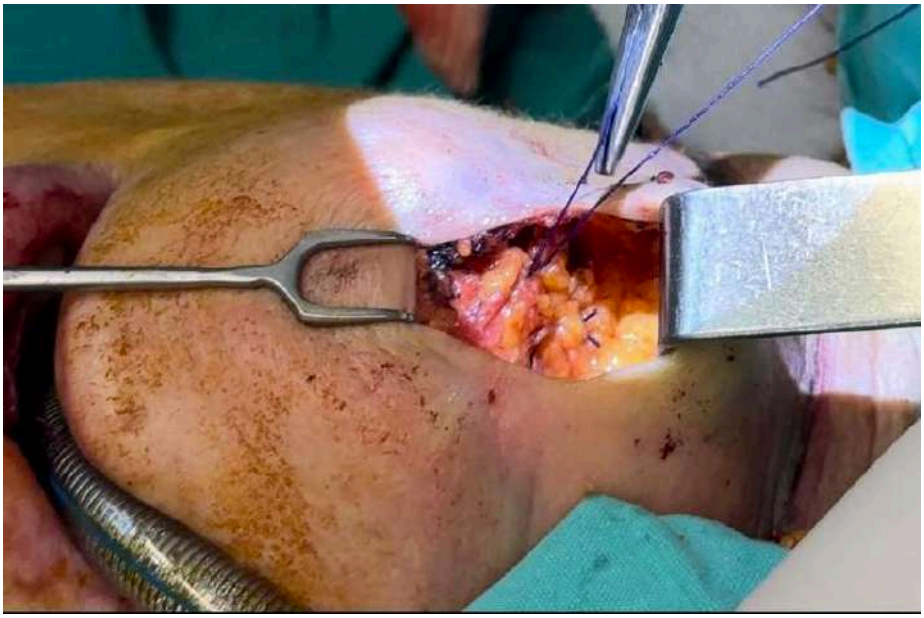

Figure 6: Medial Suturing of the PM, Suprahyoid Area, with Interrupted Stitches

Figure 7: Dissection of the Flap in Plane 2, Retroauricular and Preauricular

Figure 8: Lateral Dissection with Skin Delamination to the Platysma and Anterior Submental Dissection

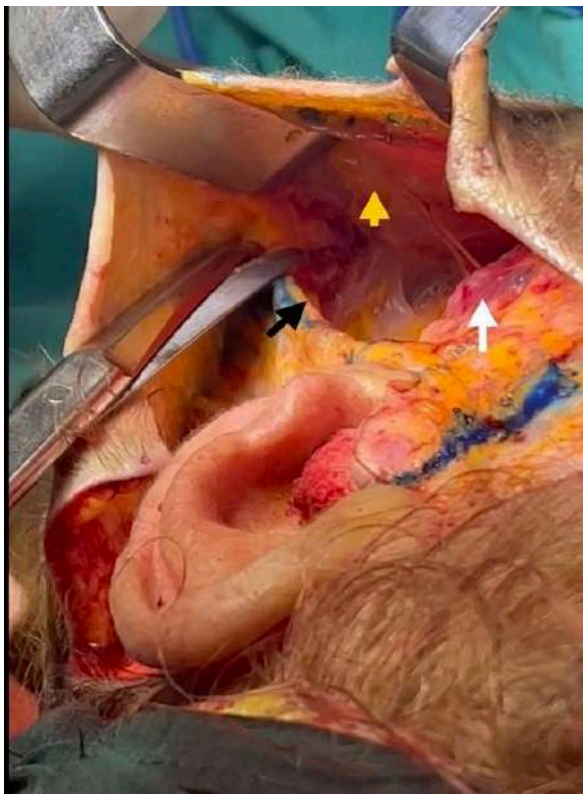

Figure 9: Posterior view of the Auricular Pavilion, Showing A Lateral Composite Cervical Flap without Delamination of the Pm

Yellow Arrow: PM adhered to Planes 1 and 2.
White Arrow: Mandibular gonion with parotid-masseteric fascia.
Black Arrow: Anterior border of the ECM.

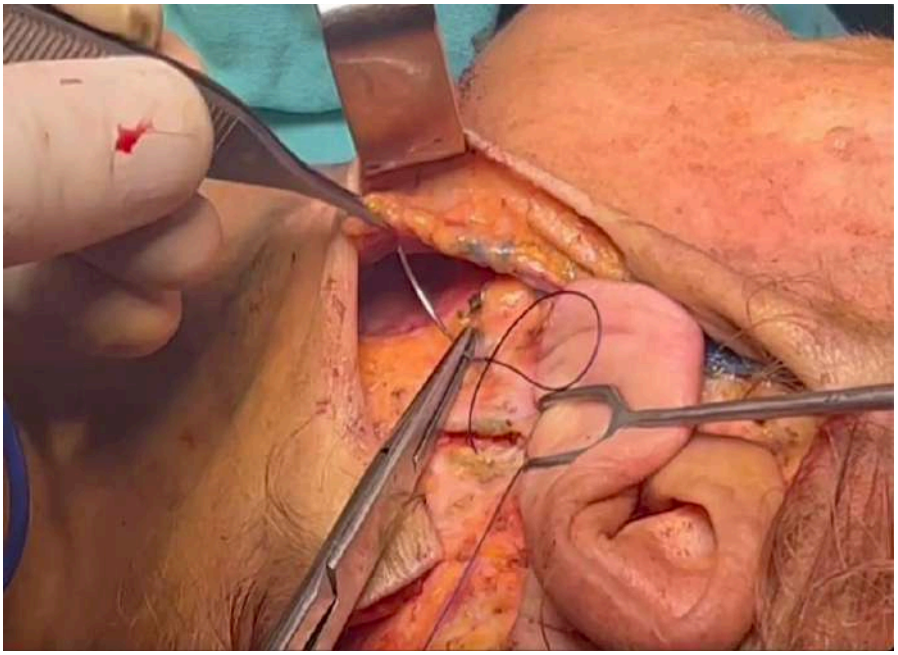

Figure 10: Suture Fixation of the Cervical Composite Flap to the Mastoid

VII. COMPLICATIONS

- *Hematoma:* These can vary in size, with large blood collections being rare. Small, isolated collections are more common. The use of the Auersvald hemostatic net is very effective in preventing these.
- *Seroma:* Generally occurs in the submental region. Treating deep fat alters lymphatic drainage. Immediate drainage is required through repeated punctures every 48 hours; if this is not feasible, a drain should be left in place.
- *Skin Retractions:* Usually occur post-seromas or untreated small hematomas.
- *Asymmetries:* Result from asymmetric reduction of deep structures.
- *Cobra Neck:* Caused by over-resection of the interdigastric fat.
- *Facial Marginal Nerve Palsy:* Can occur due to diathermy when resecting the superficial lobe of the SMG.
- *Sialomas:* Rare but can be expected with reduction of the SMG.
- *Skin Necrosis and Suffering:* Rare, typically observed with high concentrations of tranexamic acid in local anesthetic solutions. It can also occur in cases with prior energy treatments affecting the vascularization of Planes 1 and 2. In these cases, it is advised not to delaminate the PM from the skin.
- *Dry Mouth:* Rare, occurring post-SMG reduction. The SMG, along with the sublingual gland and accessory glands, maintains mouth moisture, whereas the parotid gland only functions during mastication and stimulation of food bolus. Antidepressant medication can exacerbate this complication, which is usually transient and resolves within 3 to 4 months. Treatment includes administering pilocarpine.

VIII. POST-OPERATIVE CARE

- *Pre-Surgery Information:* Inform the patient that a hard edema will develop in the submental region, lasting 4 to 6 weeks.
- *Post-Operative Education:* Instruct the patient to avoid extreme neck rotation and to avoid opening the mouth wide.
- *Massage Restrictions:* Avoid massages to reduce neck tension for 2 weeks to prevent elongation of the PM until it adheres to its new position.
- *Dietary Restrictions:* For patients who have undergone SMG treatment, avoid alcohol and citrus fruits that stimulate salivary glands for 2 weeks.
- *Sleeping Position:* For the first 48 to 76 hours, the patient should sleep semi-sitting at 25 to 30 degrees head elevation, with the nose pointing toward the ceiling to facilitate venous drainage.

Figure 11-12: Patient with an Aged Obtuse Neck and Their 20-Day Postoperative Result. Preservation Face and Neck Lift without Cervical Platysma Delamination

Figure 13: Pre- and Postoperative of a Patient with a Short Neck. Cervicofacial Lifting. Treatment type 5

Figure 14: Pre- and 2-month postoperative. Treatment type 5 with platysma delamination

Figure 15: Pre- and 2-Month Postoperative, Type 5 with Cervical Platysma Delamination

Figure 16: Pre- and 2-Month Postoperative. Cervicofacial Lifting with Lateral Approach, without Platysma Delamination. No Submental Incision. Procedure Type IV

Figures 17-18: Procedure type IV. 6 Months Postoperative

VIII. CONCLUSION

Facial aging presents distinctive characteristics compared to neck aging. In the midface, we observe deflation or reabsorption of fat compartments, accompanied by progressive laxity. The lower third reflects this same aging, adding a descent of soft tissues that migrate to the neck, causing the appearance of jowls, loss of definition of the mandibular border, and the gonion.

Current aesthetic medicine tools have shown good results in these areas, especially in faces with deflation, through volumization of the midface and simulation of a new mandibular border and gonion in the lower third. However, neck aging is characterized by a fullness effect due to laxity and descent of deep structures, along with shortening of the platysma and redistribution of subplatysmal fat, creating an incompetence between the container and its content.

Aesthetic treatments based on energy that act on the skin, subcutaneous tissue, and PM do not fully meet the expectations of patients with obtuse necks, making this area a challenging unresolved issue in the aesthetic field.

Therefore, we believe that deep neck lifting techniques, being reductive, are the ideal option to address these issues. Neck rejuvenation requires a deep understanding of anatomical structures and their dynamics during aging. This approach allows for maximizing results and minimizing complications. Accurate diagnosis is crucial for proper planning and treatment. The external shape and contour of the neck reflect its internal anatomy, similar to what happens in aesthetic rhinoplasty. Thus, thorough treatment of the deep structures of the neck is essential for improving postoperative results and prolonging their durability.

In summary, the neck today represents a new and significant challenge for plastic surgeons.

To complement our study, we conducted two informational surveys directed at plastic surgeons specialized in deep cervicofacial lifting techniques, with the following relevant results:

Treatment of the Submandibular Gland (SMG):

- 60% of respondents regularly perform submandibular gland excision as part of neck treatment.
- 10% perform it preventively.
- 50% do it only in cases of glandular hypertrophy or ptosis.
- The remaining 40% do not intervene directly in the gland, limiting treatment to ptosis with the platysma (PM) hammock technique.

Platysma Myotomy:

- 100% of respondents perform some form of platysma myotomy.
- 50% perform myotomy approximately 1 cm below the hyoid bone.
- 49% perform myotomy below the hyoid, combining it with other techniques:
  - 18% combine it with an anterior myotomy of the sternocleidomastoid muscle (ECM).
  - 31% combine it with a triangular resection below the hyoid.
  - 1% of respondents perform a total transection of the platysma.

These results highlight the diversity of approaches and techniques used in neck treatment, reflecting different preferences and experiences of specialists in the quest for optimal aesthetic and functional results.

BIBLIOGRAFIA

1. Minelli L, Yang HM, van der Lei B, Mendelson B. The surgical anatomy of the jowl and the mandibular ligament reassessed. Aesth Plast Surg.2023.
2. An Anatomic Basis for Volumetric Evaluation of the Neck Sherine S. Raveendran, MBBS, MS, FRCS Ed, EBOPRAS; D. J. Anthony, MBBS, MS, FRCS Ed; and Lucian Ion, MD, FRCS, FRCS Plast.
3. Deep Neck Contouring: Indications and Techniques Ahmad Bogari, MD1 Ozcan Cakmak 2020.
4. Deep Neck Contouring With a Focus on Submandibular Gland Vascularity: A Cadaver Study, Aesthetic Surgery Journal 2023. OXFORD.

5. Facelift Part I: History, Anatomy, and Clinical Assessment, Aesthetic Surgery Journal 2020, OXFORD.
6. Rod J. Rohrich, James M. Stuzin. Facial danger zones. Thieme MedOne.
7. Rejuvenecimiento quirúrgico facial, deep plane facelift y procedimientos complementarios. Dr. Juan Pavani. Revista Cirugía Plastica, Arg. 2024.
8. Characterization of the Cervical Retaining Ligaments During Subplatysmal Facelift Dissection and its Implications Andrew A. Jacono, MD, FACS;Aesthetic Surgery Journal 2017.
9. Importance of the Digastric Muscle in Cervical Contouring: An Update Bruce F. Connell, MD. 1999, California.
10. Volumetric Assessment of the Anterior Digastric Muscles: A Deeper Understanding of the Volumetric Changes With Aging Sean P. McCleary. 2023, Aesthetic Surgery Journal, OXFORD.
11. Age-Related Changes in the Submandibular Gland: An Imaging Study of Gland Ptosis Versus Volume, Sean P. McCleary, MD; Shahrzad Moghadam, BS; Christina Le, BS; Kevin Perez, MSc; Myung-Shin Sim, DrPH; and Jason Roostaeian, MD, Aesthetic Surgery Journal 2022, OXFORD.
12. The Short Neck: Challenges and Techniques, Auersvald L A, Auersvald A. Facial Plast Surg. 2022.
13. Limited Delamination Modifications to the Extended Deep Plane Rhytidectomy: An Anatomical Basis for Improved Outcomes AQ: au Michael Roskies, MD, MSc, FRCSC, 1,* Dominic Bray, 2 Neil A. Gordon, 3, 4 Alessandro Gualdi, 5 AQ: 1 L. Mike Nayak, 6 and Ben Talei.